Digital Photonic Receivers for Wireless and Wireline Optical Fiber Transmission Links

Guerrero Gonzalez, Neil

Publication date:
2011

Document Version
Publisher's PDF, also known as Version of record

Digital Photonic Receivers for Wireless and Wireline Optical Fiber Transmission Links

Neil Guerrero Gonzalez

Supervisors:*Professor Idelfonso Tafur Monroy* and
Assistant Professor Darko Zibar

Delivery Date: February 15th 2011

DTU Fotonik
Department of Photonics Engineering
Technical University of Denmark
Building 343
2800 Kgs. Lyngby
DENMARK

DTU Fotonik
Department of Photonics Engineering

Abstract

This PhD thesis addresses the design and performance evaluation of digital photonic receivers in hybrid optical fiber-wireless transmission systems. The research results presented in this thesis are pioneering in two areas. First, it is shown the first experimental demonstration of automatic demodulation of signals with mixed modulation formats and bit rates in a single digital coherent photonic receiver. The demodulated signals were generated on baseband and optical phase-modulated (PM) radio-over-fiber (RoF) systems. Secondly, it is presented the first known analytical and numerical investigations on the performance of data-aided optical channel estimation based on constant-amplitude zero-autocorrelation (CAZAC) sequences for 112 Gb/s polarization-diversity coherent optical fiber transmission links.

The benefits of introducing digital signal processing functions in optically envelope detected RoF systems are presented first. Subsequently, we show the robustness and flexibility of digital signal processing based receivers for coherent detection of wavelength-division-multiplexed (WDM) optical transmission system in metro-access networks supporting heterogeneous wireline and wireless services. The experimental demonstration supported the following transmissions systems: a baseband, 5 Gbps, intensity modulation system employing a directly modulated vertical cavity surface emitting laser (VCSEL), a baseband 20 Gbps non-return-to-zero quadrature phase-shift keying (NRZ-QPSK) system, an optically phase-modulated 2 Gbps impulse radio ultrawideband (IR-UWB) link and an optically phase-modulated 5 GHz OFDM radio-over-fiber transmission link. The results of the experiment are relevant for future applications in heterogeneous metro-access networks.

This thesis also introduces a novel approach to implement joint phase, frequency and modulation format estimation. The new proposed approach uses a data-aided clustering-based estimation technique based on the k-means algorithm, instead of using traditional methods based on maximum

a posteriori or maximum likelihood estimation. Firstly, the k-means algorithm is successfully applied for demodulation of very high speed radio-over-fiber signals in a WDM multichannel transmission link. The recovered 2.5 Gb/s QPSK signals at a carrier frequency of 6 GHz resulted in the highest bit rate reported until 2009 for that kind of systems. Then, an extension of the proposed k-mean algorithms is applied to higher order modulation formats. Successful experimental signal demodulation of 8 phase-shift-keying (8PSK) and 16 quadrature-amplitude-modulated (16QAM) confirm the robustness of the proposed signal demodulation approach. Finally, a reconfigurable receiver supporting burst mode transmission of signals where the modulation format and bit rate changes from "burst to burst" is introduced and experimentally validated.

This PhD thesis demonstrate the flexibility, upgradeability and robustness offered by reconfigurable digital signal processing based photonic receivers in hybrid wireless and wireline optical fiber transmission links. Furthermore, the digital signal processing framework presented in this thesis can be extended to design probabilistic-based digital photonic receivers that can find applications in cognitive heterogeneous reconfigurable optical networks.

Abstrakt

Denne ph.d.-afhandling omhandler design og evaluering af digitale, fotoniske modtagere i hybride, optiske fiber-trådløse transmissionssystemer. Forskningsresultaterne er banebrydende på to områder. For det første vises eksperimentel og automatisk demodulation af signaler med blandede modulationsformater og bithastigheder i en og samme digitale, fotoniske modtager; signalerne stammer fra basisbånd og optisk fase-modulerede (PM) radio-over-fiber (RoF) systemer. For det andet præsenteres de første, kendte, analytiske og numeriske undersøgelser af data-støttede, optiske kanalestimeringer baseret på konstant-amplitude nul-autokorrelation sekvenser for 112 Gb/s kohærente, optiske fiberforbindelser med polarisationsdiversitet.

Først præsenteres fordelene ved at indføre digital signalbehandling i optiske, RoF systemer med amplitudedetektion. Efterfølgende påvises robustheden og fleksibiliteten af digitale, signalbehandlingsbaserede modtagere til kohærent detektion af bølgelængdemultipleksede (WDM), optiske transmissionssystemer i metro-accesnet, som understøtter heterogene, kabelbaserede og trådløse tjenester. Den eksperimentelle opstilling understøtter følgende transmissionssystemer: et 5 Gb/s basisbånd, intensitetsmoduleret system, der bruger en direkte moduleret "vertical cavity surface emitting laser" (VCSEL); et 20 Gb/s basisbånd "non-return-to-zero quadrature phase-shift keying" (NRZ-QPSK) system; en optisk, fase-moduleret 2 Gb/s "impulse radio ultrawideband" (IR-UWB) forbindelse; og en optisk fase-moduleret 5 GHz OFDM-radio-over-fiber transmissionsforbindelse. Resultaterne af eksperimenterne er relevante for fremtidige anvendelser i heterogene metro-access netværk.

Afhandlingen introducerer også en ny tilgang til at realisere estimering af fælles fase, frekvens og modulationsformat. Den foreslåede, nye fremgangsmåde gør brug af en data-støttet, cluster-baseret estimeringsteknik, som er baseret på "k-means" algoritmen i stedet for de traditionelle metoder

baseret på maksimal a posteriori eller maksimal sandsynlighedsestimering. Først anvendes "k-means" algoritmen med succes til demodulation af radio-over-fiber signaler med meget høj bithastighed i en WDM multikanal transmissionsforbindelse. De gendannede 2,5 Gb/s QPSK signaler på en bærefrekvens på 6 GHz udgjorde den højeste bithastighed, som var rapporteret indtil 2009 for den slags systemer. Derefter blev en udvidelse af den foreslåede "k-mean" algoritme anvendt på højere ordens modulationsformater. Vellykkede, eksperimentelle demoduleringer af "8 phase-shift-keying" (8PSK) og "16 quadrature-amplitude-modulated" (16QAM) bekræfter den foreslåede demodulationsmetodes robusthed. Endelig blev en rekonfigurerbar modtager, der understøtter "burst mode" transmission af signaler, hvor modulationsformat og bithastighed ændrer sig fra "burst to burst", introduceret og eksperimentelt verificeret.

Ph.d.-afhandling demonstrerer den fleksibilitet, det opgraderingspotentiale og den robusthed, som omkonfigurerbare, digitale, signalbehandlingsbaserede fotoniske modtagere kan tilbyde i hybride, trådløse og kabelbaserede fiberforbindelser. Desuden kan den digitale signalbehandlingsmetode, der præsenteres, udvides til at designe sandsynlighedsbaserede, digitale fotoniske modtagere, som kan finde anvendelse i kognitive, heterogene og rekonfigurerbare optiske netværk.

Acknowledgements

During the last three years of great work at DTU, I have haven the opportunity to grow up "hand by hand" with the Metro Access group. There are no words to thank the whole group. All of you have been actively contributed to make easier and happier my life (in all dimensions) during my PhD studies.

I would like to express my most sincere gratitude to Professor Idelfonso, Darko, Xianbin, Tim, Jesper, Kamau, Alex, Antonio, Roberto, Xu, Maisara, Valeria, Robert, Xiaodan, Alexander, Thang, Bomin... the list is long. As long as a traditional colombian family.

First of all, I would like to thank my supervisor Professor Idelfonso Tafur Monroy for showing me the path of *excellence*. A path to walk during the whole life. Many thanks Professor for your precise comments, good advices and invaluable supervision through the project. I also would like to give an special thanks to Darko, my co-supervisor, for teaching me how to work with *passion and discipline*. The perfect combination to achieve any goal in life.

To my family in Colombia; Papa Reinaldo, Mama Miriam, Natalia, Diego y Ana Lucía, thanks for always being there. I did not feel the distance. This PhD thesis is one more result of all your love and support. I would like to specially thank my beautiful Claudia: thanks for kipping me alive. You are all my reasons.

Finally, I would like to close my acknowledgments offering this work to my Lord. Thanks Lord for guiding my steps up to this point. Let me continue walking with passion and discipline every day, and "hand by hand" with my family and friends, through the path of excellence.

Summary of Original Work

This thesis is based on the following original publications:

PAPER 1 Guerrero Gonzalez Neil, Prince Kamau, Zibar Darko, Tafur Monroy Idelfonso. "Re-configurable digital receiver for optically envelope detected half cycle BPSK and MSK radio-on-fiber signals", *Optical Fiber Technology*, vol. 17, no. 1, pp. 59-63, January 2011.

PAPER 2 Guerrero Gonzalez Neil, Zibar Darko, Caballero Jambrina Antonio, Tafur Monroy Idelfonso. "Experimental 2.5-Gb/s QPSK WDM phase-modulated radio-over-fiber link with digital demodulation by a K-means algorithm", *IEEE Photonics Technology Letters*, vol. 22, no. 5, pp. 335-337, March 2010.

PAPER 3 Guerrero Gonzalez Neil, Caballero Jambrina Antonio, Amaya Fernández Ferney Orlando, Zibar Darko, Tafur Monroy Idelfonso. "Experimental 2.5 Gbit/s QPSK WDM coherent phase modulated radio-over-fibre link with digital demodulation by a K-means algorithm", in *Proceedings of the 35th European Conference on Optical Communication, ECOC'2009,* Vienna, Paper P3.15, September 2009.

PAPER 4 Guerrero Gonzalez Neil, Zibar Darko, Yu Xianbin and Tafur Monroy Idelfonso. "Reconfigurable Digital Receiver for 8PSK Subcarrier Multiplexed and 16QAM Single Carrier Phase-Modulated Radio over Fiber Links", accepted for publication in *Microwave and Optical Technology Letters*, 2011.

PAPER 5 Guerrero Gonzalez Neil, Zibar Darko, Yu Xianbin, Tafur Monroy Idelfonso. "Optical phase-modulated radio-over-fiber links with k-means algorithm for digital demodulation of 8PSK subcarrier multiplexed signals", in *Proceedings of the Optical Fiber Communication Conference and Exposition and the National Fiber Optic Engineers Conference, OFC'2010,* San Diego, CA, USA., paper number OML3, March 2010.

PAPER 6 Guerrero Gonzalez Neil, Zibar Darko, Yu Xianbin and Tafur Monroy Idelfonso. "K-means Algorithm for joint Frequency and Phase Offset Compensation in Digital Receivers for Phase-Modulated Radio-over-Fiber Links", under review in *Optical Fiber Technology*, 2011.

PAPER 7 Guerrero Gonzalez Neil, Zibar Darko, Tafur Monroy Idelfonso. "Cognitive digital receiver for burst mode phase modulated radio over fiber links", in *Proceedings of the 36th European Conference on Optical Communication, ECOC'2010,* Torino, Italy, Paper P6.11, September 2010.

PAPER 8 Guerrero Gonzalez Neil, Caballero Jambrina Antonio, Borkowski Robert, Arlunno Valeria, Thang Pham Tien, Rodes Roberto, Zhang Xu, Binti Othman Maisara, Prince Kamau, Yu Xianbin, Jensen Jesper B., Zibar Darko and Tafur Monroy Idelfonso. "Reconfigurable Digital Coherent Receiver for Metro-Access Networks Supporting Mixed Modulation Formats and Bit-rates", accepted for oral presentation at *the Optical Fiber Communication Conference and Exposition and the National Fiber Optic Engineers Conference OFC'2011,* Los Angeles, USA., paper number OMW7, March 2011.

PAPER 9 Arlunno Valeria, Borkowski Robert, **Guerrero** Gonzalez Neil, Caballero Antonio, Prince Kamau, Jensen Jesper B., Zibar Darko, Larsen Knud J. and Tafur Monroy Idelfonso. "Adaptive order n-QAM Optical OFDM Link with Optical Phase Modulation and Digital Coherent Detection", under review in *Microwave and Optical Technology Letters* 2011.

PAPER 10 Pham Tien-Thang, **Guerrero** Gonzalez Neil, Yu Xianbin,

Zibar Darko, Dittmann Lars and Tafur Monroy Idelfonso. "Robust BPSK Impulse Radio UWB-over-Fiber Systems Using Optical Phase Modulation," accepted for oral presentation at *the Optical Fiber Communication Conference and Exposition and the National Fiber Optic Engineers Conference OFC'2011,* Los Angeles, USA., paper number OTuF6, March 2011.

PAPER 11 Rodes Lopez Roberto, Yu Xianbin, Caballero Jambrina Antonio, Jensen Jesper B., Gibbon Timothy Braidwood, **Guerrero** Gonzalez Neil, Tafur Monroy Idelfonso. "Range extension and channel capacity increase in impulse-radio ultra-wideband communications", *Tsinghua Science and Technology*, vol. 15, no. 2, pp. 169-173, April 2010.

PAPER 12 Gibbon Timothy Braidwood, Yu Xianbin, Gamatham Romeo, **Guerrero** Gonzalez Neil, Rodes Lopez Roberto, Jensen Jesper B., Caballero Jambrina, Antonio, Tafur Monroy Idelfonso. "3.125 Gb/s impulse radio ultra-wideband photonic generation and distribution Over a 50 km Fiber With Wireless Transmission", *IEEE Microwave and Wireless Components Letters*, vol. 20, no. 2, pp. 127-129, February 2010.

PAPER 13 Prince Kamau, Jensen Jesper B., Caballero Jambrina Antonio, Yu Xianbin, Gibbon Timothy Braidwood, Zibar Darko, **Guerrero** Gonzalez Neil, Osadchiy Alexey Vladimirovich, Tafur Monroy Idelfonso. "Converged wireline and wireless access over a 78-km deployed fiber long-reach WDM PON", *IEEE Photonics Technology Letters*, vol. 21, no. 17, pp. 1274-1276, September 2009.

Other scientific reports associated with the project:

PAPER 14 Guerrero Gonzalez Neil, Zibar, Darko, Yu Xianbin, Tafur Monroy Idelfonso. "Experimental demonstration of a digital maximum likelihood based feedforward carrier recovery scheme for phase-modulated radio-over-fibre links," in *Proceedings of the 21st Annual Meeting of the IEEE Lasers and Electro-Optics Society LEOS'2008,* Newport Beach, CA, USA., paper number ThN2, November 2008.

PAPER 15 Zibar Darko, Caballero Jambrina Antonio, **Guerrero** Gonzalez Neil, Schaeffer Christian, Tafur Monroy Idelfonso. "Digital coherent receiver employing photonic downconversion for phase modulated radio-over-fibre links," in *Proceedings of the International Microwave Symposium Digest IMS'2009,* Boston, USA., December 2009.

PAPER 16 Andres Soriano Ruben, **Guerrero** Gonzalez Neil, Zibar Darko and Tafur Monroy Idelfonso. "Polarization Rotation Monitoring Using 2D-Pattern Recognition in Digital Coherent Receivers," in *the 2010 Benelux Symposium,* Holland, November 2010.

Contents

List of Figures

List of Tables

Chapter 1

Introduction

A strong upgrade of existing wireless and fiber-based access networks is needed in order to respond to the exponential increase of bandwidth demand from modern information societies. Moreover, it is expected that next generation access networks will guarantee access to high bandwidth services, as well as multimedia applications, to end users any time and anywhere.

On one hand, the wide set of heterogeneous multimedia services provided by wireless access networks have implanted the idea of an omnipresent telecommunication network in users' minds. Indeed, immediate access to information is currently offered by wireless access networks. Telecommunication wireless services, however, do not have enough bandwidth to allow access to services such as high definition TV (HDTV) or multimedia applications with transmission rates in the order of thousands of Mb/s. To date, the highest transmission rate offered by the wireless local area network (LAN) technology is still 10 times below the data transmission capacity necessary to support the new generation of video-based telecommunication services [1].

To increase the data transmission rate of current telecommunication wireless services from hundred of Mb/s up to multi-Gb/s, new research fronts on wireless access networks are exploring the unlicensed 60 GHz frequency band for wireless signal transmission [1, 2]. However, the high atmospheric attenuation of mm-waves at this frequency band will demand the installation of a large number of antenna base-stations (BSs) in order to compensate for signal power losses and guarantee the quality of service to customers. In conclusion, while the use of the 60 GHz frequency band is good for efficient spectral utilization for in-building communication ap-

plications, it also implies an increase of the system energy consumption. Therefore, a new approach to decrease system power consumption and at such high frequency band supporting high data transmission capacity is urgently needed in wireless access networks [1, 2].

On the other hand, wired access networks based on fiber-to-the-home (FTTH) technology are a promising approach to increase data transmission capacity due to the large bandwidth offered by the optical fiber [3], [1,2]. Indeed, FTTH deployment has recently surpassed thirty million users worldwide and the trend is predicted to continue at a rapid rate [3]. Various FTTH solutions have been implemented using passive optical networks (PONs). Passive optical networks provide much higher bandwidth for data transmission applications than current solutions such as digital subscriber lines (DSL), as well as lower network energy consumption because of the use of only passive elements such as passive combiners, couplers and splitters in the signal's path. The aggregated data transmission capacity on PON access has rapidly increased from orders of Gb/s up to 40 Gb/s over the last 10 years [1]. In fact, transmission rates above 10 Gb/s have been reported by PON systems based on optical fiber access technologies such as Time Division Multiple Access (TDMA), Wavelength Division Multiplexed (WDM) and optical Orthogonal Frequency Division Multiple Access (OFDMA) [4]. Furthermore, recent experimental demonstrations of data rate transmission of 25 Ghz-spaced, 320x114Gb/s dense-WDM (DWDM) transmission through 580 km been reported [5].

Among the already mentioned optical fiber access technologies, WDM-PON is the most promising solution for implementing future broadband access networks [6, 7]. These systems, however, rely on demultiplexing by fixed wavelength filters such as fiber Bragg gratings or arrayed waveguide grating (AWGs). This adds complexity to the PON architecture, and makes future upgrades of capacity and number of users problematic. In our group we proposed in [8], the introduction of coherent detection with digital signal processing (DSP) as a flexible and future-proof candidate for next generation PONs. The proposed solution is based on multi wavelength optical transmission over the existing PON architecture while avoiding the restrictions imposed by AWGs for demultiplexing. Moreover, the system will support both wireline and wireless over fiber types of signals, as well as bidirectional single fiber transmission.

1.1 Hybrid fiber wireless networks

The use of a WDM-PON infrastructure to distribute microwave and millimeter waveband signals is envisaged as the next technology to increase data transmission capacity in wireless access services. Such technology is known as Radio-over-Fiber (RoF). Furthermore, since the same optical fiber infrastructure to distribute RoF signals can also support optical digital signals, the convergence of RoF-based optical-wireless networks and WDM-PON systems are regarded as the most promising solution to increase the capacity, coverage, bandwidth and mobility in future hybrid broadband access networks (see Fig. 1.1) [9–15]. The convergence of wireless-based and fiber-based access networks is known as hybrid fiber wireless networks.

The implementation of hybrid fiber wireless networks is not straightforward and issues of spectrum allocation, performance optimization and integration with existing infrastructures must be considered [16]. An approach to achieve dynamic spectrum allocation have been recently reported by using optical-frequency-interleaved techniques and optical path switching to perform dense WDM (DWDM) grid assignment [1]. An additional important aspect for hybrid fiber wireless networks is to fulfil power budget, dispersion, and other quality requirements for both signal types.

In **PAPER 13** we reported an experimental demonstration of a 78.8 km WDM-PON supporting converged transport of 21.4 Gbit/s NRZ-DQPSK, optical phase modulated 5 GHz radio-over-fiber, fiber and air transmission

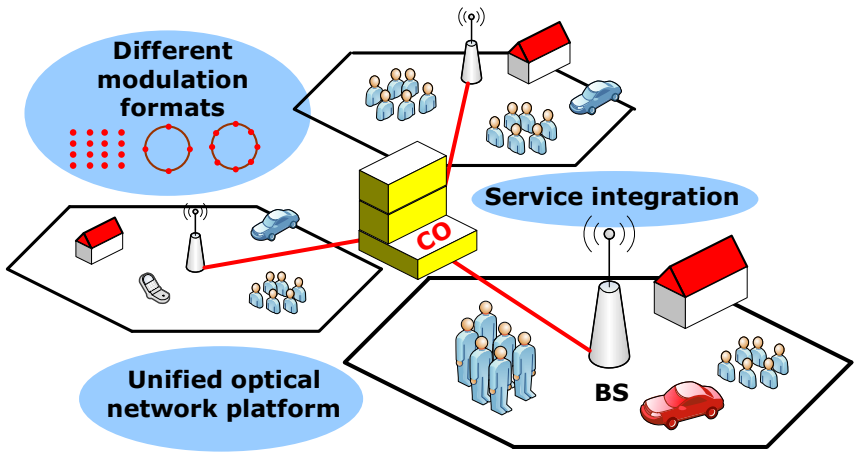

Figure 1.1: Radio−over−fiber network: urban scenario. BSU, base station unit; CO, central office

of 3.125-Gb/s pulse ultra-wideband and 256-QAM WiMAX. This was the first known demonstration of seamless coexistence of various wireless and wireline signals toward future converged broadband access networks.

A powerful method to achieve successful implementation of hybrid fiber wireless networks is the use of digital signal processing (DSP) algorithms for transmission impairment compensation and signal conditioning and demodulation. Recent advances in high-speed DSP techniques and analog-to-digital (A/D) converters (ADC) have enabled the integration of DSP-based receivers into fiber-based communication systems. Digital receivers to perform signal demodulation of intensity-modulated/direct-detected (IM/DD) hybrid fiber wireless systems are known as digital direct detection receivers. **PAPERS 1, 11 and 12** report on the contributions of two representative IM/DD hybrid fiber wireless technologies: optical envelope detected systems and photonic ultra-wideband (UWB) systems.

1.2 IM/DD hybrid fiber wireless networks

Optical envelope detected systems allow an easy integration of microwave wireless communications schemes with wired access networks based on optical fiber technology. Optical envelope detection emerges as a promising technology to reduce the complexity of radio-frequency (RF) resources at the receiver side since RF down-conversion is performed by direct photodetection of the optical signal instead of heterodyne RF mixing techniques [17]. Experimental validation has been reported with various RF modulated signal types, including 5.5 Gbit/s amplitude shift keying (ASK) [18], and 40 Mbaud 16 QAM and quadrature phase shift keying (QPSK) [19].

In **PAPER 1** we demonstrated the first known integration of a DSP-based receiver into optical envelope detected systems. The benefits introduced by the integration of DSP modules for signal demodulation can be summarized as follows: easy receiver system reconfiguration on a single software-platform, and simple digital implementation of coding and encoding tasks.

The other relevant contribution reported here on IM/DD hybrid fiber wireless systems regards the development of photonic UWB systems. UWB has been proposed as an alternative air interface for Wireless Personal Area Networks (WPAN) because of its low power spectral density, high data rate, and robustness for multi-path fading [20]. For broadcast applications such as high definition TV, this approach has the added benefit that the UWB transmission equipment can be localized in a central office, thereby dis-

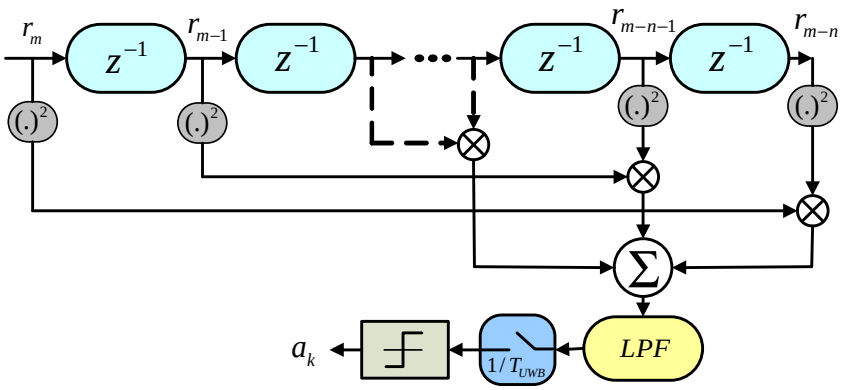

Figure 1.2: Digital UWB receiver

tributing costs among many users. However, the realization of these UWB benefits faces the challenge of low-complexity high-performance receiver schemes where clock synchronization constitutes the major issue due to the low-power UWB transmit waveforms [21, 22].

In **PAPERS 11 and 12**, we reported successful signal detection and demodulation of 2 and 3.125 Gb/s photonic impulse radio ultra-wideband signal over 50 km of fiber and wireless transmission over 2.9–3.3-m. I have contributed to this topic by developing the direct digital detection receiver for signal demodulation of photonic UWB signals. The schematic structure of the implemented UWB receiver is shown in Fig. 1.2.

1.3 Optical phase-modulated hybrid fiber wireless networks

The stringent linearity link requirements of a multicarrier transmission techniques such as orthogonal frequency division multiplexing RoF signal transmission, are challenging to meet with IM/DD RoF systems [16, 23]. Currently, new research fronts in hybrid access networks are focused on phase-modulated (PM) links to improve linearity and power receiver sensitivity [24, 25].

Coherent optical detection has been demonstrated to perform linear signal demodulation of millimeter and mm-wave signals encoded onto the phase of an optical carrier [26–28]. The main advantages offered by coherently detected PM RoF systems over traditional IM/DD RoF systems

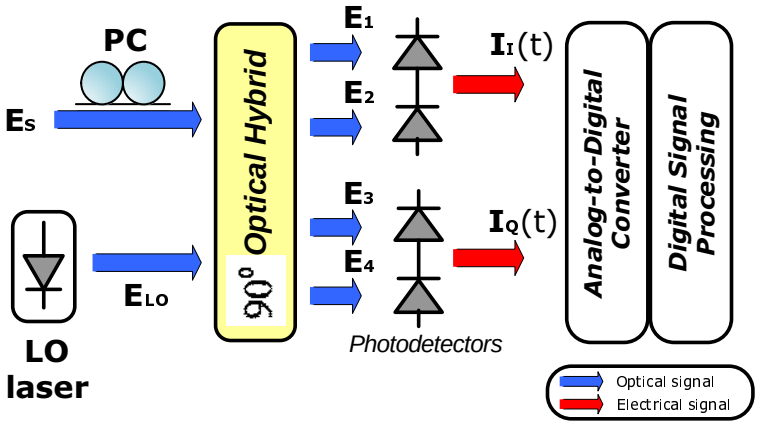

Figure 1.3: Homodyne phase-diversity receiver. LO: local oscillator; PC: polarization controller.

are: 1) larger spur-free dynamic range (SFDR) [26,27], 2) higher spectrally efficient optical data transmission of advanced modulated microwave signals, 3) larger bandwidth and channel selectivity and 4) lower transmission signal power requirements [11].

Coherent optical communication emerged 30 years ago to overcome limitations in receiver sensitivity by using local oscillator (LO) with a large power level. Optical coherent receivers are also applied for narrow optical filtering of closely spaced WDM channels in WDM-PON systems and optical phase signal detection to increase data transmission capacity [29]. The first demonstration of digital carrier-phase estimation in 2005 [30] opened a new stage in optical communication systems integrating high-speed DSP-based modules and coherent receivers [31,32]. In PM RoF systems the role of the DSP-based coherent receiver is to reconstruct the transmitted microwave signal from the phase of the received optical carrier and perform the subsequent signal demodulation.

The main advantages that digital photonic receivers can offer compared to the traditional optical signal demodulation techniques include [33]: 1) cost effectiveness and compactness [34, 35], 2) adaptive compensation of channel impairments in the electronic domain using signal processing techniques [36], and 3) design versatility and robust operation by enabling reception of different formats using the same receiver hardware [37–43].

1.4 DSP algorithms for optical PM hybrid fiber wireless links

DSP algorithms for optical coherent communication systems can be grouped into two classes: 1) digital filtering for optical transmission impairment monitoring and compensation and 2) transmitter-receiver synchronization. DSP functions for transmitter-receiver synchronization can be further classified in four subgroups: 1) timing recovery, 2) carrier recovery parameters [37–43] and 3) decoding and symbol estimation.

Algorithms for optical transmission impairments monitoring groups algorithms for linear estimation and compensation of most of the optical linear transmission impairments such as chromatic dispersion (CD), higher order polarization mode dispersion (PMD) and polarization dependent loss (PDL) among others in the digital domain. This class of algorithms is based on finite-impulse response (FIR) realizations [44], as well as adaptive digital equalization to compensate time varying impairments such as the state of polarization and polarization mode dispersion (PMD) [45, 46].

New techniques for linear estimation of signal transmission impairments based on digital coherent receivers are currently receiving the attention of the optical communication community. The target of such techniques, known as optical performance monitoring (OPM), is to provide information for signal quality estimation, fault localization and system diagnosis to perform dynamic and future impairment-aware routing in the levels of network management and network control [47, 48]. In this PhD thesis, I present the results of numerical investigations of the use of a special type of sequences belonging to the class of poly-phase sequences called CAZAC (constant-amplitude zero-autocorrelation) for data-aided optical channel estimation. The new method for OPM based on CAZAC sequences is presented in chapter 2.

1.4.1 The digital coherent receiver for PM RoF links

Fig. 1.4 shows the block diagram of a digital coherent receiver for PM RoF systems. The first two blocks of the digital coherent receiver transfer the full optical field to the electrical domain. Once detected, photocurrents are digitized using a digital sampling oscilloscope (DSO) and the third block then uses a carrier-recovery digital phase-locked loop (PLL) [28] to remove the optical frequency/phase offset between the tunable local oscillator and the incoming optical carrier recovery. Next, a linear signal demodulation

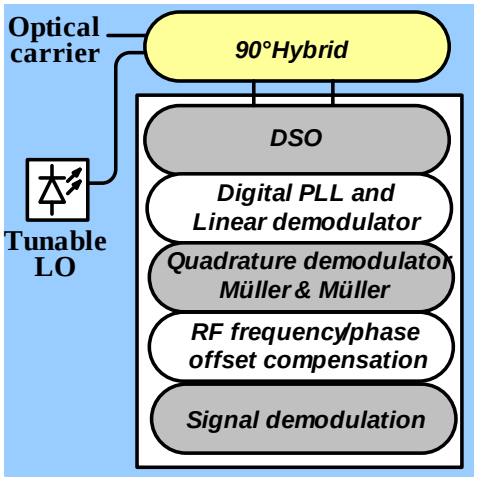

Figure 1.4: Digital coherent receiver for PM RoF systems.

[28] is implemented to recover the encoded RF signal from the phase of the optical carrier. In the RF domain, RF frequency down-conversion and the subsequent timing recovery are performed in the digital domain. RF frequency and phase offset compensation perform signal conditioning before signal demodulation.

1.4.2 Beyond the state-of-the-art on PM RoF links

Recently, our group has reported experimental transmission records on maximum bit rate (4 Gb/s) and maximum RF carrier frequency (40 GHz) [49] for DSP-based coherently detected phase-modulated RoF links.

I have extended on the state of the art on hybrid fiber wireless systems by experimentally demonstrating unified support for signal detection on highly heterogeneous next generation metro-access networks. **PAPER 8** reported on the first validation of a reconfigurable digital coherent receiver operating in a real-world test including 78 km of installed optical fiber, which was part of a Danish commercial optical fiber communications network. The novel concept of a reconfigurable digital photonic receiver integrating the benefits of coherent detection and digital signal processing was tested in a wavelength-division-multiplexing (WDM) scenario composed of four signals from different optical access technologies. The heterogeneous metro access network was composed of the following subsystems:

1. 5 Gbps directly modulated vertical cavity surface emitting laser (VC-

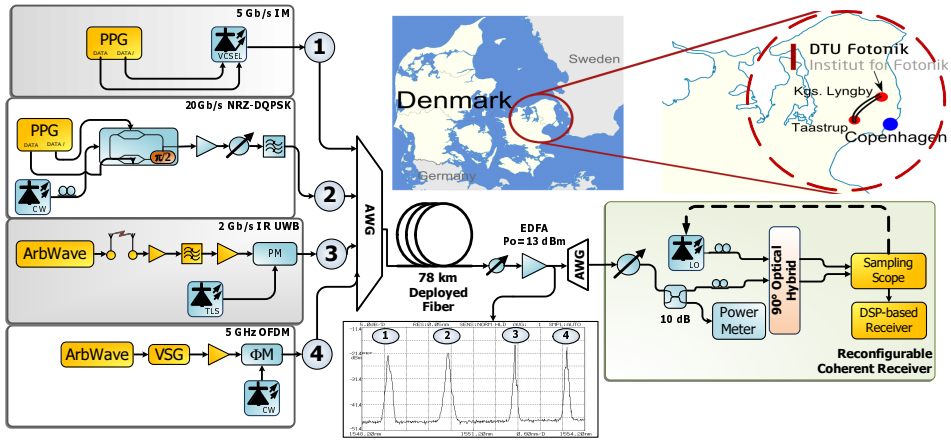

Figure 1.5: Experiment layout of the heterogeneous optical network reported in PAPER 8, showing optical and electrical RF spectra at key points; route of installed optical fiber are also shown. Reconfigurable receiver construction allows local oscillator (LO) tuning for channel selection. PPG: pulse pattern generator; ArbWave: arbitrary waveform; VSG: vector signal generator.

SEL).

2. Baseband 20 Gbps non-return-to-zero quadrature phase-shift keying (NRZ-QPSK).

3. Optically phase-modulated 2 Gbps impulse radio ultrawideband (IR-UWB).

4. optically phase-modulated 5 GHz OFDM radio-over-fiber.

PAPER 8 is currently nominated as a finalist in the 2011 Corning Outstanding Student Paper Competition in the Optical Fiber Communication Conference and Exposition and the National Fiber Optic Engineers Conference (OFC/NFOEC 2011). The novel concept on reconfigurable digital coherent receivers has the potential to enable signal detection and demodulation on the expected highly heterogeneous next generation metro-access networks. Fig. 1.5 shows a block diagram of the heterogeneous optical network and setup used in the experiment.

Nevertheless, the capabilities of the use of DSP in RoF systems can be extended to perform time-varying operations such as adaptive signal parameters estimation supported by pattern recognition techniques [50].

1.5 DSP-based signal parameters estimation

This PhD thesis contributes to the topic of adaptive signal parameters estimation in PM RoF systems by applying a clustering technique called the k-means algorithm [51]. The novel reconfigurable digital coherent receiver integrates functional operations for carrier phase recovery, carrier frequency compensation and automatic modulation format detection based on a single clustering approach on the constellation diagram. The proposed signal parameters estimation approach adds design versatility of digital receivers as well as flexibility and robustness to phase-modulated radio-over-fiber systems for signal demodulation in scenarios with mixed formats and mixed bit-rates.

Since phase-modulated radio-over-fiber systems have the information encoded into the phase of the RF carrier which then modulates the phase of the optical carrier, DSP-based signal parameters estimation in phase-modulated radio-over-fiber systems are divided into two stages: optical and RF signal parameters estimation.

Signal parameters estimation includes carrier frequency and phase offset estimation and compensation. Optical carrier frequency and phase offset are mainly caused by the phase noise which is the major impairment in coherent optical communications [38, 40]. To compensate the optical frequency/phase mismatch between the local oscillator (LO) and the optical carrier, a digital phase-locked-loop (DPLL) is implemented [28] at he first stage of the signal parameters estimation process.

In the RF domain, carrier phase and frequency offset are caused by two facts: residual uncompensated optical frequency offset by the DPLL at the first stage of the signal parameters estimation process and the phase mismatch between the extracted RF data signal from the phase of the optical carrier by the linear demodulator and the digital local carrier used for RF frequency down-conversion at the receiver.

Fig. 1.6 illustrates the effect of frequency and phase offset on a schematic QPSK constellation diagram. Frequency offset is represented as time-varying rotations of the constellation diagram. In phase-modulated radio-over-fiber links, the frequency offset comes from the limitation of the DPLL to track values in the range of kHz due to the very high computational cost required by numerical methods to increase the resolution of the spectral analysis of the signal. Signal demodulation cannot be achieved in the presence of RF frequency offset since data-symbols are continuously rotating on the constellation diagram. Assuming perfect RF frequency offset

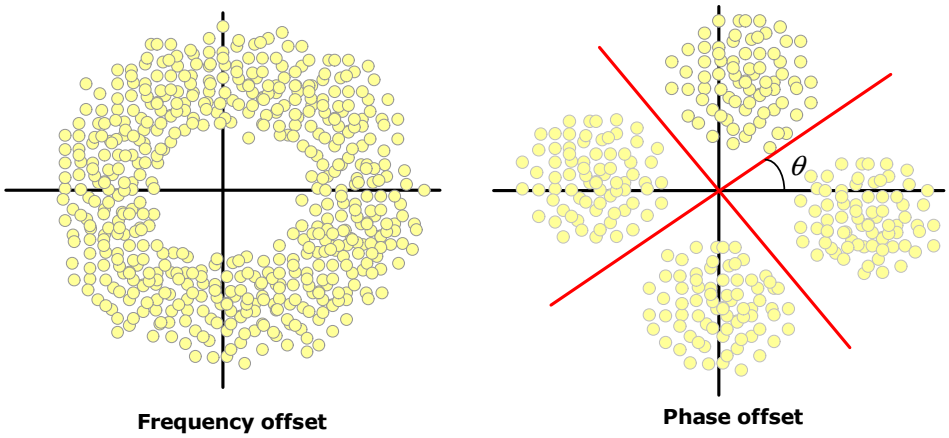

Figure 1.6: Schematic diagram of an impaired QPSK constellation.

compensation; RF phase offset is represented as constant rotations of the constellation diagram.

Since the angular frequency difference between the optical local oscillator and the optical carrier signal varies slowly in a real transmission system, frequency offset can be estimated readily by existing methods [43, 52]. The best possible estimate of the carrier phase that can be made given the recovered data symbols is achieved by the maximum a posteriori (MAP) estimate [38, 40]. Carrier phase estimation based on the MAP solution finds the set of signal parameters which maximize the conditional probability density function of the received data signal [38, 40]. However, this joint maximization problem does not yield a closed-form solution. Several phase estimation (PE) methods based on feedback and feedforward architectures have been recently proposed and demonstrated having the MAP phase estimation as a baseline for estimation performance evaluation [37–43].

On the other hand, automatic signal modulation format detection has started to be addressed by the research community on signal processing and the wireless communication community [53–56]. Automatic modulation format detection (AMFD) can be described as a statistical process to estimate the modulation format of an unknown signal based on a set of multiple hypothetical modulation formats with a certain probability of success in a short observation time. A variety of techniques have been proposed for AMFD in wireless systems such as higher-order moments, fuzzy logic, counting, and wavelengths techniques. The application of existing AMFD techniques to hybrid fiber wireless systems has not been reported to date.

The heterogeneous environment of future hybrid fiber wireless networks has brought a new set of challenges to be faced by the next generation of adaptive algorithms for signal parameter estimation and demodulation. Such challenges include: reconfigurable approaches for signal parameters estimation on time-varying transmission settings, and modular DSP algorithms for feasible implementation on digital parallel processors. The most recent advances on signal parameters estimation for optical communications systems are presented below.

1.6 State-of-the-art

In general, feedforward-based phase estimation (PE) methods are preferred due to the fact that digital processors in the coherent receivers are very likely to have a parallel structure. Because of the inherent loop delay in feedback-based PE methods such as the PLL solution, the performance of feedforward architectures is usually higher than PE methods based on feedback structures [57, 58].

Most feedforward PE methods estimate the carrier phase separately from the received data sequence in order to minimize computation resources. One way to achieve carrier-phase/data-symbol estimation separately is to remove the effect of data modulation by raising the signal to the M-th power, where M is equal to the order of the modulation format. This method is widely known as the Viterbi- and-Viterbi (V-V) algorithm or the power-law algorithm [39]. The V-V method simply averages over M-th powered symbols to estimate the carrier phase, under the assumption that the carrier phase would remain constant within the average duration. However, this basic assumption is not always satisfied in real transmissions, for instance, when there is frequency offset between the optical carrier and the local oscillator [59]. Moreover, aside from its complexity for higher order modulation formats, additional modifications on the V-V algorithm are required in order to be extended to quadrature amplitude modulated (QAM) signals [60–63]. In general, carrier PE based on the law-power method has the disadvantage that it suffers from cycle slips even when the phase noise is low [40].

Other carrier PE algorithms have been proposed by employing the Wiener filter [38, 64] and a modification of the Kalman filter [65] to complement the V-V algorithm. Even though the combined power-law/Wiener PE method provides good phase estimation, it may not be suitable for implementation in a digital parallel architecture due to feedback-loops present

in the filtering processing. In addition, knowledge of the statistics of the phase noise and the additive noise is required to design the filters. Such requirements may be impractical, especially in a reconfigurable optical system [66]. Decision-aided (DA) carrier PE has recently been proposed to avoid the need to know the statistics of the system noise [66]. However, the method requires additional synchronization stages since a known data training sequence is needed to start the carrier phase estimation process. The requirement of a training data symbol as well as feedback loops inside the architecture may also be impractical for real-time realizations.

In conclusion, although all reported carrier PE approaches show successful signal PE estimation in static environments (e.g. QPSK data transmission), investigations on carrier PE approaches in time-varying transmission settings such as mixed modulation formats and bit rates have not been reported to date. **PAPERS 2-7** report a flexible solution capable of extracting knowledge from the signal and tracking dynamic variations of transmission settings such as modulation format and bit rate. The proposed methodology for signal parameters estimation is based on clustering operations over data-symbols on the constellation diagram.

1.7 Beyond the state of the art

The best solution to the problem of data-signal phase estimation is achieved by the method of MAP estimation, maximizing a conditional joint probability density function (pdf) of the received data-signal y_k.

The received data-signal y_k can be represented as follows:

$$y_k = x_k e^{j\theta_k} + n_k \tag{1.1}$$

where x_k is a complex-valued symbol transmitted at the k-th symbol period, θ_k is the carrier phase and n_k is the additive white Gaussian noise (AWGN) which includes local oscillator (LO) spontaneous beat noise as well as shot and thermal noises produced by the receiver. The AWGN is assumed with zero mean and variance $N_0/2$ per dimension.

To estimate the carrier phase θ_k, the conditional joint pdf of the received data-signal y_k to be maximized is given by:

$$p(y_k|x_k,\theta_k) = \frac{1}{\pi N_0} \exp\left(-\frac{\left|y_k - x_k e^{j\theta_k}\right|^2}{N_0}\right) \tag{1.2}$$

Since x_k and θ_k are independent, the MAP estimates of the transmitted symbol and the carrier phase are:

$$(\hat{x}_k, \hat{\theta}_k) = \max_{x_k, \theta_k} p(y_k|x_k, \theta_k)p(x_k)p(\theta_k) \tag{1.3}$$

One method of evaluating 1.3 is to discretize phase to a set of values $[\theta]$ and then compute the cost function 1.3 for different pairs of $(x_m, [\theta_k])$; the pair that maximize 1.3 will be the MAP estimate.

This approach is computationally expensive specially for dense modulation formats like 16-QAM and unsuitable for high-bit-rate systems. Additionally, all reported phase estimation algorithms based on MAP or maximum likelihood approaches at the receiver side assume an a priori knowledge about the finite modulation alphabet used for signal modulation at the transmitter. Furthermore, the evaluation of 1.3 on each single data-symbol y_k to estimate the phase parameter θ_k make difficult the tracking of time-varying transmission settings such as signal modulation format on heterogeneous environments or dynamic effects on the constellation diagram such as continuous rotations of data-symbols y_k because of residual frequency offset between the LO and the optical carrier at the coherent receiver.

Instead of data signal parameters estimation based on MAP or maximum likehood estimation, we show that by characterizing the received data-signal y_k represented on its two-dimensional constellation diagram, the problem of data-signal parameters estimation on time-varying transmission settings and dynamic system impairments become a two-dimensional clustering problem. This clustering-based data signal parameters estimation leads to a simplification of the estimation process itself and allows to take into account at the same time parameters estimation which usually would have to be considered separately such as phase, frequency and signal modulation format estimation.

The main principle is to deal directly with the estimation of two parameters after the clustering process on the constellation diagram: the number of estimated symbols and the coordinates of those estimated. Data signal phase and frequency offset estimation as well as signal modulation format detection are then easily derived from the number of estimated clusters and the coordinates of such estimated clusters on the constellation diagram. **PAPERS 2-7** report how to perform phase and frequency estimation as well as signal modulation format detection after a clustering process on the constellation diagram. Fig. 1.7 shows an schematic description of the

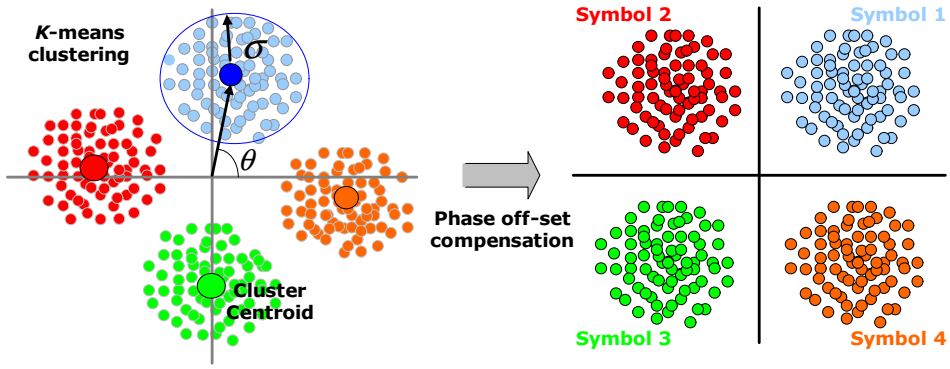

Figure 1.7: Carrier phase recovery based on the k-means algorithm.

proposed clustering-based signal parameters estimation on a QPSK constellation diagram.

1.7.1 The k-means clustering algorithm

An iterative clustering algorithm called the k-means [51] can be applied to the two-dimensional data-symbols mapped into the constellation diagram for signal parameters estimation purposes [67]. Signal parameters estimation approaches based on the k-means algorithm can be classified as a special type of feedforward data-aided (DA) method since data-symbols carrying information are always present in the estimation process. However, training sequences are not required since the clustering algorithm is applied directly on the constellation diagram.

Advantages introduced by the carrier recovery approach based on the k-means algorithm over classical carrier parameters estimation methods are:

- **Easy software reconfiguration:** the principle of operation for carrier recovery can be extended to different modulation formats.
- **Feasible real time implementation:** the feedforward structure of the carrier recovery based on the k-means algorithm allows implementation in parallel digital modules. Additionally, no complex M-power operations are required.
- **Multi-operational signal demodulation:** since the k-means algorithm is a DA method, statistical values over data-symbols such

as variances, means and relations among them allow additional operations to carrier recovery. Frequency-offset compensation and automatic modulation format detection can be performed in addition to phase-offset estimation and compensation.

Applications of the k-means algorithm for carrier phase and frequency offset compensation are reported in **PAPERS 2-6**. **Paper 7** reports the integration of an automatic modulation format detection (AMFD) module to the reconfigurable carrier phase recovery approach proposed in **PAPERS 2, 3, 4 and 5**. The automatic modulation format detection operation is based on metrics of symmetry in the constellation diagram as well as metrics derived from the histogram of the signal.

1.7.2 Automatic modulation format detection

Fig. 1.8 shows a schematic diagram of the automatic modulation format detection (AMFD) function based on our proposed reconfigurable signal phase estimation approach. A total amount of N data-symbols $\chi = \{\bar{x}_1, \bar{x}_2, ..., \bar{x}_N\}$ enter the AMFD module. AMFD is based on the statistical analysis of the signal and will provide the updating information to the carrier recovery module for subsequent demodulation. A first step is the estimation of the number of clusters (or expected m-PSK/QAM complex symbols) on the 2D constellation diagram as well as the number of levels on the histogram (hypothesis stage). The operation of finding the number of clusters is achieved by the k-means clustering algorithm on the constellation diagram. After features extraction from the histogram and the clustering process, a testing stage based on rules follows.

Rules for AMFD are derived according to modulation type characteristics and stored on a knowledge database. The two criteria to be judge for AMFD are the number of levels on the magnitude histogram of vectors formed by the complex data symbols, and the number of clusters on the constellation diagram. In the case of classification between QAM and PSK signals, AMFD is based on the number of levels detected on the histogram (first rule).

For AMFD among m-PSK modulation formats, a condition of symmetry must be satisfied after clustering operation on the constellation diagram. If the condition is not satisfied, the initial state of the k-means algorithm (the number of expected clusters to be found) is varied. This k-means reinitialization plays the role of the learning process in our digital receiver and it will go through all possible formats in the knowledge database until

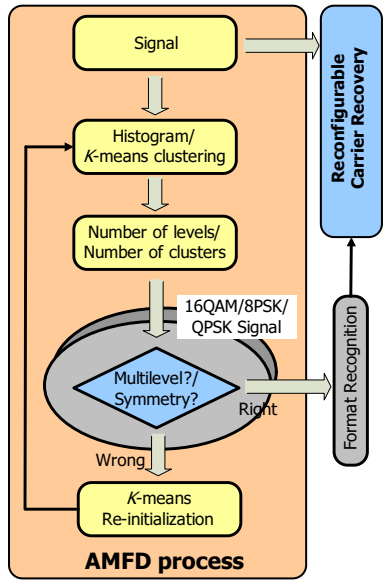

Figure 1.8: Schematic diagram of the automatic modulation format detection module.

successful detection is achieved. Successful automatic modulation format detection is achieved when the symmetry condition is satisfied for the number of clusters found on the constellation.

The symmetry condition: for complex constant modulus m-PSK symbols, a metric of symmetry (s) defined as the statistical variance of a vector composed of distances between expected m-PSK symbols and their closest expected neighbors on the constellation diagram (see Fig. 1.9) is proposed. AMFD among m-PSK signals is an iterative process of clustering followed by an evaluation of the symmetry condition over all possible formats in the knowledge database. Successful AMFD (true format detection) is achieved for the smallest s value after clustering.

The proposed automatic modulation format detection (AMFD) was experimentally demonstrated for optical phase-modulated radio-over-fiber links transporting burst mode mixed modulation formats (QPSK, 8PSK and 16QAM) in **Paper 7**.

AMFD was implemented as a sliding time-window. Fig. 1.10 shows the performance of the AMFD module as a function of the number of complex m-PSK data samples (DS) required to satisfy the symmetry condition for "true QPSK detection" for two different values of optical signal-to-noise ratio (OSNR). Both curves varies between values of symmetry of 1^{-3} and 4^{-3}

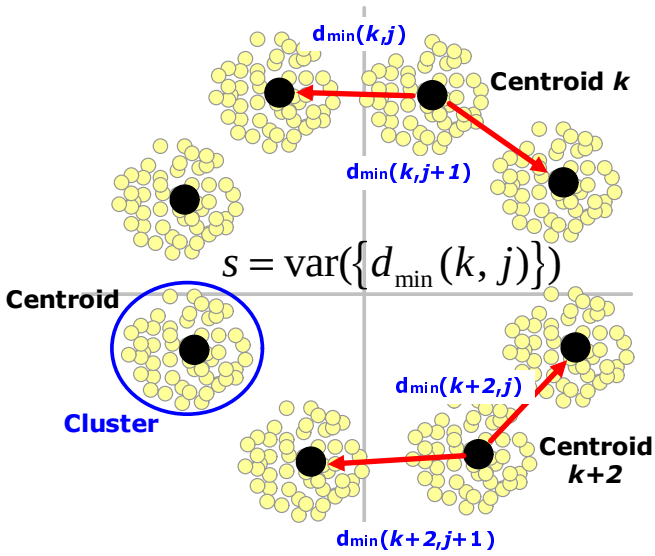

Figure 1.9: Schematic illustration of the proposed symmetry condition for m-PSK signal detection.

after 100 data samples and reaches a stable state after 200 data samples. We also observe in Fig. 1.10 that for the case of true detection, the highest value achieved is below 7^{-3}. Moreover, for the case of wrong QPSK detection (the expected modulation format by the MFD module was 8PSK), Fig. 1.10 (inset) shows that the value of symmetry is around 18^{-3}. The threshold is defined for values between 1^{-3} and 3^{-3}. In the experiment reported in PAPER 5, successful classification is achieved after 30 data samples for an OSNR of 24 dB. The proposed self-configurable burst-mode digital receiver shows prospect for next generation access networks due its adaptability, flexibility and fast format detection.

1.8 Main contributions and outline of the thesis

This thesis is based on a set of articles submitted for publication, articles already published in journals, and conference proceedings. This thesis presents results obtained during the course of my doctoral studies into the design and experimental validation of digital photonic receivers for wireless and wireline optical fibre transmission links. The implemented reconfigurable digital receiver enables reception of different formats and mixed bit rates using the same software-platform.

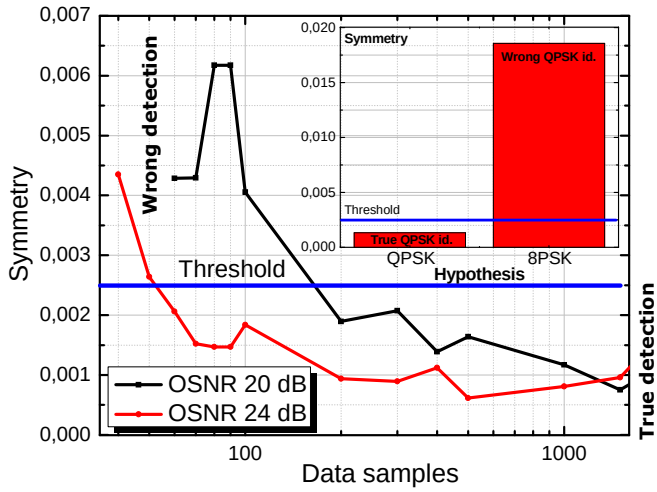

Figure 1.10: Modulation format detection performance as a function of the number of date samples for two different values of OSNR. Inset: thresholding operation for *true* and *wrong* QPSK detection.

PAPER 1 presents the first known integration of a digital receiver into optically envelope detected RoF systems. I have expanded on the state of the art in signal demodulation of optical envelope detected systems by designing and integrating a reconfigurable digital receiver into this type of system. The digital receiver consists of a reconfigurable scheme for two different types of optical envelope detected wireless signals, while keeping the complexity of used optical components low. Experimental validations on both 416.6 Mbit/s HC-BPSK and 104.17 Mbit/s MSK radio-frequency modulated signals after 30 km of fiber transmission demonstrate successful performance of the proposed reconfigurable digital receiver.

In **PAPERS 2 and 3**, I report a novel carrier phase recovery approach based on the k-means clustering algorithm for quadrature phase-shift-keying (QPSK) signals. We expand on the state of the art on the design of digital coherent receivers phase-modulated RoF signals by designing a simple and flexible signal phase estimation technique based on the k-means algorithm. The proposed clustering-based phase estimation approach can be additionally extended to other signal demodulation functions such as signal frequency offset compensation and automatic modulation format detection over the same software-platform. The principle is

experimentally validated on a wavelength division multiplexed (WDM) 2.5 Gbit/s QPSK phase-modulated RoF system, resulting in the highest bit rate reported before 2009 for that kind of systems.

PAPERS 4 and 5 present the extension of the proposed carrier phase recovery approach in **PAPERS 2 and 3** to 8PSK and quadrature-amplitude-modulated (QAM) signals. The reconfigurable scheme is introduced based on metrics derived from the constellation diagram and is robust to signal power level variations. Experimental validations on three, 50 Mbaud, 8PSK subcarrier multiplexed signals and a 312.5 Mbaud, 16QAM single carrier after 40 km single mode fiber transmission confirm the robustness and simplicity of the proposed approach.

In **PAPER 6**, I present a joint frequency/phase offset compensation approach based on the k-means algorithm. The proposed scheme is based on iterative phase-offset compensation on consecutive time-blocks of the data-signal. Experimental validations on 312.5 Mbaud 8PSK RoF signal after 40 km of optical transmission show successful compensation up to a value of 30 khz of frequency offset.

In **PAPER 7**, I report for the first time on phase-modulated RoF systems, a digital module for automatic modulation format detection (AMFD) integrated to the reconfigurable RF carrier phase recovery approach proposed in **PAPERS 2, 3, 4 and 5**. The automatic modulation format detection operation is based on metrics of symmetry in the constellation diagram as well as metrics derived from the histogram of the data-signal. Experimental validations of the reconfigurable digital receiver are carried out for bursts of mixed modulation formats at 312.5 Mbaud QPSK, 8PSK and 16QAM data payloads.

PAPER 8 reports an assessment of the performance of a reconfigurable digital coherent receiver operating in a real-world test including 78 km of installed optical fiber, which was part of a Danish commercial optical communications network. We have extended on the state of the art on hybrid fiber wireless systems by experimentally demonstrating unified support for signal detection on highly heterogeneous next generation metro-access networks. To test the novel concept of the single reconfigurable digital coherent receiver, four signals from different optical access technologies were WDM multiplexed onto the same fiber. The heterogeneous metro access network

was composed of the following subsystems: 1) 5 Gbps directly modulated vertical cavity surface emitting laser (VCSEL). 2) Baseband 20 Gbps non-return-to-zero quadrature phase-shift keying (NRZ-QPSK). 3) Optically phase-modulated 2 Gbps impulse radio ultrawideband (IR-UWB) and 4) optically phase-modulated 5 GHz OFDM radio-over-fiber. The experimentally demonstrated digital reconfigurable coherent receiver has the potential to enable unified support for signal detection on highly heterogeneous next generation metro- access networks.

In **PAPER 9** we demonstrate successful digital coherent demodulation of asynchronous optical PM adaptive order QAM (4, 16 and 64) OFDM signals by using a single reconfigurable digital receiver after 78 km of deployed optical fiber.

In **PAPER 10** we investigate on the impact of fiber dispersion on the performance of optical phase modulated impulse radio-ultra-wideband (IR-UWB) signals. 2Gbps BPSK IR-UWB over 78km fiber transmission is successfully achieved by using digital coherent detection.

This thesis is composed of two more chapters. Chapter 2 reports a novel optical performance monitoring technique based on a special type of poly-phase sequences called CAZAC sequences. A brief state of the art in OPM as well as numerical investigations on CD and PMD estimation are also presented in Chapter 2. Finally, concluding remarks are presented in chapter 3.

Chapter 2

Data-aided DSP algorithms for optical performance monitoring

Toward dynamically reconfigurable all-optical networks, optical performance monitoring (OPM) enables dynamic and future impairment-aware routing by providing information for signal quality estimation, fault localization and system diagnosis [47, 68–70]. Recent advances in coherent detection in combination with electronic signal processing have shown the feasibility of estimating and compensating most of the optical transmission impairments such as chromatic dispersion (CD), higher order polarization mode dispersion (PMD) and polarization dependent loss (PDL) among others in the digital domain [47, 48].

OPM exploits the fact of having the estimated inverse optical channel response related to the filter impulse response at the digital coherent receiver given an optimum adaptation process for the FIR equalizer. Hence, in principle, all linear channel distortions contributing to the total channel response can be compensated without any additional device to the equalizer.

A wide range of approaches are used for optical channel estimation. The non-data-aided (NDA) approach offers the possibility to increase the bandwidth efficiency since no preamble is used whereas the data-aided (DA) algorithm offers high parameter estimation accuracy at the cost of slight bandwidth efficiency degradation when dealing with slowly varying synchronization parameters. Recently, several OPM strategies based on NDA approaches have been reported in the literature [69]. In this chapter, we

present the results of numerical investigations of the use of a special type of sequences belonging to the class of poly-phase sequences called CAZAC (constant-amplitude zero-autocorrelation) for DA optical channel estimation. To overcome the limitations on the number of filter taps in time domain and the subsequent low resolution in the frequency domain for CD and PMD estimation, we estimate directly in the frequency domain the inverse channel transfer function by applying the zero-forcing (ZF) principle.

In summary, we have contributed to the state of the art in OPM by *designing a DA approach in the frequency domain for optical channel estimation, independent of memory lengths and update algorithms for FIR filter taps convergence.* Section 2.1 introduces the optical channel model and the zero-forcing equalizer. Section 2.2 presents the DA channel estimation based on the CAZAC sequence. Section 2.3 discusses results obtained along the investigation.

2.1 Channel model and the zero-forcing (ZF) equalizer

In general, the transmitter sends complex valued signals:

$$\bar{s}(f) = [s_X(f), s_Y(f)]^T \tag{2.1}$$

on both X and Y polarizations. The optical channel cross-couples information between both polarizations, which can be described by:

$$\bar{r}(f) = \bar{H}(f)\bar{s}(f)+\bar{n}(f) = \begin{pmatrix} H_{XX}(f) & H_{YX}(f) \\ H_{XY}(f) & H_{YY}(f) \end{pmatrix} \begin{pmatrix} s_X(f) \\ s_Y(f) \end{pmatrix} + \begin{pmatrix} n_X(f) \\ n_Y(f) \end{pmatrix} \tag{2.2}$$

The linear channel transfer matrix is composed of the transfer function $D(f)$ and $\bar{E}_i$ concatenated elements and $\bar{U}_i(f)$, accounting for PDL and higher order PMD, as in

$$\bar{H}(f) = D(f) \prod_{i=1}^{N} \bar{E}_i \bar{U}_i(f) \tag{2.3}$$

The PMD matrices:

$$\bar{U}_i(f) \;=\; \begin{pmatrix} u_i(f) & v_i(f) \\ -v_i^*(f) & u_i^*(f) \end{pmatrix} \tag{2.4}$$

$$= \begin{pmatrix} e^{j(\varphi_i+2\pi f\tau_i)/2} & 0 \\ 0 & e^{-j(\varphi_i+2\pi f\tau_i)/2} \end{pmatrix} \begin{pmatrix} \cos\alpha_i & \sin\alpha_i \\ -\sin\alpha_i & \cos\alpha_i \end{pmatrix}$$

induce a phase shift φ_i and a DGD τ_i between the two orthogonal fast and slow axes of the birefringent element. The angle between the slow and the polarization state of s_X is α_i. The instantaneous DGD $\langle\tau(f)\rangle$ defines the average over the DGD spectrum $\tau(f)$. Individual realizations $\tau(f,t)$ follow a Maxwellian distribution with mean value $\langle\tau(f,t)\rangle = \sqrt{8/(3\pi)}D_p\sqrt{N}$, given a PMD parameter D_p in $[ps/\sqrt{Km}]$. The Hermitian PDL elements:

$$\bar{E}_i = \begin{pmatrix} 1 & 0 \\ 0 & k_i \end{pmatrix} \tag{2.5}$$

attenuate one polarization relative to the other with attenuation factor $0 < k_i < 1$ and $PDL_i[dB] = -20lok(k_i)$. Analogous to PMD, the instantaneous PDL that depends on rotation angles α_i is Maxwellian distributed around a mean value $\langle PDL(t)[dB]\rangle = \sqrt{8/(3\pi)}D_{PDL}\sqrt{N}$ for PDL parameter $D_{PDL}[dB/\sqrt{Km}]$. The linear transfer function:

$$D(f) = H_{CD}(f)H_{AF}(f) \tag{2.6}$$

Contains the all-pass transfer function:

$$H_{CD}(f) = \exp(jf^2\psi) \tag{2.7}$$

With $\psi = -CD\lambda^2\pi/c$ responsible for residual CD and an amplitude filter (AF) function $H_{AF}(f)$ with a linear phase accounting for any bandpass filtering during transmission or LP filtering after demodulation in the receiver.

2.1.1 The zero-forcing (ZF) equalizer

Meeting channel requirements, the filtering is described by:

$$\bar{z}(f) = \bar{W}(f)\bar{r}(f) = \begin{pmatrix} W_{XX}(f) & W_{YX}(f) \\ W_{XY}(f) & W_{YY}(f) \end{pmatrix} \begin{pmatrix} r_X(f) \\ r_Y(f) \end{pmatrix} \tag{2.8}$$

With the filtering function $\bar{W}(f)$ and the filtered signal:

$$\bar{z}(f) = [z_X(f), z_Y(f)]^T \tag{2.9}$$

Provided that the channel memory does not exceed the equalizer memory length, the filter adapts to the ZF solution:

$$\bar{W}(f) = \bar{H}^{-1}(f) \tag{2.10}$$

Which is an optimum solution regarding parameter extraction for optical performance monitoring (OPM). However, inverting the AF component that typically follows a low-pass characteristic $H_{AF}^{-1}(f)$ strongly enhances noise in the regions of the stop band of $H_{AF}(f)$. With the ZF assumption equation evolves into:

$$\bar{W}(f) = \bar{H}^{-1}(f) = D^{-1}(f) \prod_{i=N,-1}^{1} \bar{U}_i^{-1}(f)\bar{E}_i^{-1} \tag{2.11}$$

By inverting equation with the aid of individual properties described in equations **??**−, we can now separate the components for extracting the desired parameters. Although the inverse of each element $D(f)$, $\bar{E}_i$ and $\bar{U}_i(f)$ can be calculated easily; a general description with a large number of PDL and PMD elements cannot be obtained. However, due to the unitary nature of the PMD matrices $\bar{U}_i(f)$, the square root of the determinant of $\bar{W}(f)$ becomes:

$$\begin{aligned} \sqrt{\det(\bar{W}(f))} &= \left(D^{-2}(f) \prod_{i=N,-1}^{1} \det(\bar{U}_i^{-1}(f)) \det(\bar{E}_i^{-1}) \right)^{1/2} \\ &= D^{-1}(f) \prod_{i=1}^{N} (k_i)^{1/2} \end{aligned} \tag{2.12}$$

which eliminates the PMD contributions. Given than the amplitude filter $H_{AF}^{-1}(f)$ has a linear phase in the transmission band, the phase:

$$\arg(\hat{H}_{CD}^{-1}) = \arg(\sqrt{\det(\bar{W}(f))}) = -f^2\psi \tag{2.13}$$

only depends on the quadratic transfer function imposed by CD. In contrast, the amplitude transfer function:

$$\hat{H}_{PDL}(f) = \left| \sqrt{\det(\bar{W}(f))} \right| = |H_{AF}(f)|^{-1} \prod_{i=1}^{N} (k_i)^{-1/2} \tag{2.14}$$

clearly becomes a function of the PDL attenuation. Normalizing $\bar{W}(f)$ by the square root of its determinant, we obtain:

$$\begin{aligned} \bar{W}_{UE}(f) &= \frac{\bar{W}(f)}{\sqrt{\det(\bar{W}(f))}} \\ &= \prod_{i=N,-1}^{1} \begin{pmatrix} u_i^*(f) & -v_i(f) \\ v_i^*(f) & u_i(f) \end{pmatrix} \begin{pmatrix} k_i^{1/2} & 0 \\ 0 & k_i^{-1/2} \end{pmatrix} \\ &= \begin{pmatrix} u_I(f) & v_I(f) \\ v_{II}(f) & u_{II}(f) \end{pmatrix} \end{aligned} \tag{2.15}$$

A reliable DGD estimation can be achieved after two steps. In a first step, the derivative of the matrix elements $u_I(f)$, $u_I I(f)$, $v_I(f)$ and $v_I I(f)$ of $\bar{W}_{UE}(f)$ with respect to the angular frequency indexed by ω are estimated. Then, equation 2.16 is applied to cancel PDL contributions for further DGD mean value estimation:

$$\tau_{estimated}(f) = 2\sqrt{u_{I,\omega}(f)u_{II,\omega}(f) - v_{II,\omega}(f)v_{II,\omega}(f)} \tag{2.16}$$

The estimation of the mean value over the DGD spectrum $\langle \tau_{estimated}(f) \rangle$ is limited to a certain bandwidth.

2.2 Data-aided channel estimation based on CAZAC sequence

Prior to parameter estimation the channel transfer function 2.1.1 has to be obtained. In general, the training sequence for the $2x2$ multi-input multi-output (MIMO) system can be composed of four independent blocks $C_{Tx,X}, C_{Tx,Y}, NS_{Tx,X}, NS_{Tx,Y}$. The training sequence is repeated regularly, as shown in Fig. 2.2. We choose CAZAC sequences, which provide optimum framing synchronization.

The CAZAC is a complex-valued phase-noise (PN) sequence with a constant amplitude and periodic zero-autocorrelation [71]. The discrete CAZAC is defined as follows:

$$c[n] = \begin{cases} \exp(jK_c\pi n^2/L_c), & L_c : even \\ \exp(jK_c\pi(n-1)^2/L_c), & L_c : odd \end{cases} \tag{2.17}$$

where L_c denotes the number of samples per CAZAC and K_c is a constant integer. The discrete CAZAC sequence has constant amplitude and

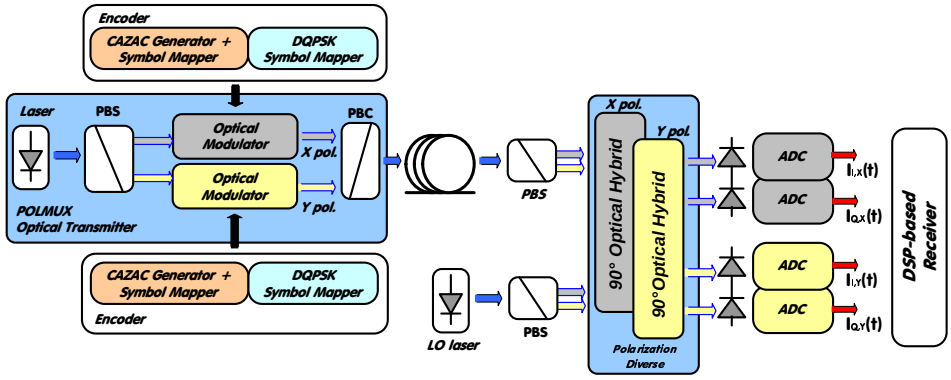

Figure 2.1: System model of PDM-DQPSK optical transmission with coherent detection. PBS=polarization beam splitter; PBC=polarization beam combiner; LO=local oscillator; ADC=analog to digital converter.

the sample values are on the unit circle. The CAZAC sequence is additionally zero-mean. To demonstrated CD and DGD estimation, we simulate a 112 Gb/s polarization multiplexed (POLMUX) differential quadrature phase-shift keying (DQPSK) transmission over a wide range of random channel parameters. Fig. 2.1 shows the system model of the POLMUX-DQPSK transmission used to demonstrate CD and DGD parameter estimation based on CAZAC sequences and the zero-forcing criteria. At the receiver, after the polarization-diverse 90^o hybrid, an analog-to-digital converter (ADC) stage digitizes the received signal at 2 samples per symbol.

In order to separate the signal components transmitted by the two principal states of polarization (PSP), an accurate knowledge of the multiple-input multiple-output (MIMO) channel is necessary. The MIMO signal processing could be performed as soon as the MIMO channel impulse response is known. To achieve that, the training sequences at the different transmit polarization should be time orthogonal by transmitting only one CAZAC sequence at one polarization state whereas no signal is transmitted by the other polarization state (see Fig. 2.2). Since this scheme is not efficient in terms of bandwidth efficiency because of the introduction of a guard interval every time before the CAZAC sequence is transmitted; we propose as a future work to investigate a second concept based on the perfect autocorrelation characteristics of the CAZAC sequence. For now, we demonstrate in this work a successful chromatic dispersion (CD) and differential group delay (DGD) estimation by using zero-forcing (ZF) channel estimation having CAZAC sequences as a training sequence.

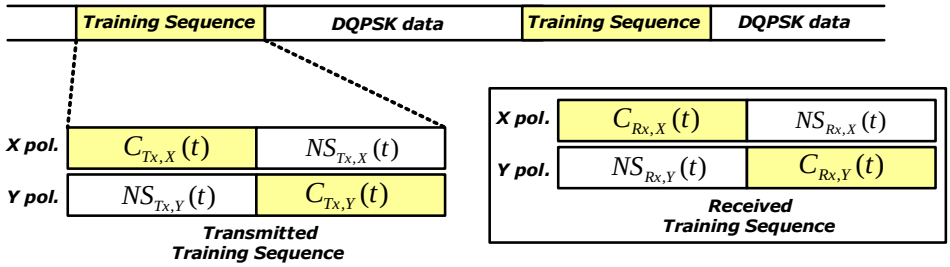

Figure 2.2: Schematic diagram of the transmitted and received training sequences for both polarizations to estimate the MIMO optical channel.

In order to estimate the optical channel, a training sequence of length $2n$ is divided into two sub-sequences and sent it respectively over the two polarizations X and Y. One of the transmitted sub-sequences is a CAZAC sequence of length n ($C_{Tx,X}(t)$ for polarization X) which is allocated in orthogonal time-slots from polarization to polarization (see the red-block in Fig. 2.2). The other transmitted sub-sequence is a non-signal (NS) sequence of length n ($NS_{Tx,X}(t)$ for polarization X). The four MIMO components of the inverse channel transfer function $\bar{W}_{ZF}(f)$ can be estimated applying the zero-forcing criteria to calculate the relations shown in equation 2.18.

$$\bar{W}_{ZF}(f) = \begin{pmatrix} W_{xx}(f) & W_{yx}(f) \\ W_{xy}(f) & W_{yy}(f) \end{pmatrix} = \begin{pmatrix} \frac{C_{Rx,X}(f)}{C_{Tx,X}(f)} & \frac{NS_{Rx,X}(f)}{C_{Tx,Y}(f)} \\ \frac{NS_{Rx,Y}(f)}{C_{Tx,X}(f)} & \frac{C_{Rx,Y}(f)}{C_{Tx,Y}(f)} \end{pmatrix} \tag{2.18}$$

The received CAZAC and NS sub-sequences can be described as:

$$\begin{aligned} C_{Rx,X}(t) &= C_{Tx,X}(t) + \eta(t) \\ NS_{Rx,X}(t) &= NS_{Tx,X}(t) + \eta(t) \end{aligned} \tag{2.19}$$

where the term $\eta(t)$ represents the additive noise involved in the whole transmission system.

2.2.1 Chromatic dispersion estimation

To estimate ψ and the residual CD from equation 2.19, it is firstly defined the function $Z(f)$ as:

$$Z(f) = \sqrt{\det(\bar{W}_{ZF}(f))} \tag{2.20}$$

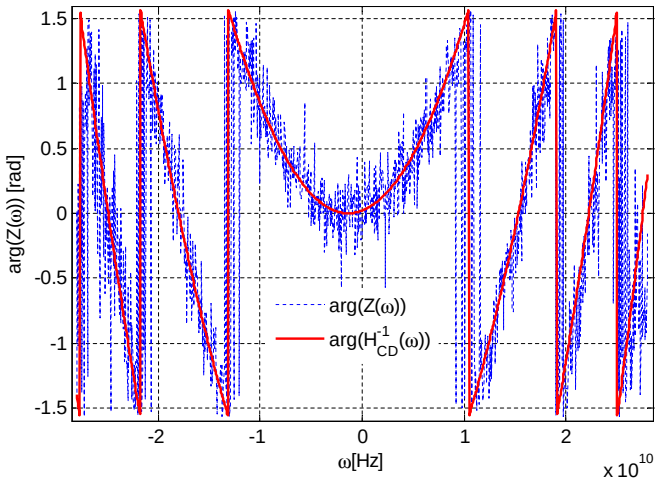

Figure 2.3: Phase transfer function of $Z(f)$ after MIMO channel estimation based on the CAZAC sequence and the estimated CD dispersion function by the quadratic function.

The phase transfer function $\hat{H}_{CD}^{-1}$ can be estimated with a quadratic fit after unwrapping the $pi-$ ambiguity from the phase transfer function of $Z(f)$. Fig. 2.3 shows the noisy parabolic function calculated from the phase transfer function of $Z(f)$ and the subsequent estimated phase transfer function $\hat{H}_{CD}^{-1}$ after the quadratic fit. In this case, we have transmitted a CAZAC sequence of length equal to 512 taps with 2 samples per symbol (1024 taps of resolution in frequency domain).

2.2.2 Polarization effects estimation (DGD and PMD

Within the polarization effects, this work is focused on the mean value of DGD. Since such effect varies over time, the instantaneous value is of high interest to monitor the transients. Depending on the signal bandwidth and the mean DGD in the link, several orders of PMD can be present. The DGD is the magnitude of the first-order derivative of the PMD vector and fully describes all statistical properties of the all-order PMD [68], [47]. A reliable DGD estimation can be achieved by averaging the DGD spectrum over a certain bandwidth as it is shown in Fig. 2.4. equations and describe mathematical operations required to cancel CD and PDL contributions for DGD estimation.

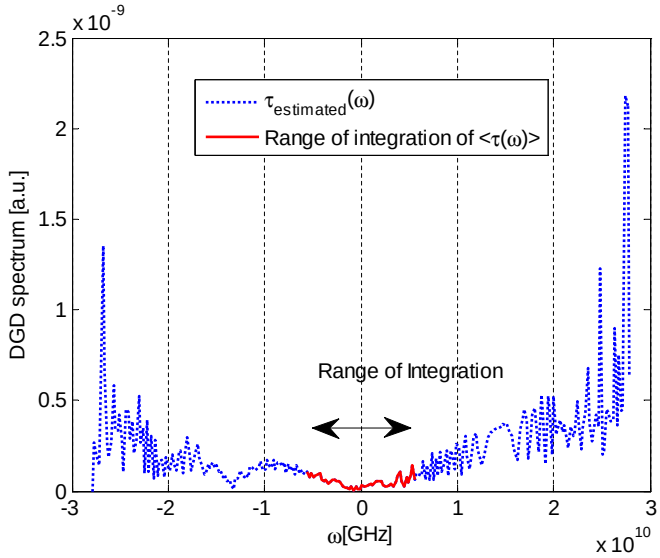

Figure 2.4: Illustration of the range of integration over a DGD spectrum for estimation of $\langle \tau(f) \rangle$.

$$\begin{aligned} \bar{W}_{UE}(f) &= \frac{\bar{W}_{ZF}(f)}{Z(f)} \\ &= \prod_{i=N,-1}^{1} \begin{pmatrix} u_i^*(f) & -v_i(f) \\ v_i^*(f) & u_i(f) \end{pmatrix} \begin{pmatrix} k_i^{1/2} & 0 \\ 0 & k_i^{-1/2} \end{pmatrix} \\ &= \begin{pmatrix} u_I(f) & v_I(f) \\ v_{II}(f) & u_{II}(f) \end{pmatrix} \end{aligned} \tag{2.21}$$

$$\tau_{estimated}(f) = 2\sqrt{u_{I,\omega}(f)u_{II,\omega}(f) - v_{II,\omega}(f)v_{II,\omega}(f)} \tag{2.22}$$

Fig. 2.4 shows a DGD spectrum for an inverse channel transfer function. A CAZAC sequence of length 128 was used for giving a total resolution of 256 taps for the DGD spectrum (since 2 samples per symbol were implemented for simulating purposes). A mean value of simulated DGD equal to 22 ps was calculated for a value of optical signal to noise ratio (OSNR) equal to 50 dB.

2.3 Results and discussion

2.3.1 Estimation of CD

The CD was estimated for the combination of a randomly given CD ranging from 0 to 1200 ps/nm in combination with a given mean PDL of 6 dB and a mean PMD of 25 ps. Fig. 2.5(a) shows the histogram of CD estimation error after 1000 realizations for three different values of OSNR (10 dB, 15 dB and 20 dB of OSNR values), for a given CD range between [0 : +1200] ps/nm in combination with a given mean PDL of 6 dB and a mean of all-order order PMD of 25 ps. The CAZAC sequence used for simulations was of length 128 (which means a resolution of 256 taps in the frequency domain because of the fact of 2 samples per symbol used for simulations). On the other hand, Fig. 2.5(b) shows the histogram of CD estimation error for three different scenarios with CAZAC sequences of lengths equal to 128, 256 and 512 taps for a specific OSNR value of 10 dB. In order to evaluate the performance of the estimator, the statics of the CD estimation have been evaluated with respect to the deviation of the mean value:

$$m_{CD} = \frac{1}{N}\sum_{i=1}^{N} CD_{given,i} - CD_{estim,i} \tag{2.23}$$

which indicates an offset of the estimation. Furthermore, it has been defined the deviation σ_{CD} as:

$$\sigma_{CD} = \sqrt{\frac{1}{N}\sum_{i=1}^{N} (CD_{given,i} - CD_{estim,i})^2} \tag{2.24}$$

Table 2.1 summarizes the mean and deviation values of the estimated CD parameter applying the quadratic fit over the phase transfer function of $Z(f)$. It can be clearly seen that the worst-case CD estimation error spreads to ± 50 ps/nm for an OSNR value of 10 dB. For a given OSNR value of 10 dB, it can be also observed a better accuracy of the CD estimation process for higher resolution of the phase transfer function of $Z(f)$. Fig. 2.5(b) shows how the offset in the estimation as well as the deviation value with respect to the estimated mean value are improved when a CAZAC sequence of length equal to 512 (1024 taps because of the fact of 2 samples per symbol used for simulation purposes) is used. This behavior is because higher resolution facilitates more accurate quadratic fit approximation of the CD function. In Fig. 2.5(a) it can be also observed an improvement of

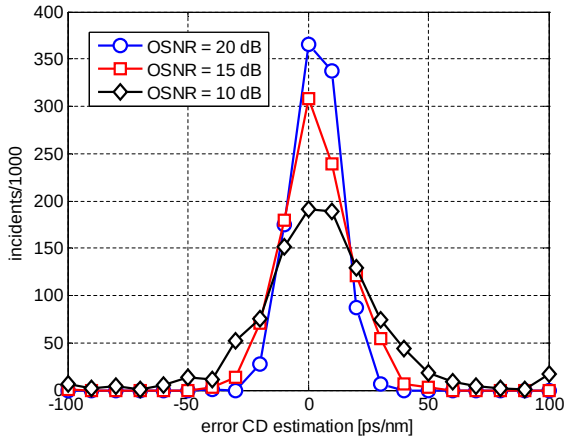

(a) OSNR values of 10 dB, 15 dB and 20 dB

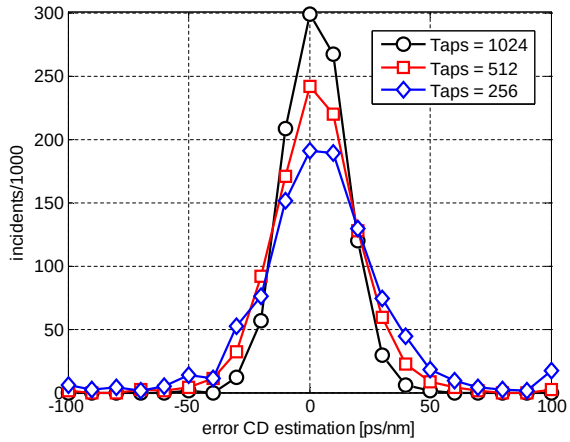

(b) CAZAC sequences with length of 128, 256 and 512 taps

Figure 2.5: Performance evaluation of the CD estimator after 1000 realizations

the CD estimation process for higher values of OSNR when the length of the CAZAC sequence is fixed to 128 taps.

2.3.2 Estimation of PMD

Since the given DGD $\langle \tau(f) \rangle$ varies for each individual case, we have calculated the deviation of the mean value as follows:

OSNR (dB)	**Number of taps**	m_{CD}	σ_{CD}
10	256	7.5172	50.1325
10	512	4.0048	34.3923
10	1024	2.5240	12.5384
10	256	7.5172	50.1325
15	256	2.7493	20.3875
20	256	2.9101	9.4226

Table 2.1: Summary of mean and deviation values of the CD estimation process for six different simulated scenarios. The first three rows report the estimation statistics when an OSNR value is fixed and the length of the CAZAC sequence vary. The last three rows report the estimation statistics when the length of the CAZAC sequence is fixed while the OSNR values vary

$$m_{DGD} = \frac{1}{N}\sum_{i=1}^{N} DGD_{given,i} - DGD_{estim,i} \tag{2.25}$$

and the biased error σ_{DGD} as:

$$\sigma_{DGD} = \sqrt{\frac{1}{N}\sum_{i=1}^{N} (DGD_{given,i} - DGD_{estim,i})^2} \tag{2.26}$$

The DGD mean value has been estimated for the combination of a given DGD value ranging from 10 to 35 ps following a Maxwellian distribution with mean value of 25 ps, in combination with a constant given CD of 1000 ps/nm and an OSNR value of 50 dB. After 1000 realizations, Fig. 2.6(a) shows the histogram of DGD estimation error for three different simulated scenarios with CAZAC sequences of length 128, 256 and 512 taps respectively. In this case, the averaging range to estimate $\langle \tau(f) \rangle$ has been fixed to the 5 per cent of central taps over the DGD spectrum. It can be observed how the offset in the estimation increase according to higher resolution analysis on the spectrum (which it is proportional to the number of taps used in the CAZAC sequence).

Fig. 2.6 shows how the mean value of the DGD estimation process is highly sensitive to the range of integration over the DGD spectrum. However, it is interesting to see the fact of no variation in the deviation of the estimation process. Fig. 2.6(b) shows the effect on the DGD estimation when the range of integration varies around the central tap over the DGD spectrum. The number of taps in the CAZAC sequence has been fixed to

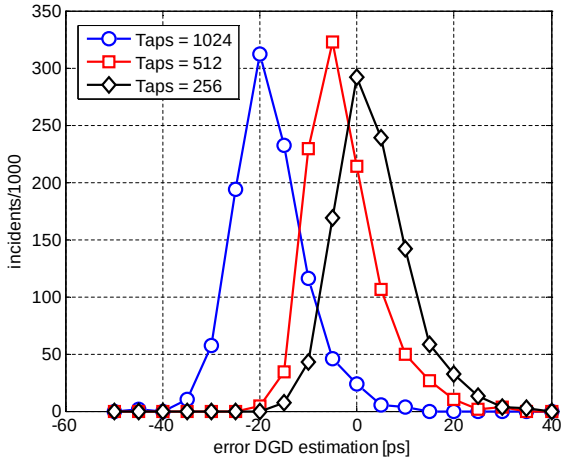

(a) CAZAC sequences with length 128, 256 and 512 taps.

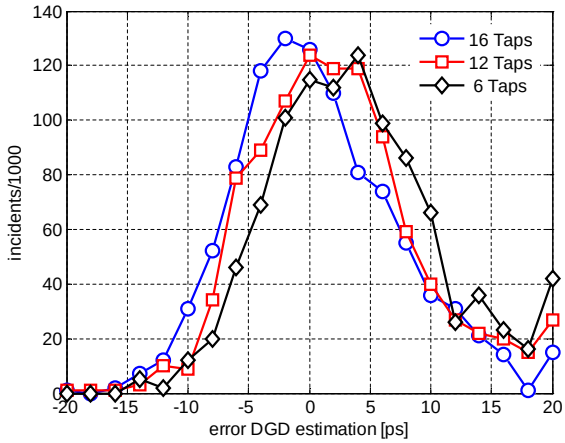

(b) Different range of integration with a fixed CAZAC sequence length of 128 taps.

Figure 2.6: Performance evaluation of the DGD estimator. The OSNR and CD values were fixed to 50 dB and 1000 ps/nm respectively.

128. It can be observed again the shift of the estimated DGD mean value while the deviation keeps almost constant. Table 2.2 summarizes the mean and deviation values of the DGD estimation process illustrated in Fig. 2.4.

Resolution (tabs)	**Range of averaging (taps)**	m_{DGD}	σ_{DGD}
256	16	4.0558	7.5744
256	12	2.3545	7.1209
256	8	0.7863	6.8502
1024	14	-17.9779	7.0947
512	14	-2.6859	7.1412
256	14	3.2632	7.5401

Table 2.2: Summary of mean and deviation values of the DGD estimation process for six different simulated scenarios. The first three rows report the estimation statistics when the length of the CAZAC sequence is fixed and the range of integration around the central tap on the DGD spectrum vary. The last three rows report the estimation statistics when the length of the range of integration is fixed and the length of the CAZAC sequence vary.

2.4 Conclusions

Constant Amplitude Zero Autocorrelation (CAZAC) sequences have been demonstrated as a promising training sequence candidate for data-aided optical channel estimation in 112 Gbit/s polarization-diversity coherent systems. Extensive numerical investigations show accurate chromatic dispersion estimation for different OSNR conditions including the case for 10 dB. In addition to different noisy scenarios, the robustness of the estimation has been demonstrated over a wide range of combined distortions including random PMD contributions ranging from 10 to 35 ps and 6 dB of PDL. Despite of non-data-aided approaches, estimation processes using CAZAC sequences and the zero-forcing criteria are independent of memory lengths and update algorithms for FIR filter taps convergence. Additionally, an estimation approach of instantaneous differential group delay parameter has been demonstrated for high values of OSNR. Therefore, data-aided channel estimation based on the principle of zero-forcing and using CAZAC sequences as training sequences, opens the door to accurate and low complexity approaches toward real time implementation of optical performance monitoring algorithms.

Chapter 3

Conclusions and future work

3.1 Conclusions

This PhD thesis addresses the design and performance evaluation of digital photonic receivers in hybrid optical fiber-wireless- transmission systems. The research results presented in this thesis are pioneering in two areas: first experimental demonstrations of automatic demodulation of signals with mixed modulation formats and bit rates in a single digital coherent photonic receiver including baseband and optical phase-modulated (PM) radio-over-fiber (RoF) systems and the first known analytical and numerical investigations on the performance of data-aided optical channel estimation based on constant-amplitude zero-autocorrelation (CAZAC) sequences for 112 Gb/s polarization-diversity coherent optical fiber transmission links.

3.1.1 DSP-based photonic receivers on heterogeneous fiber wireless scenarios

PAPERS 1, 8 and 11, respectively report on the experimental performance evaluation of digital photonic receivers, as well as communications systems demonstrating envelope-detected radio-over-fiber systems, heterogeneous metro-access networks and photonic impulse-radio (IR) ultra wideband (UWB) signal generation and transmission.

Based on recent advances of DSP-based receivers in the area of 40-G and 100-G optical coherent systems, it is seen that the wide applicability of DSP technology across several fields of technology will continue to reduce the cost of integrating such technologies into systems requiring modest levels of data processing. It has already become apparent that DSP technology has been

successfully integrated into diverse communications systems, including data modems for ADSL applications, wireless radio transceivers, and electronic dispersion compensation modules for long-distance signalling. It is therefore not a great leap in imagination to anticipate the introduction of such systems into low-cost reconfigurable optical transceivers for metropolitan and access network systems.

The advantages of integrating flexible and reconfigurable digital photonic receivers into optical envelope detection lies on the adaptability of DSP modules to emerging standards and modulation formats. Furthermore, signal demodulation employing reconfigurable digital photonic receivers in optically intensity-modulated systems using carrierless amplitude phase (CAP) modulation techniques may enable the implementation of multi-dimensional modulation formats. Recent experiments in our group using DSP-based receivers, report successful transmission of higher modulation formats employing two-dimensional carrierless amplitude phase modulation (CAP) with 16 and 64 levels.

In **PAPER 1**, the first integration of a digital receiver into optically envelope detected radio-over-fiber systems is demonstrated. The proposed digital photonic receiver is experimentally validated on 416.6 Mbit/s half-cycle binary phase shift keying (HC-BPSK) and 104.17 Mbit/s MSK radio-frequency modulated signals after 30 km of optical fiber transmission. Additionally, the maximum relation bit-rate/carrier-frequency for BPSK signals is achieved with the proposed HC-BPSK modulation. The digital photonic receiver implemented uses common digital functions for both types of signals, reducing the complexity of the receiver and enabling easy reconfiguration on a single software-platform.

PAPER 8 reported on the first validation of a reconfigurable digital coherent receiver operating in a real-world test including 78 km of installed optical fiber, which was part of a Danish commercial optical communications network. The novel concept of a reconfigurable digital photonic receiver integrating the benefits of coherent detection and digital signal processing was tested in a wavelength-division-multiplexing (WDM) scenario composed of four signals from different optical access technologies. The heterogeneous metro access network was composed of the following subsystems:

1. 5 Gbps directly modulated vertical cavity surface emitting laser (VCSEL).

2. Baseband 20 Gbps non-return-to-zero quadrature phase-shift keying

(NRZ-QPSK).

3. Optically phase-modulated 2 Gbps impulse radio ultrawideband (IR-UWB).

4. optically phase-modulated 5 GHz OFDM radio-over-fiber.

PAPER 8 is currently nominated as a finalist in the 2011 Corning Outstanding Student Paper Competition in the Optical Fiber Communication Conference and Exposition and the National Fiber Optic Engineers Conference (OFC/NFOEC 2011). The novel concept on reconfigurable digital coherent receivers has the potential to enable signal detection and demodulation on the expected highly heterogeneous next generation metro-access networks.

Additionally, **PAPER 9** demonstrates the robustness and flexibility of optical phase-modulated links in the linear transport of orthogonal frequency division multiplexed (OFDM) microwave signals. Successful demodulation of an asynchronous optical phase-modulated adaptive-order OFDM signal composed of 4, 16 and 64 quadrature amplitude modulated (QAM) sub-carriers was demonstrated using a DSP-based reconfigurable photonic receiver.

Finally, in **PAPER 11**, a DSP-based receiver was used for signal demodulation to demonstrate the furthest (50 km of optical fiber transmission followed by 2.9 m of wireless transmission) and highest bit rate wireless transmission of an IR-UWB signal (3.125 Gb/s) generated in the photonic domain.

3.1.2 Reconfigurable digital photonic receivers for PM RoF systems

We considered the theoretical point of view on the design of reconfigurable digital photonic receivers for optical phase-modulated links. It has also been shown that data-signal parameters estimation including carrier phase and frequency offset estimation as well as signal modulation format detection can be jointly performed and simplified by using a clustering-based estimation approach, instead of using traditional approaches based on maximum a posteriori (MAP) or maximum likelihood (ML) estimation.

The novel clustering-based estimation approach is based on the estimation of two parameters after the clustering process on the constellation diagram: the number of estimated symbols represented by the geometrical center of each identified cluster and the coordinates of those estimated

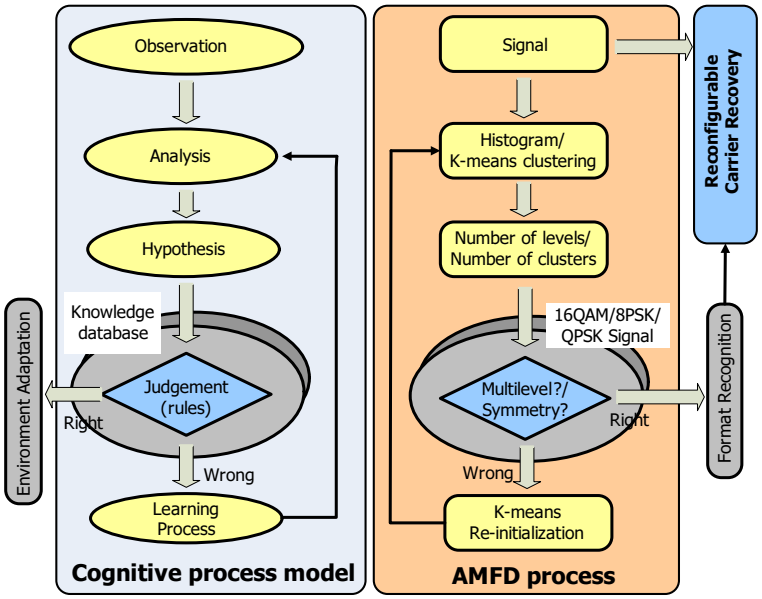

Figure 3.1: Schematic diagrams of cognitive process model and the automatic modulation format detection module.

cluster-centers on the constellation diagram. Data-signal phase and frequency offset estimation as well as signal modulation format detection can be easily derived from the number and coordinates of the identified clusters. **PAPERS 2-7**report how to perform phase and frequency estimation and compensation as well as signal modulation format detection based on the k-means clustering algorithm. Successful signal detection and demodulation of QPSK, 8PSK and 16QAM phase-modulated radio-over-fiber signals was achieved using the novel clustering-based approach and supported by experimental validations on wavelength-division-multiplexing (WDM), subcarrier multiplexed and burst mode phase-modulated radio-over-fiber systems.

PAPERS 7 also developed a parallel between a schematic diagram of a generic cognitive process model and the corresponding automatic modulation format detection (AMFD) function integrated in our proposed digital receiver (see Fig. 3.1). The proposed reconfigurable burst-mode digital coherent receiver shows prospect for next generation access networks due its adaptability, flexibility and expandable format detection principle.

3.1.3 Data-aided optical channel estimation

Constant Amplitude Zero Autocorrelation (CAZAC) sequences are investigated in Chapter 2 and developed as a strong candidate for performing training sequence-aided optical channel estimation in 112 Gbit/s polarization-diversity coherent detected optical transmission systems. Low-complexity channel estimation can rapidly be achieved for each training block overcoming current drawbacks in blind OPM approaches with blind, non-data aided (NDA) filter update. This system is also adaptable, overcoming limitations introduced, for example, by finite time-domain filter taps (causing low parameter range and low precision estimation); CAZAC length may be adapted to fit within the FFT-size of the feedforward equalizer.

Extensive numerical investigations showed accurate chromatic dispersion estimation for different OSNR conditions, including the case for 10 dB. In addition to different OSNR scenarios, the robustness of the estimation is demonstrated in chapter 2 over a wide range of combined distortions including random PMD contributions ranging from 10 to 35 ps and 6 dB of PDL. Additionally, the proposed estimation approach of the instantaneous differential group delay parameter based on the CAZAC sequence was demonstrated for high values of OSNR.

Instead of non-data-aided approaches, the use of data-aided optical channel estimation with the zero-forcing criteria has allowed accurate CD and PMD estimation, independent of memory lengths and update algorithms for FIR filter tap convergence. Therefore, data-aided channel estimation based on the principle of zero-forcing criteria in the frequency domain, and use of CAZAC training sequences, has enabled accurate and low complexity optical performance monitoring approaches toward real time realizations.

3.2 RoF systems: 100-G systems and optical microwave signal generation

The trend in radio-over-fiber systems is to increase the microwave carrier frequency to cover the huge growth of data capacity (multigigabt wireless systems) demanded for end users [24]. Several frequency bands in the millimeter wave frequency regime (60, 70/80, >100 GHz, etc.), have a few gigahertz of available bandwidth, which could potentially enable gigabit wireless transmissions [9, 10, 24, 72–74]. Hence, more attention must be paid to fiber dispersion, as a direct consequence of increasing microwave

carrier frequency.

One equally important topic in RoF systems is the optical-domain generation and transmission of high-fidelity microwave and millimeter-wave signals.There have been reports in the scientific literature of two different techniques for generating microwave signals: the optoelectronic oscillator [80–86] and the heterodyning of optical carriers with different wavelengths [87–92].

3.3 Toward cognitive optical networks

The Internet of the future is a new concept arising from the fact that the current Internet structure will not be able to meet future demands for bandwidth capacity, flexibility and indispensable easy manageability of its complex infrastructure. A simple incremental growth and development will not suffice. The very concept of the Internet will need to evolve, not only at the level of its physical layer infrastructure, but also at the level of providing efficient and manageable connectivity of real and virtual worlds, for sustainable energy consumption and the provision of new services with security and privacy guarantees.

Therefore, future optical networks supporting the Future Internet, are envisioned as intelligent systems, capable of self-adjusting network resources to support the continuing demand of new and diverse bandwidth-hungry services [2]. Cognitive optical networks based on models of human-brain abilities integrated into the network are expected as a breakthrough technology to implement future optical communication networks. Indeed, the integration of cognitive processes into the network will allow perceiving optical network conditions for optimum data-signal routing as well as efficient network management in order to optimize network resources utilization and reduce system power consumption.

The most relevant research challenges to exploit the full potential of cognitive optical networks are how to implant cognitive entities (devices) into the existing optical network architecture and map intelligence into such devices. The proposed clustering-based approach developed within in my PhD for signal parameter estimation enables the use of machine learning techniques for advance signal demodulation approaches and data-signal modeling in optical networks. For instance, additional signal parameters such as cluster-variances and measurements of the distances and angles between the clusters on the constellation diagram can be estimated by extending the proposed clustering-based approach using the k-means algorithm.

Such an extension consists of adding posterior probabilities to the clustering process to make a *soft* assignment of data-symbols to clusters, instead of the *hard* assignment performed by the k-means algorithm in which each data-symbol is associated uniquely with one cluster.

The resultant extension is known as the expectation-maximization (EM) algorithm. EM is a general technique for finding maximum likelihood estimators in latent variable models such as Gaussian mixture (GoM) models. GoM models can be interpreted as a simple linear superposition of Gaussian components and it is a strong class of density model to exploit in digital communications. For example, data-signal parameters estimation based on GoM models would lead at least to two interesting enhancements to the optical network functions: optical performance monitoring based on cluster-shape variations analysis on the constellation diagram and signal detection and demodulation of multi-cluster modulation formats, enabling novel multiplexing methods based on clusters allocation on the constellation diagram.

Paper 1: Re-configurable digital receiver for optically envelope detected half cycle BPSK and MSK radio-on-fiber signals

Guerrero Gonzalez Neil, Prince Kamau, Zibar Darko, Tafur Monroy Idelfonso. "Re-configurable digital receiver for optically envelope detected half cycle BPSK and MSK radio-on-fiber signals", *Optical Fiber Technology*, vol. 17, no. 1, pp. 59-63, January 2011.

Optical Fiber Technology 17 (2011) 59–63

Contents lists available at ScienceDirect

Optical Fiber Technology

www.elsevier.com/locate/yofte

Re-configurable digital receiver for optically envelope detected half cycle BPSK and MSK radio-on-fiber signals

Neil Guerrero Gonzalez *, Kamau Prince, Darko Zibar, Idelfonso Tafur Monroy

DTU Fotonik, Technical University of Denmark, Oersteds Plads 343, DTU Campus, 2800 Kgs. Lyngby, Denmark

ARTICLE INFO

Article history:
Received 27 May 2010
Revised 20 August 2010
Available online 20 November 2010

Keywords:
Envelope detection
Hybrid wireless-fiber systems
Radio-on-fiber
Digital receiver

ABSTRACT

We present the first known integration of a digital receiver into optically envelope detection radio-on-fiber systems. We also present a re-configurable scheme for two different types of optically envelope detected wireless signals while keeping the complexity of used optical components low. Our novel digital receiver consists of a digital signal processing unit integrating functions such as filtering, peak-powers detection, symbol synchronization and signal demodulation for optically envelope detected half-cycle binary phase-shift-keying and minimum-shift-keying signals. Furthermore, radio-frequency signal down-conversion is not required in our proposed approach; simplifying evens more the optical receiver front-end. We experimentally demonstrate error-free optical transmission (bit-error rate corresponding to 10^{-3} related to FEC-compatible levels) for both 416.6 Mbit/s half-cycle binary phase-shift-keying and 104.17 Mbit/s minimum-shift-keying radio-frequency modulated signals after 30 km of fiber transmission.

1. Introduction

Digital receivers based on digital signal processing (DSP) for optical communication systems have attracted the attention of the optical community in the last years because its cost effectiveness and compactness, adaptive compensation of fiber impairments in the electronic domain, and its versatility and robustness [1,2]. Moreover, an increase over the information capacity reached by intensity-modulation/direct-detection (IM/DD) schemes has been recently demonstrated by combining coherent detection and digital receivers based on DSP [3,4]. Furthermore, digital coherent receivers based on DSP have been reported as a part of the integration of microwave wireless communications schemes with fixed optical access links such as the radio-on-fiber (RoF) technology [5]. RoF is also a promising candidate for simultaneous distribution of wired and wireless services over a unified networking platform [6,7].

Despite the improvement on information capacity, coherent detection tends to be more complex than envelope detection due to the optical mixing methods required for re-constructing the electrical field of the signal. Also heterodyne methods for radio frequency (RF) down-conversion and detection are more complex than envelope detection of RF signals. Thus, optical envelope detection emerges as a promising technology to keep the complexity of optical components low as it requires only direct photodetection of the optical signal [8]. Moreover, complex RF mixers and local oscillator stages can be avoided as well [9,10]. The main challenge lies on the receiver side since emerging services from the convergence of wired and wireless networks may have diverse modulation formats and mixed bit rates. Digital receivers based on DSP enable easier re-configurable schemes to switch between different modulation and standards such as quadrature amplitude modulated (QAM) and minimum-shift-keying (MSK) signals [11] and may also be further adapted to support future advances in wireless signaling technology.

Recently, optical envelope detection has been successfully demonstrated with various RF modulated signal types, including 5.5 Gbit/s amplitude shift-keying (ASK) [9], and 40 Mbaud 16 QAM and quadrature phase-shift-keying (QPSK) [10]. However, the advantages and benefits of digital receivers incorporated into optical envelope detection have not yet been investigated. We present in this paper the first known integration of a digital receiver based on DSP to optical envelope detection systems. By taking advantage of the flexibility of digital receivers, we also present a re-configurable scheme for both optically envelope detected half-cycle binary phase-shift-keying (HC-BPSK) and MSK RoF signals. We propose HC-BPSK as a modification of binary phase-shift-keying (BPSK) to reach the maximum relation bit-rate/carrier frequency possible by encoding information symbols in half cycles of the carrier. Based on the same principle of HC-BPSK detection, we also propose a method for MSK signals with direct detection.

* Corresponding author. Address: DTU Fotonik, Technical University of Denmark, Oersteds Plads 343, DTU Campus, Office 214, 2800 Kgs. Lyngby, Denmark. Fax: +45 4593 6581.
E-mail address: nggo@fotonik.dtu.dk (N.G. Gonzalez).

1068-5200/$ - see front matter © 2010 Elsevier Inc. All rights reserved.
doi:10.1016/j.yofte.2010.10.005

We designed and implemented a single set of flexible filtering and synchronization DSP modules that were used for both types of signals, although separate demodulation modules were used in the receiver for the MSK and HC-BPSK modulated channels. We have successfully demonstrated the performance of our proposed receiver by achieving bit-error rate (BER) values below 10^{-3} (on the forward error correction level) after transmission for both 416.6 Mbit/s half-cycle and 104.17 Mbit/s MSK RF modulated signals after 30 km of fiber transmission.

2. Experimental details

We consider a communications scheme as shown in Fig. 1. The RF signal is HC-BPSK and MSK modulated. The base station unit (BSU) interfaces to the wireless communications network and imposes the received RF signal onto an optical carrier. At the central office (CO), the incoming optical signal is photo-detected before the data content is recovered by a DSP-enabled receiver.

The block diagram of the experimental setup is presented in Fig. 2. The RF waveform emulating the received wireless signal was obtained from an Agilent N8241A arbitrary waveform generator (AWG). The AWG produced a 416.6 Mbit/s HC-BPSK modulated signal at an intermediate frequency of 208.33 MHz, and a 104.17 Mbit/s MSK modulated signal by using two different carrier frequencies fixed at 104.17 MHz and 416.66 MHz for representing logic symbols "one" and "zero". This RF signal was used to drive a Mach–Zehnder optical intensity modulator (MZM) biased for linear operation, which modulated an optical carrier of wavelength 1554.42 nm. The RF voltage driving the MZM was set to 4.5 V peak-to-peak. A polarization controller was used at the MZM input to maximize optical modulation depth. The amplitude-modulated optical signal was launched into the standard single mode fiber (SMF) with an average optical power level of −5.74 dBm and transmitted over 30 km. The average optical received power level was measured to be −11.15 dBm. A 10 GHz photodiode (PD) was used at the receiver. The PD output was sampled at a rate of 40 Gs/s using a 13 GHz-bandwidth real time oscilloscope (Agilent Infinium DSO80000B), and processed offline using our proposed DSP algorithms.

The digital receiver includes common filtering and synchronization steps for both half cycle BPSK and MSK signals. Post-processing of the digitized data consists of a digital Gaussian filter to improve

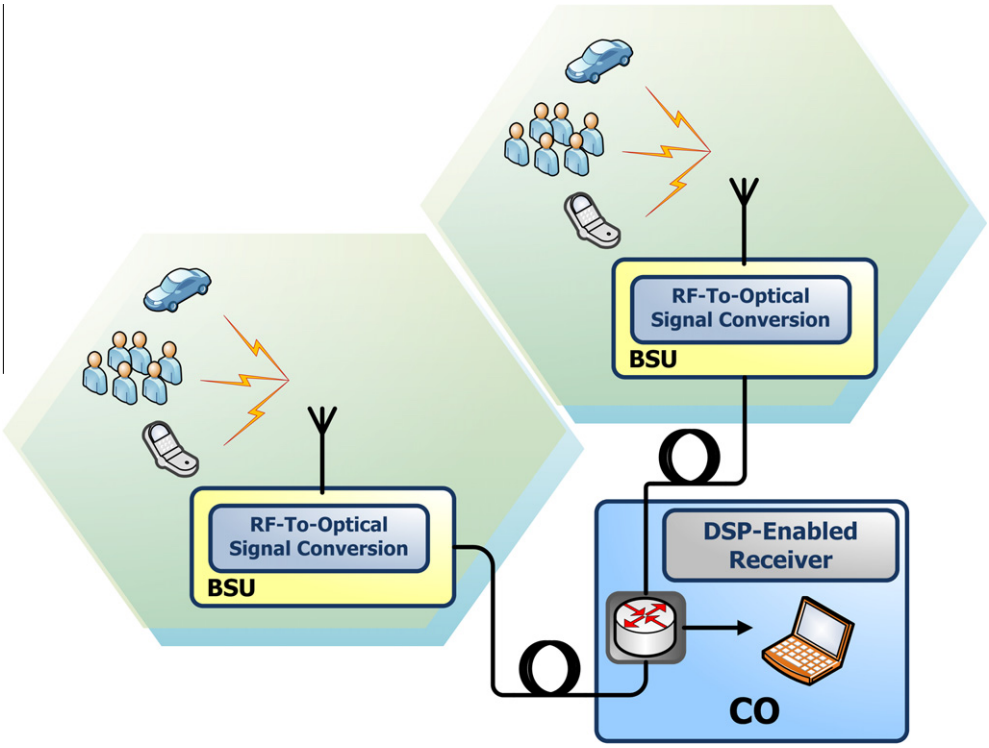

Fig. 1. Urban scenario. BSU, base station unit; CO, central office.

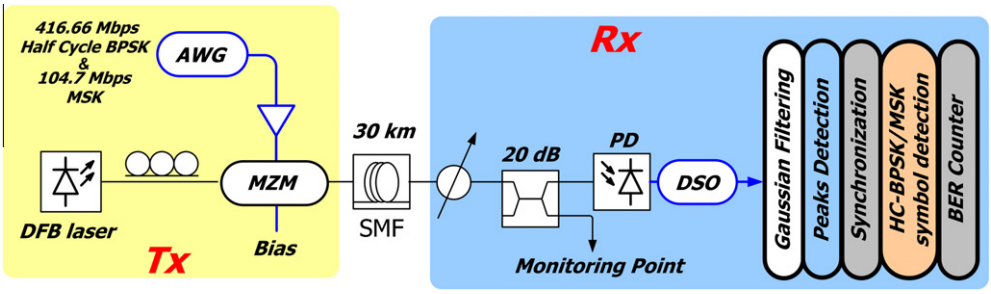

Fig. 2. Experimental layout. The intensity-modulated RoF signal is optically envelope detected after transmission. DSO, digital sampling oscilloscope; AWG, arbitrary waveform generator.

receiver signal-to-noise ratio (SNR), a synchronization module for peak-power samples detection and a demodulation module adapted for both the HC-BPSK and the MSK signals. Finally, the data pattern was recovered and the bit-error rate (BER) calculated.

2.1. HC-BPSK modulation principle

The HC-BPSK modulation format is based on a BPSK modulation with a symbol rate of twice the value of the carrier frequency. Thus, half periods of the carrier are used for representing information bits. The modulation process includes an encoding rule which consists of a π phase shift of the RF carrier to represent logic "zero", and a preservation of carrier phase in the other case.

2.2. MSK signal generation

The MSK signal was generated by using two different carrier signals to represent logic symbols "one" and "zero", with continuous phase in the transition. Carrier frequencies were fixed to 104.17 MHz and 416.66 MHz and the bit rate was fixed at 104.17 MHz.

3. The digital receiver

After photodetection, the PD output is digitized using a sampling oscilloscope at 40 GSa/s for offline processing. Fig. 3 shows the signal flow chart of the DSP receiver. The proposed demodulation algorithm implemented is based on the number of peak-powers samples detected per symbol period in both HC-BPSK and MSK signals.

Firstly, the HC-BPSK/MSK signal samples, denoted by $y(\frac{m}{N}T_s)$, sampled at a rate higher than the symbol rate (every $(m/n)T_s$ seconds where $m \leqslant n$), are divided into streams of N values according to the HC-BPSK/MSK symbol period T_s and post-processed in a DSP receiver. We can write the sampled signal as:

$$y\left(\frac{m}{N}T_s\right) = \sum_k \left(\sum_{m=1}^{N} b_k\left(\frac{m}{N}T_s - kT_s\right) + n\left(\frac{m}{N}T_s\right) \right) \tag{1}$$

where b_k represents a sinusoidal signal whose frequency values are describing in Eq. (2) and $n(\frac{m}{N}T)$ is a gaussian sample noise. Three different values for carrier frequency are switched according to the modulation format to be implemented. Thus, as it is described in Eq. (2), logical symbol '0' for the MSK signal will have a carrier frequency four times higher than the sampling frequency at the receiver.

$$b_k = \sin(2\pi f_k t) \rightarrow \begin{cases} f_k = \frac{1}{4T_s} & \text{for MSK}_0 \\ f_k = \frac{1}{T_s} & \text{for MSK}_1 \\ f_k = \frac{2}{T_s} & \text{for HC-BPSK} \end{cases} \tag{2}$$

The digital receiver consists of a digital Gaussian filter with adjustable standard deviation (σ) factor whose input is a stream of N data samples. Since the digital Gaussian filter is a low pass filter whose bandwidth is adjustable by σ, and bandwidth requirements for signal demodulation are different from HC-BPSK and MSK, the reconfiguration process implies a new selection of the σ. After filtering operation, samples (denoted by $\tilde{y}(\frac{m}{N}T_s)$) are passed through a tapped delay line of length 2 to calculate the first and second derivative of the signal. Eq. (3) describes the derivative operation.

$$\Delta^2\tilde{y}\left(\frac{m}{N}T_s\right) = \tilde{y}\left(\frac{m}{N}T_s - 2\right) - \tilde{y}\left(\frac{m}{N}T_s - 1\right) + \tilde{y}\left(\frac{m}{N}T_s\right) \tag{3}$$

Secondly, a peak-power samples detection block (denoted as "peak detection" in Fig. 2) extracts from the second derivative of the signal, all peak-power samples in a symbol period. Since these peak-power samples may represent local (because of the effect of the Gaussian noise) and global (values required for timing clock recovery) maximums in a symbol period, a synchronization block is required. All peak-power samples are fed to the synchronization block where peak-power samples higher than a threshold (denoted by μ) value are selected for timing recovery. The function *thres*(·) whose output is a vector ($M = [m_1, \ldots, m_j]$) containing the discrete time index of samples above μ is defined in Eq. (4).

$$thres\left(\sum_{m=1}^{N}\Delta^2\tilde{y}\left(\frac{m}{N}T_s\right), \mu\right) = \left\{m; \quad \Delta^2\tilde{y}\left(\frac{m}{N}T_s\right) \geqslant \mu\right. \tag{4}$$

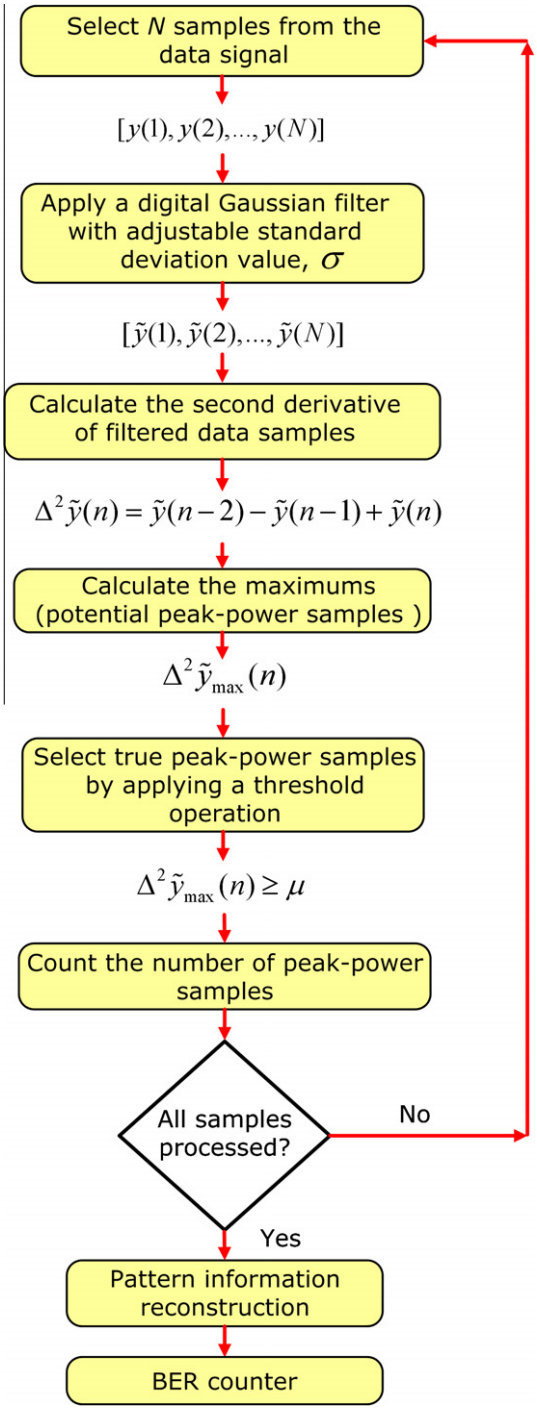

Fig. 3. Signal flow chart of the DSP-enabled receiver for HC-BPSK and MSK signal demodulation.

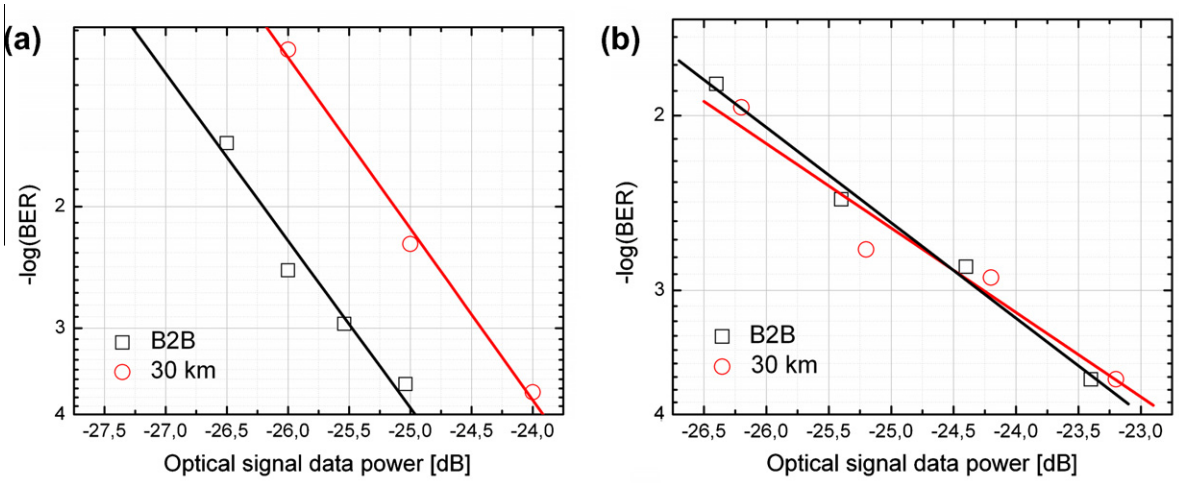

Fig. 4. Showing transmission penalty (BER vs. received optical power) results for (a) 416.7 Mbit/s HC-BPSK and (b) 104.17 Mbit/s MSK signaling.

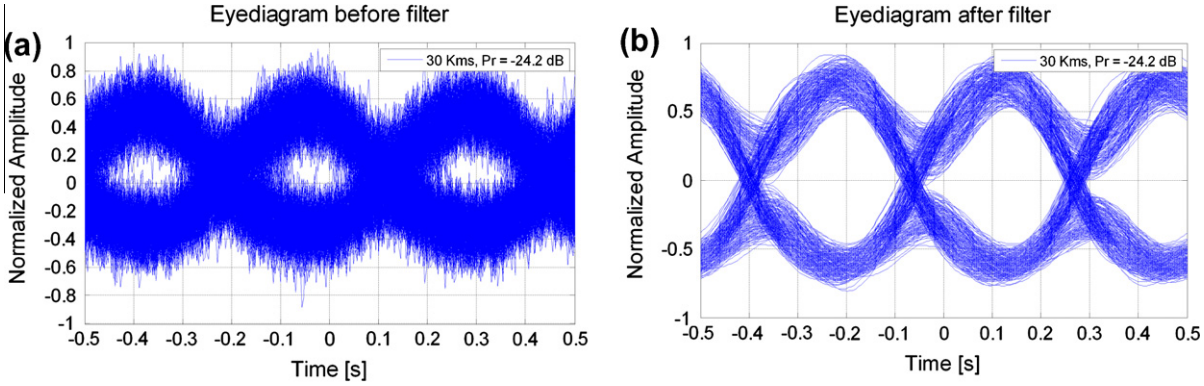

Fig. 5. Eye diagrams obtained (a) before and (b) after filtering at the receiver.

Finally, after peak-powers detection and synchronization, the information of the discrete time index from vector M is used by the HC-BPSK/MSK symbol detection block to reconstruct the binary data information before the bit-error rate (BER) counter.

Filtering and synchronization DSP modules are used for both types of signals. However, different demodulation modules have been developed to demodulate MSK and HC-BPSK modulated signals separately. HC-BPSK signals are associated with one peak-power sample per symbol (since only half cycle of the carrier is modulated) while for MSK signals the number of peak-power samples per symbol varies from one logic symbol to the other one. This is because of the different number of full carrier cycles depending of the logical symbol recovered (since different carrier frequencies are used for each logical symbol). For instance, four peak-power samples will be found for the symbol represented by the frequency fixed at 416.66 MHz with a symbol rate fixed at 104.17 MHz. On the other hand, only one power peak will be detected for the symbol represented by the frequency fixed at 104.17 MHz.

4. Results

We assessed BER sensitivity of the system as a function of the average received optical power, and present the results for 416.7 Mbit/s HC-BPSK in Fig. 4a and 104.17 Mbit/s MSK in Fig. 4b. BER calculations were done at the transmitter output (B2B) and after 30 km SMF by analyzing a total amount of 15,524 bits. Optical power losses after transmission were measured at 6 dB approximately. For both signals, we obtained BER below 10^{-3}. It is observed in Fig. 4a that there is a penalty in received power (for BER at 10^{-3}) of approximately 1 dB for a value of 0.55 of the digital Gaussian filter standard deviation factor (σ). For Fig. 4b, the DSP based receiver was reconfigured to MSK signal demodulation by adjusting the σ value to 0.65. No penalty in received power was observed for BER at 10^{-3} between the back-to-back (B2B) and transmission scenario.

In Fig. 5, we present an eye diagram obtained after 30 km optical transmission, before and after filtering of the half cycle BPSK modulated signal (at a received power level of Prec = −24.2 dBm). Eye diagrams were calculated by using 7000 of bits to illustrate the effect of the digital Gaussian filter. An open eye diagram was observed after filtering, confirming the low probability of errors reported in Fig. 4a at −24.2 dBm of optical received power (a log value of the BER of 3.89 corresponds to 2 errors over the total amount of bits considered for BER calculations).

5. Conclusions

A re-configurable digital receiver for optically envelope detected HC-BPSK and MSK signals for radio-on-fiber has been presented. We have experimentally demonstrated successful demodulation of both 416.6 Mbit/s HC-BPSK and 104.17 Mbit/s MSK RF modulated signals, after transmission over a 30 km of SMF. The proposed digital receiver uses common digital functions for both types of signals reducing the complexity of the receiver and does

not required RF signal down-conversion due to the demodulation method based on the peak-power detection implemented. The maximum relation bit-rate/carrier-frequency for BPSK signals is achieved with the proposed HC-BPSK modulation. By using a digital receiver for optically envelope detected wireless signals, higher order modulation formats can be implemented; increasing the capacity of the system without increasing the complexity of the optical receiver. In addition to encoding tasks and signal demodulation of advanced modulation formats, digital receivers based on DSP also enable easy reconfiguration to different modulations formats and standards on a single platform. This fact makes digital receivers more feasible for implementing the next generation of access networks.

References

[1] L.G. Kazovsky, G. Kalogerakis, W.-T. Shaw, Homodyne phase-shift-keying systems: past challenges and future opportunities, J. Lightw. Technol. 24 (12) (2006) 4876–4884.
[2] S.J. Savory, Electronic signal processing in optical communications, Proc. SPIE 7136 (2008). 71362C-1–71362C-9.
[3] G. Goldfarb, G. Li, DSP-enabled coherent optical communications, Proc. SPIE 6572 (2007) 657202.1–657202.7.
[4] M. Kuschnerov, F.N. Hauske, K. Piyawanno, B. Spinnler, M.S. Alfiad, A. Napoli, B. Lankl, DSP for coherent single-carrier receivers, J. Lightw. Technol. 27 (16) (2009) 3614–3622.
[5] D. Zibar, X. Yu, C. Peucheret, P. Jeppesen, I. Tafur Monroy, Digital coherent receiver for phase-modulated radio-over-fiber optical links, IEEE Photon. Technol. Lett. 21 (3) (2009) 155–157.
[6] N.J. Gomes, M. Morant, A. Alphones, B. Cabon, J.E. Mitchell, C. Lethien, M. Csörnyei, A. Stöhr, S. Iezekiel, Radio-over-fiber transport for the support of wireless broadband services, J. Opt. Networking 8 (2) (2009) 156–178.
[7] Y. Pi, Z. Dong, L. Chen, J. Yu, A radio-over-fiber system for simultaneous generation of wired and wireless services, Proc. SPIE 7136 (2008). 71361K-1–71361K-9.
[8] H. Paul, K.-D. Kammeyer, Equivalent baseband channels of systems using envelope detection, Int. J. Electron. Commun. 63 (2009) 533–540.
[9] K. Prince, I. Tafur Monroy, J. Seoane, P. Jeppesen, All-optical envelope detection for radio-over-fiber links using external optical injection of a DFB laser, Opt. Exp. 16 (3) (2008) 2005–2014.
[10] I. Tafur Monroy, K. Prince, J. Seoane, X. Yu, Optically envelope detected QAM and QPSK RF modulated signals in hybrid wireless-fiber systems, Microw. Opt. Technol. Lett. 51 (3) (2009) 864–866.
[11] H. Schwetlick, A. Huhn, A universal receiver concept for multi-system LR-WPAN, in: Proceedings of the 13th IEEE International Symposium on Consumer Electronics (ISCE2009), 2009, pp. 761–764.

Neil Guerrero received the B.Sc. degree in electronics engineering from the Universidad Nacional de Colombia, Manizales, in 2005; a Graduate Diploma in M.Eng.Sc. degree from the Universidad Nacional de Colombia, Manizales, in 2007. He is currently pursuing a Ph.D. in Photonics at the Technical University of Denmark, with the metro-access and short range systems research group of the department of Photonics Engineering.

Kamau Prince received the B.Sc. degree (first class honors) in electrical engineering from the University of the West Indies, St. Augustine, Trinidad, in 1999; a Graduate Diploma in telecommunications engineering and M.Eng.Sc. degree from the University of Melbourne, Victoria, Australia, in 2003 and 2006, respectively. He is currently pursuing a Ph.D. in optical communications engineering at DTU Fotonik, Technical University of Denmark.

Darko Zibar was born on December 9th, 1978, in Belgrade former Yugoslavia. He received the M.Sc. degree in Telecommunication in 2004 from the Technical University of Denmark and the Ph.D. degree in 2007 from the Department of Communications, Optics and Materials, COM·DTU within the field of optical communications. He was a Visiting Researcher with Optoelectronic Research Group led by Prof. John E. Bowers, at the University of California, Santa Barbara (UCSB) from January 2006 to August 2006, and January 2008 working on coherent receivers for phase-modulated analog optical links. From February 2009 until July 2009, he was Visiting Researcher with Nokia-Siemens Networks working on digital clock recovery for 112 Gb/s polarization multiplexed systems. Currently, he is employed at DTU Fotonik, Technical University of Denmark as the Assistant Professor. His research interests are in the area of coherent optical communication, with the emphasis on digital demodulation and compensation techniques.
He is a recipient of the Best Student Paper Award at the IEEE Microwave Photonics Conference (MWP) 2006, for his work on novel optical phase demodulator based on a sampling phase-locked loop as well as Villum Kann Rasmussen postdoctoral research grant in 2007.

Idelfonso Tafur Monroy received the M.Sc. degree in multichannel telecommunications from the Bonch-Bruevich Institute of Communications, St. Petersburg, Russia, in 1992, the Technology Licenciate degree in telecommunications theory from the Royal Institute of Technology, Stockholm, Sweden, and the Ph.D. degree from the Electrical Engineering Department, Eindhoven University of Technology, The Netherlands, in 1999.
He is currently Head of the metro-access and short range communications group of the Department of Photonics Engineering, Technical University of Denmark. He was an Assistant Professor until 2006 at the Eindhoven University of Technology. Currently, he is a Professor at the Technical University of Denmark. He has participated in several European research projects, including the ACTS, FP6, and FP7 frameworks (APEX, STOLAS, LSAGNE, MUFINS). At the moment, he is in involved the ICT European projects Gi-GaWaM, ALPHA, BONE, and EURO-FOS. His research interests are in hybrid optical-wireless communication systems, coherent detection technologies and digital signal processing receivers for baseband and radio-over-fiber links, optical switching, nanophotonic technologies, and systems for integrated metro and access networks, short range optical links, and communication theory.

Paper 2: Experimental 2.5-Gb/s QPSK WDM phase-modulated radio-over-fiber link with digital demodulation by a K-means algorithm

Guerrero Gonzalez Neil; Zibar Darko ; Caballero Jambrina, Antonio ; Tafur Monroy, Idelfonso. "Experimental 2.5-Gb/s QPSK WDM phase-modulated radio-over-fiber link with digital demodulation by a K-means algorithm", *IEEE Photonics Technology Letters*, vol. 22, no. 5, pp. 335-337, March 2010.

Experimental 2.5-Gb/s QPSK WDM Phase-Modulated Radio-Over-Fiber Link With Digital Demodulation by a K-Means Algorithm

Neil Guerrero Gonzalez, Darko Zibar, Antonio Caballero, and Idelfonso Tafur Monroy

***Abstract*—Highest reported bit rate of 2.5 Gb/s for optically phase-modulated radio-over-fiber (RoF) link, employing digital coherent detection, is demonstrated. Demodulation of 3×2.5 Gb/s quadrature phase-shift-keying modulated wavelength-division-multiplexed RoF channels is achieved after 79 km of transmission through deployed fiber. Error-free performance (bit-error rate corresponding to 10^{-4}) is achieved using a digital coherent receiver in combination with a K-means algorithm for radio-frequency phase recovery.**

***Index Terms*—Carrier recovery, coherent communication, digital receivers, digital signal processing (DSP), phase-modulation, radio-over-fiber (RoF).**

I. Introduction

COHERENTLY detected optically phase-modulated radio-over-fiber (RoF) links are a promising technology for future applications in wireless photonic networks where a large bandwidth and channel selectivity, and low transmit power is required [1]. Optically phase-modulated RoF links can potentially enable large dynamic range, high-capacity and spectral efficiency, and simplified antenna base stations implementation. However, phase-modulated links require an optical coherent receiver combined with digital signal processing (DSP) modules for detection and linear signal demodulation [2]. We have recently proposed and experimentally demonstrated a novel digital coherent receiver for phase-modulated wavelength-division-multiplexed (WDM) RoF optical links employing a simple binary phase-shift-keying (BPSK) and quadrature phase-shift-keying (QPSK) modulation format with a relatively low bit rate of 50 Mb/s for a radio-frequency (RF) carrier at 5 GHz [2]. Since phase-modulated RoF systems have the information encoded into the phase of an RF carrier which then modulates the phase of the optical carrier, two frequency/phase-compensation modules are required. The first module (the digital phase-locked-loop (DPLL) [2], [3]) removes the frequency/phase offset between the local oscillator (LO) and the incoming signal. A second module is needed to remove the RF phase offset (RF carrier recovery) before signal demodulation. For RF carrier recovery feedback, decision-directed (DD) and feedforward nondecision-aided (NDA) algorithms are used to compensate the RF phase offset [3]. Feedforward phase estimation algorithms are preferred since they avoid feedback which can cause system instability and also they can be more easily parallelized which is important for high-speed real-time implementation. For M-ary phase-shift keying (M-PSK) modulation formats, feedforward algorithms as the classical Viterbi & Viterbi (V&V) algorithm are typically well suited; however, they suffer from complexity as we scale up to higher order modulation formats [3]. In this work, we propose a novel feedforward application of the k-means algorithm for RF carrier recovery. In addition to its adaptability to a wide variety of modulation schemes, the k-means algorithm is less complex than the V&V algorithm since complex multiplications are not required to remove the data modulation decreasing its complexity for digital implementation. It is important to decrease the number of complex multiplications because more hardware resources are used for real-time implementation and the range of resolution for representing float numbers is reduced [3].

We experimentally demonstrate a three-channel WDM, 2.5-Gb/s QPSK optical phase-modulated uplink RoF link and a 6-GHz RF carrier frequency, including a transmission over a 78.8 km of deployed fiber. We achieve an error-free performance of 10^{-4}, for the center demodulated channel and three simultaneous demodulated channels for back-to-back (B2B) case and after fiber transmission.

II. Setup Description

The experimental setup is shown in Fig. 1. The transmitter consists of three tunable distributed-feedback (DFB) lasers, with a linewidth of $\sim$3 MHz. The output of the transmitter laser array is then connected to an optical phase modulator (PM). The spacing between the optical channels was at 50 GHz. Two independent output signals from a pulse pattern generator (PPG) at 1.25 Gb/s are used to feed the in-phase and quadrature (I/Q) mixer of a vector signal generator (VSG), which performs QPSK modulation at 6-GHz carrier frequency. The RF power driving the PM is set to 18 dBm, corresponding to 0.86 modulation index. The optically phase-modulated signal is launched into the field-deployed optical fiber at -0.7 dBm and transmitted over 78.8 km. The optical power received was at -24.32 dBm. The fiber is a G.652 standard single-mode fiber (SMF) type. The deployed link incorporates dispersion compensation by using a matched length of dispersion-compensating

Manuscript received September 18, 2009; revised November 18, 2009; accepted December 16, 2009. First published January 12, 2010; current version published February 10, 2010.

The authors are with DTU Fotonik, Technical University of Denmark, Kgs-Lyngby 2800, Denmark (e-mail: nggo@fotonik.dtu.dk).

Color versions of one or more of the figures in this letter are available online at http://ieeexplore.ieee.org.

Digital Object Identifier 10.1109/LPT.2009.2039640

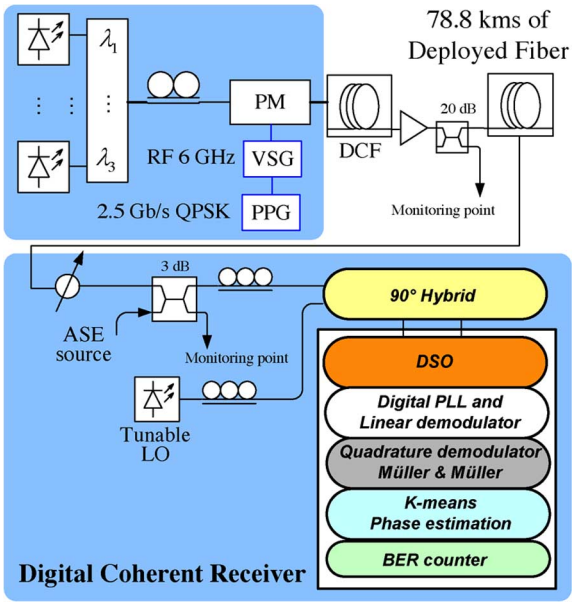

Fig. 1. General outline for the experimental setup for demonstration of WDM 2.5-Gb/s QPSK phase-modulated RoF optical link using the digital coherent detection.

fiber (DCF) whose loss is compensated by an erbium-doped fiber amplifier (EDFA). As an LO, a tunable external cavity laser is used, with ~100-kHz linewidth and 0-dBm input power was delivered to the 90° optical hybrid. The I/Q resultant signals after the 90° optical hybrid are detected with two pairs of balance photodiodes, with 7.5-GHz bandwidth. The detected photocurrents are digitalized using a sampling oscilloscope (DSO) at 40 Gs/s (Agilent Infinium DSO91304A) for offline processing. The employed digital receiver uses carrier-recovery DPLL and linear signal demodulation [2], the quadrature demodulator for RF down-conversion [3], the Müller and Müller algorithm for timing recovery [3], and the k-means algorithm for RF phase estimation and signal demodulation.

Once the signal after photodetectors is digitized, the DPLL removes the difference in frequency and phase between the transmitter and LO lasers. The DPLL can track frequency offset in the range of approximately 400 MHz [2]. Next, we linearly demodulate the phase encoded RF signal. Then quadrature demodulator is used to down-convert the RF signal to baseband and a Müller and Müller synchronizer is applied to select the best sample per symbol. Finally, we apply k-means algorithm to make clustering before signal demodulation.

III. K-Means Algorithm for RF Phase Recovery

This section is intended as an introduction to our proposed k-means algorithm [4], [5] whose signal flowchart is presented in Fig. 2. The general setting of our k-means approach is as follows: clusters represent the four phase-states of a QPSK signal in the presence of phase offset in the I/Q plane. The RF phase offset θ is found by calculating the angle of the cluster centroids [see Fig. 2(d)]. The cluster's centroids estimation starts after the Müller and Müller synchronization block (see Fig. 1). N two-dimensional (2-D) vectors $x(n) = [x_i(n) \quad x_q(n)]$ formed by their I/Q data sample pair are mapped into the I/Q complex

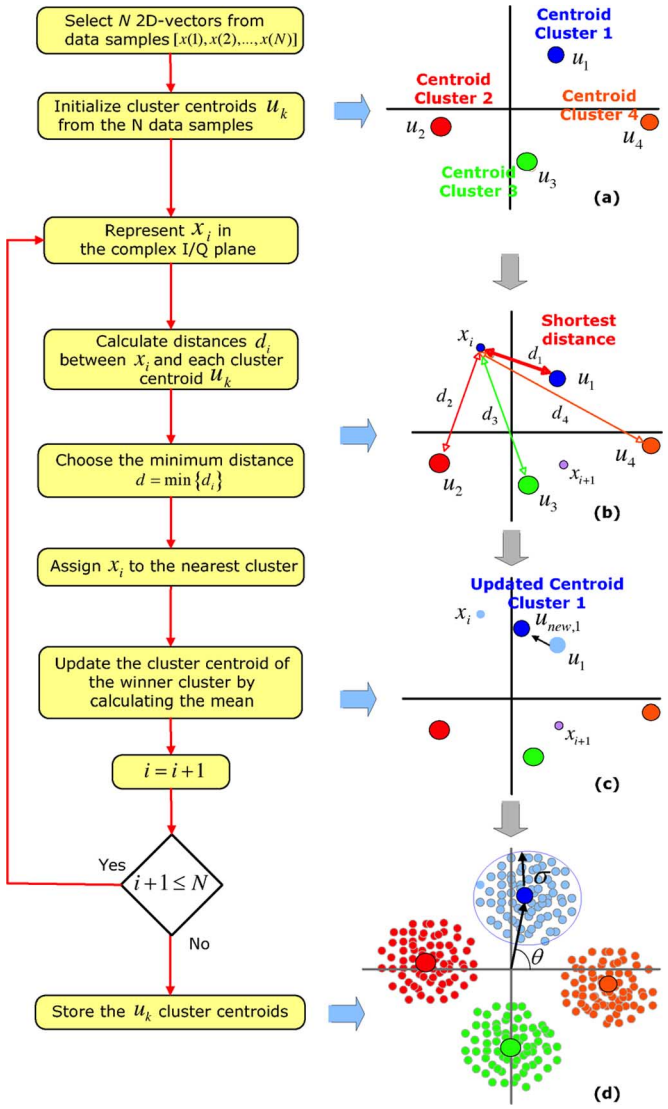

Fig. 2. K-means training flowchart.

plane, as shown in Fig. 2(d). Since QPSK signals have four phase-states, four clusters of data points are found. In order to start the estimation of the phase offset θ, four initial representative cluster prototypes u_k with $k = 1, 2, 3, 4$, representing the cluster number, are placed into the I/Q complex plane extracted from the initial N samples [see Fig. 2(a)]. The distance $d_k = |x(n) - u_k|$ between each 2-D vector $x(n)$ and each prototype u_k is calculated. Fig. 2(b) illustrates the distance calculation for the first single 2-D vector $x(1) = [x_i(1) \quad x_q(1)]$ when $n = 1$. Vector $x(n)$ is assigned to the cluster whose distance d is the minimum (the winner cluster) and the position of its prototype is updated by calculating the mean between the vector $x(n)$ and the winner prototype u_k [Fig. 2(c)]. The process is repeated for $n = 1, \ldots, N$ and the algorithm reaches its stable-state after certain number of iterations.

IV. Results

Fig. 3 shows the measured electrical spectrum of the QPSK signal with 2.5-GHz double sideband bandwidth at 6-GHz RF carrier frequency. As we expect, the spectra is centered at 6 GHz

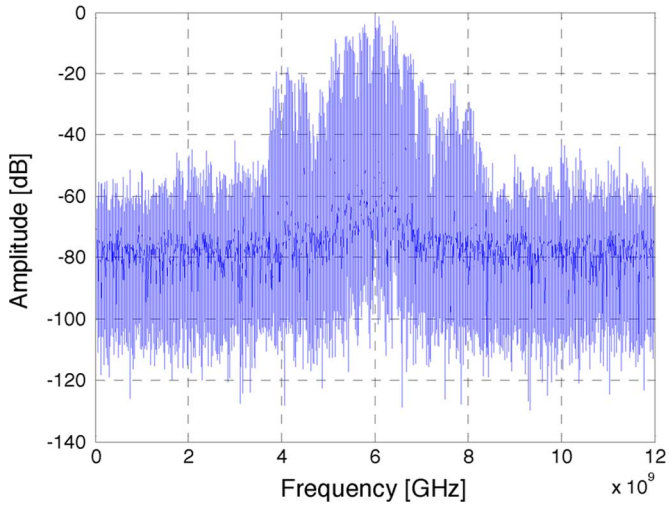

Fig. 3. Measured electrical spectra of 2.5-Gb/s QPSK RF signal.

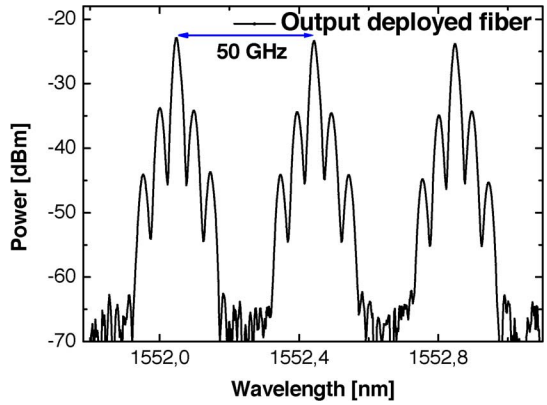

Fig. 4. Measured optical spectra of WDM phase-modulated RoF signal.

with nulls at 7.25 GHz, showing a QPSK phase-modulated RF carrier at 1.25 Gbaud. Fig. 4 shows the measured optical spectrum of the optical data signal. The spacing between the optical channels is set to 50 GHz, in order to comply with standardized International Telecommunication Union (ITU) grid. Amplified spontaneous emission (ASE) noise was loaded as a method to vary the optical signal-to-noise ratio (OSNR) at 0.1-nm resolution bandwidth.

To assess the performance of our system, we have computed the bit-error-rate (BER) curve as a function of OSNR for two different scenarios. The first scenario was fixed for a single wavelength ($\lambda_2 = 552.44$ nm) for B2B and after 78 km of fiber transmission. The second scenario was fixed for three simultaneous channels spaced ~50 GHz ($\lambda_1 = 1552.048$ nm, $\lambda_2 = 1552.44$ nm, and $\lambda_3 = 1552.85$ nm) after 78 km of fiber transmission.

Fig. 5 shows the offline computed results for these two cases. In order to analyze neighboring effects for a WDM system, only results for the center channel λ_2 are provided since it is the one that experiences the most crosstalk.

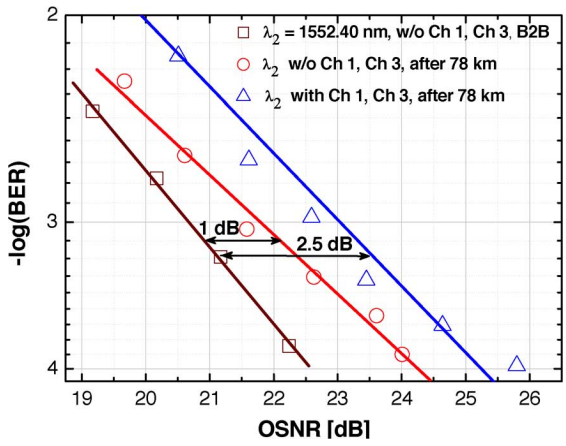

Fig. 5. BER of the demodulated 2.5-Gb/s QPSK signal at wavelength 1552.4 nm for a WDM channel spacing of 50 MHz, for B2B and after 78 km of deployed fiber transmission.

A penalty of 1 dB for a BER at 10^{-3} is observed for a single wavelength ($\lambda_2 = 1552.44$ nm) after 78.8 km of fiber transmission with respect to its B2B performance and approximately 2.5 dB of penalty for the case of two added neighbor channels.

The reason for the observed penalty, we believe, is associated to the system drift of the deployed fiber setup. We believe that although no postequalization algorithms were used, they may improve the overall system performance.

V. Conclusion

We have experimentally demonstrated successful coherent detection and digital demodulation of a three-channel WDM optically phase-modulated RoF link, at a bit rate of 2.5 Gb/s per channel and 6-GHz RF carrier frequency, after transmission over 78.8 km of field deployed fiber. To the best of our knowledge, this is the highest reported bit rate for optical phase-modulated RoF, coherent optical links. The k-means algorithm is used for RF phase recovery and it is a promising RF carrier phase approach for higher order modulation formats due its flexible configurationally and simplicity for digital implementation.

References

[1] N. J. Gomes, M. Morant, A. Alphones, B. Cabon, J. E. Mitchell, C. Lethien, M. Csörnyei, A. Stöhr, and S. Iezekiel, "Radio-over-fiber transport for the support of wireless broadband services," *J. Opt. Netw.*, vol. 8, pp. 156–178, Feb. 2009.

[2] D. Zibar, X. Yu, C. Peucheret, P. Jeppesen, and I. T. Monroy, "Digital coherent receiver for phase-modulated radio-over-fiber optical links," *IEEE Photon. Technol. Lett.*, vol. 21, no. 3, pp. 155–157, Feb. 1, 2009.

[3] H. Meyr, M. Moeneclaey, and S. A. Fechtel, *Digital Communication Receivers: Synchronization, Channel Estimation and Signal Processing*. Hoboken, NJ: Wiley, 1998, ch. 5.

[4] J. G. Proakis, *Digital Communications*. New York: McGraw-Hill, 1989, ch. 2, pp. 120–126.

[5] K. F. Conner and C. W. Baum, "A new method for block demodulation without channel estimation," in *Proc. IEEE Military Communications Conf. (MILCOM 98)*, Oct. 1998, vol. 3, pp. 852–856.

Paper 3: Experimental 2.5 Gbit/s QPSK WDM coherent phase modulated radio-over-fibre link with digital demodulation by a K-means algorithm

Guerrero Gonzalez Neil, Caballero Jambrina Antonio, Amaya Fernández Ferney Orlando, Zibar Darko, Tafur Monroy Idelfonso. "Experimental 2.5 Gbit/s QPSK WDM coherent phase modulated radio-over-fibre link with digital demodulation by a K-means algorithm", in *the 35th European Conference on Optical Communication, ECOC'2009,* Vienna, Paper P3.15, September 2009.

Experimental 2.5 Gbit/s QPSK WDM Coherent Phase Modulated Radio-over-Fibre Link with Digital Demodulation by a K-means Algorithm

N. Guerrero [(1)], A. Caballero[(1)], F. Amaya[(1,2)] D. Zibar[(1)] and I. Tafur Monroy[(1)]

[(1)] DTU Fotonik, Technical University of Denmark, DK-2800 Kgs. Lyngby, Denmark, nggo@fotonik.dtu.dk
[(2)] GIDATI Research Group, Universidad Pontificia Bolivariana, Medellín, Colombia, foafe@fotonik.dtu.dk

Abstract *Highest reported bit rate of 2.5 Gbit/s for optically phase modulated radio-over-fibre link employing coherent detection is demonstrated. Demodulation of 3x2.5 Gbit/s QPSK modulated WDM channels, is achieved after 79km of transmission through deployed fiber.*

Introduction

Coherently detected optically phase-modulated radio over fiber (RoF) links are a promising technology for future applications in wireless networks where a large bandwidth, channel selectivity and low transmit power is required[1]. Optically phase modulated RoF links can potentially enable large spurious–free dynamic range, high-capacity, high-spectral efficiency, enhanced receiver sensitivity and simplified antenna base stations implementation. However, phase modulated links require an optical coherent receiver for detection and linear signal demodulation[2]. A promising approach for linear signal demodulation is a digital coherent receiver that comprised stages for removing frequency offset between the local optical local oscillator and incoming signal, carrier recovery, timing recovery, radio frequency (RF) phase estimation and signal demodulation. We have recently proposed and experimentally demonstrated a novel DSP based digital coherent receiver for phase-modulated WDM RoF optical links employing a simple BPSK modulation format at 50 Mbit/s for RF carrier over 25 km of SMF[3]. In this paper, we experimentally demonstrate a 3 channel wavelength division multiplexing (WDM), 2.5 Gbit/s quadrature phase-shift keying (QPSK) optical phase modulated RoF, including transmission over a 78.8 km long field deployed optical fibre in the Copenhagen area. QPSK signal is generated by a Pulse Pattern Generator (PPG) and demodulation is performed offline employing a k-means algorithm featuring low complexity and simplicity for digital implementation.

Setup Description

The experimental setup is shown in Fig. 1. The transmitter consists of 3 tuneable Distributed Feedback Laser (DFB) lasers, with an average optical output power of 1 dBm and a linewidth of ~3 MHz. The output of the transmitter laser array is then connected to an optical phase modulator (PM). The wavelengths of the channels were spaced at 50 GHz from 1552.444 nm to 1552.048 nm. Two independent output signals from a PPG at 1.25 Gbit/s are used to feed the I&Q mixer of a Vector Signal Generator (VSG), which performs QPSK modulation at 6 GHz carrier frequency.

The RF power driving the PM is set to 18 dBm, corresponding to 0.8662 modulation index. The optically phase modulated signal is transmitted over a 78.8 km of field-deployed optical fiber. The fiber is a G.652 standard single mode fiber (SMF) type. The total link loss was measured to be 25 dB. This deployed link incorporates dispersion compensation by using a matched length of dispersion compensating fiber (DCF) whose loss is compensated by an erbium doped fiber amplifier (EDFA).

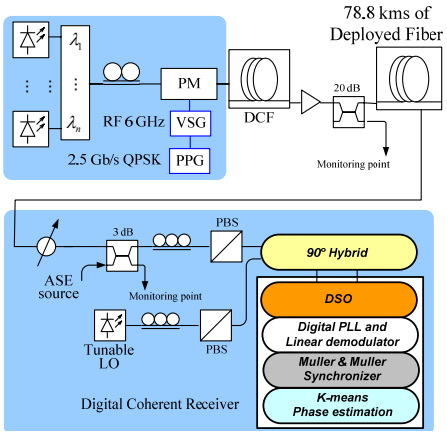

Fig. 1: Experimental setup

As a Local Oscillator (LO), a tuneable external cavity laser is used, with ~100 kHz linewidth and 0 dBm input power was delivered to the 90° optical hybrid. Both signals are passed through Polarization Beam Splitters (PBS) so the beating of both lasers is maximized. In practice, a polarization diversity scheme or polarization tracking can also be implemented. The in-phase and quadrature signals resultant after the 90° Hybrid coherent receiver are detected with two pairs of balance photodiodes, with 7.5 GHz bandwidth. The detected photocurrents are digitalized using a sampling oscilloscope at 40 Gs/s (Agilent Infinium DSO91304A) for offline processing. The employed digital receiver uses carrier-recovery digital phase-locked loop (PLL), linear signal

978-3-8007-3173-2

demodulation[2], and k-means algorithm for RF phase estimation and signal demodulation.

K-means Algorithm for RF phase recovery

In contrast to using phase rotation methods to align a recovered constellation, an iterative clustering approach called k-means algorithm[4] can be applied to the complex QPSK data mapped into the In-phase and quadrature space. This algorithm subdivides the constellation iteratively into L clusters (or classes) once the centroid of every cluster is found. Complex multiplications to rotate the constellation and certain number of data to estimate the phase are not required for signal demodulation.

An example of phase recovery for our QPSK signal using k-means is shown in Fig. 2.

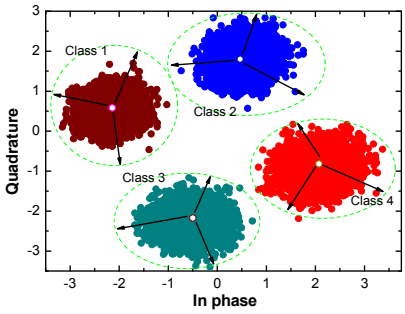

Fig. 2: Phase recovery by k-means algorithm

Experimental Results

Fig. 3 shows the electrical spectrum of the QPSK signal with 2.5 GHz double side-band bandwidth.

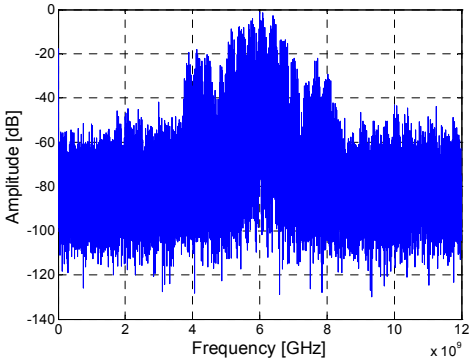

Fig. 3: Electrical spectrum of digital demodulated QPSK signal, 2.5 Gbit/s at 6 GHz carrier frequency

Fig. 4 shows the measured optical spectrum of the 50 GHz WDM space signals. Amplified spontaneous emission (ASE) noise was added to the system using two cascades EDFA with a tuneable filter in between to measure the optical signal to noise ratio (OSNR) at 0.1 nm of resolution.

To assess the performance of our system, we have computed the BER curve as a function of OSNR for the central wavelength channel alone and for the case of two added, simultaneous neighbouring channels spaced 50 GHz. Fig. 5 shows the offline computed results for Back-to-Back (B2B) transmission and after the deployed fibre.

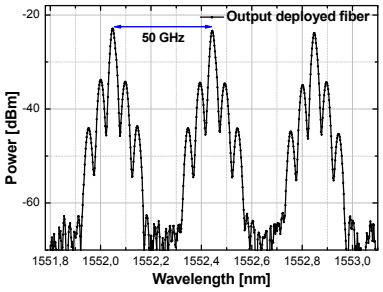

Fig. 4: Optical spectrum of WDM channels

A penalty of 1 dB is observed for a single wavelength ($\lambda_2 = 1552.44$ nm) after 78.8 km of transmission with respect to its B2B performance and approximately 2.5 dB of penalty for the case of two added neighbour channels. The reason for the observed penalty, we believe, it is associated with polarisation dispersion issues in the field deployed fibre.

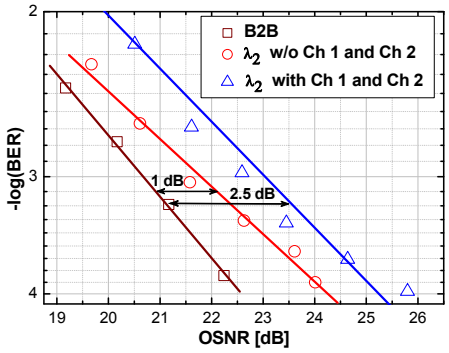

Fig. 5: BER curve for back-to-back (B2B), and after transmission for one and three wavelengths, simultaneously

Conclusions

We have experimentally demonstrated successful coherent detection and digital demodulation for 3xWDM of 2.5 Gbit/s QPSK phase modulated RoF optical link after transmission over a 78.8 km of field deployed fibre. The k-means algorithm is used for RF phase recovery. To the best of our knowledge, this is the highest reported baud rate for optical phase modulated RoF, coherent optical links.

References

1 N.J. Gomes et al., J. Optical Networking. **8**, 156-178 (2009).
2 D. Zibar et al., PTL **21**, 155-157 (2009).
3 D. Zibar et al., Proc. ECOC'08, TU.3.E.1.
4 J. G. Proakis, *Digital Communications*. McGraw-Hill (1989).

Paper 4: Reconfigurable Digital Receiver for 8PSK Subcarrier Multiplexed and 16QAM Single Carrier Phase-Modulated Radio over Fiber Links

Guerrero Gonzalez Neil, Zibar Darko, Yu Xianbin and Tafur Monroy Idelfonso. "Reconfigurable Digital Receiver for 8PSK Subcarrier Multiplexed and 16QAM Single Carrier Phase-Modulated Radio over Fiber Links", accepted for publication in *Microwave and Optical Technology Letters*, 2011.

Reconfigurable Digital Receiver for 8PSK Subcarrier Multiplexed and 16QAM Single Carrier Phase-Modulated Radio over Fiber Links

Neil Guerrero Gonzalez, Darko Zibar, Xianbin Yu and I. Tafur Monroy

Abstract— A reconfigurable digital radio frequency carrier recovery scheme based on the *k*-means algorithm is proposed for phase-modulated subcarrier multiplexed and quadrature amplitude modulated single carrier phase-modulated radio-over-fiber links. We report on experimental results for 40 km single mode fiber transmission link with three, 50 Mbaud, 8PSK subcarrier multiplexed signals and a 312.5 Mbaud, 16QAM single carrier at 5 GHz frequency, demonstrating the adaptability and feasibility of our proposed scheme for higher order modulation formats in order to achieve service integration on a unified networking platform.

***Index Terms*— *k*-means, coherent communication, radio-over-fiber, phase modulation, digital signal processing (DSP), digital receivers, carrier recovery.**

I. INTRODUCTION

The next generation broadband access networks are striving for convergence of wired and wireless service delivery to the end users over a unified networking platform (see Fig. 1). Radio over fiber (RoF) technology is a promised candidate to realize an effective unified network platform because of its transparent transmission of various types of radio services [1].

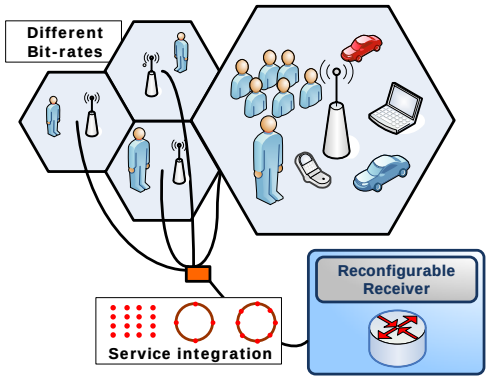

Fig. 1. Next generation broadband access networks supporting mixed services, mix bit rate and diverse modulation formats.

However, in addition to accommodate the increasing demand for greater bandwidth, access networks will need to be flexible to support emerging services while keeping the overall cost and complexity low. Diversity of emerging services is presenting a new set of challenges to be faced in the design of receivers such as transparency and adaptability to advance modulation formats and different bit rates. Recently, we proposed quadrature phase shift keying (QPSK) modulated subcarrier multiplexed signals (SCM) in coherently detected optical phase-modulated radio-over-fiber (RoF) systems for achieving increased spectral efficiency and link linearity [2]. In addition, SCM in phase-modulated RoF systems present higher robustness against fiber nonlinearities than the scenario for intensity modulation and direct detection (IM/DD) systems. To accomplish it, an optical coherent receiver supported by digital signal processing is required for linear signal demodulation. For moving toward higher order modulation formats such as quadrature amplitude modulated (QAM) signals; reconfigurable algorithms for digital RF carrier recovery have been investigated [3, 4].

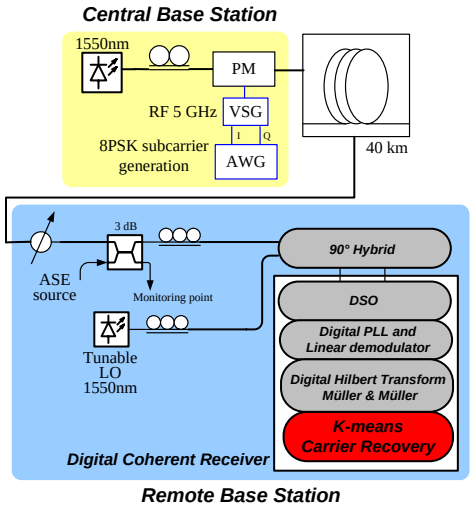

Fig. 2. Experimental setup for demonstration of three-channel SCM phase-modulated optical signal, employing 50 Mbaud 8PSK (frequency band: 4.6 GHz – 5.4 GHz) and 312.5 Mbaud 16QAM modulation and using digital coherent detection.

Recently we have proposed and experimentally demonstrated a novel approach for radio frequency (RF) carrier recovery for QPSK modulated Wavelength Division Multiplexed (WDM) RoF channels based on the flexible *k*-means algorithm [5]. In this paper, we present an upgrade of the *k*-means algorithm to demodulate three 8PSK SCM signals for increasing the transmission capacity of our phase-modulated RoF optical link. We also present an adaptation of our carrier recovery scheme

All authors are with the DTU Fotonik-Department of Photonics Engineering, Technical University of Denmark, DK-2800 Kgs. Lygnby, Denmark. (E-mail: ngo@fotonik.dtu.dk).

for 16QAM signals demonstrating its feasibility for a wide variety of modulation formats. We successfully demonstrate for a phase-modulated RoF downlink a signal demodulation of 3 channels subcarrier multiplexed optically phase-modulated RoF link, employing 50 Mbaud 8PSK modulation format of subcarriers around a 5 GHz frequency after 40 km of standard Single Mode Fibre (SMF) transmission. Signal demodulation of a 312.5 Mbaud 16QAM single carrier at 5 GHz is also demonstrated after 40 km of transmission.

II. Experimental Setup

The experimental setup for a phase-modulated radio-over-fibre optical link employing multi-channel subcarrier modulation is shown in Fig. 2. The transmitter consists of a tuneable Distributed Feedback Laser (DFB), with a linewidth of ~3 MHz in the range of 1550 nm. The output of the transmitter laser is then connected to an optical phase modulator (PM).

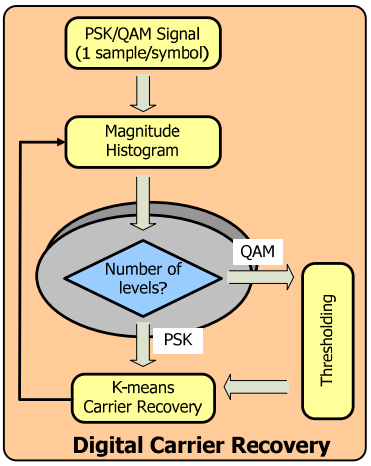

Fig. 3. Schematic diagram of the digital carrier recovery approach based on the k-means algorithm.

We use an Agilent N8241A arbitrary waveform generator (AWG) to generate three 50 Mbaud 8PSK and a 312.5 Mbaud single carrier 16QAM modulated digital data streams. The PSK generated digital data signals are then modulated onto 3 subcarriers with frequencies at 0, 200 and 400 MHz. Square root of raised-cosine filter is applied to the digital data streams in order to limit the signal bandwidth and reduce Interference Inter-symbols (ISI) between subcarriers. The outputs of the AWG are I and Q components of the modulated subcarriers and are then simultaneously fed to the Vector Signal Generator (VSG) where they are up-converted to a 5GHz carrier frequency. The output of the VSG is a 50 Mbaud multichannel SCM in the frequency range from 4.6 GHz to 5.4 GHz. The RF power driving the PM is set to 11 dBm. The optically phase modulated signal is launched into the optical fiber with an average power level of -1.8 dBm and transmitted over 40 km. The received optical power level was measure to be -9.5 dBm. The fiber is a standard single mode fiber (SMF) type. As a Local Oscillator (LO), a tuneable external cavity laser is used, with ~100 kHz linewidth and 0 dBm input power was delivered to the 90° optical hybrid. The in-phase and quadrature resultant signals after the 90° optical hybrid are detected with two pairs of balance photodiodes, with 7.5 GHz 3-dB bandwidth. The detected photocurrents are digitized using a sampling oscilloscope at 40 GSa/s for offline processing. The employed digital receiver uses carrier-recovery digital phase-locked loop (PLL) [2], linear signal demodulation [2], and a subcarrier demodulation approach including a digital Hilbert transform [2], our proposed *k*-means algorithm is used for RF phase estimation and signal demodulation.

III. Reconfiguration of the Carrier Recovery Approach for QAM Signals

The *k*-means is a scalable and flexible clustering algorithm which estimates centroids of clusters on a two dimensional (2D) space. Since the phase-offset is a constant rotation of the 2D constellation diagram of RF signals, *k*-means can be used for phase-offset estimation by calculating the angle of centroids after the clustering process [5]. Assuming perfect frequency estimation and synchronization, PSK carrier recovery based on the *k*-means algorithm can be reconfigured for 16QAM signals. Fig. 3 shows the schematic diagram of the reconfigurable carrier recovery approach based on the *k*-means algorithm. In the beginning, to identify among PSK and QAM signals, the number of amplitude levels is calculated by analysing the magnitude histogram. For the case of QAM signals (multilevel signals), the input signal must be adjusted before clustering by the extraction of QAM symbols whose magnitude on the constellation diagram correspond to the lowest amplitude level (thresholding, see Fig. 4). The QAM extracted symbols are in any case a sub-QPSK constellation and then, the already demonstrated carrier recovery approach based on the *k*-means algorithm is applied. It is important to notice the reduction of complexity in the case of QAM signals in terms of computational operations since only four clusters from the constellation are used for phase estimation.

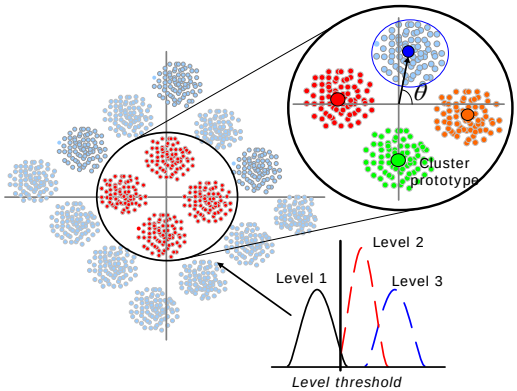

Fig. 4. Principle of operation of *k*-means for multilevel signals.

IV. Experimental Results

Fig. 5(a) shows the frequency spectrum of the three-channel subcarrier-multiplexed phase-modulated optical signal. It is shown that the reconstruction of the whole optical field is achieved after removing the frequency offset between the lasers by the DPLL. Double-sideband subcarriers occupying the frequency range from 4.6 to 5.4 GHz are clearly observed in the shown frequency spectrum. Fig. 5(a) also shows that the

subcarriers located at 4.8 and 4.6 GHz have their respective amplitudes 10 and 20 dB lower than the amplitude on the frequency spectrum of the central subcarrier as a consequence of the frequency response of the used AWG. This amplitude difference is also reflected in Fig. 6(a) and explained in the next paragraph. Fig. 5(b) shows an example of the constellation of demodulated 8PSK SCM signal for 11 dB optical-signal-to-noise-ratio (OSNR). The constellation points look clear and well separated.

The bit error rate (BER) curves as a function of the OSNR for the three 8PSK SCM channels for back-to-back (B2B) and after 40 km of fiber transmission are presented in Fig. 6(a). At BER value of 10^{-3}, OSNR penalties of 8 dB and 14 dB, compared to that of the subcarrier at 5GHz, can be observed for the subcarriers at 4.8 GHz and 4.6 GHz, respectively. This is due the difference in amplitude on the frequency spectrum between subcarriers shown in Fig. 5(a).

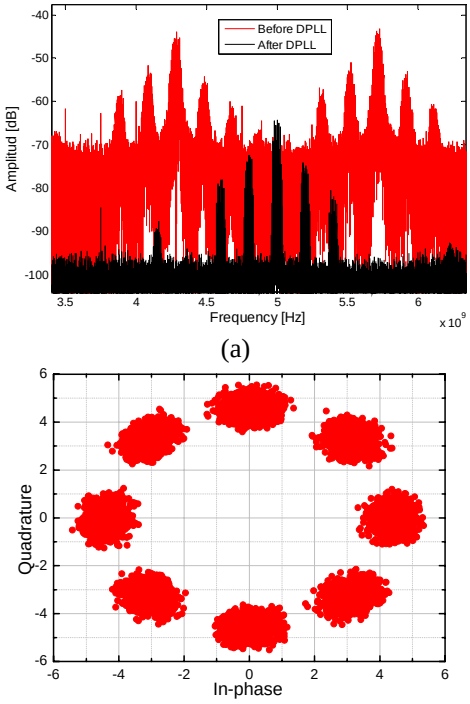

Fig. 5. (a) Frequency spectrum of the sampled complex optical signal before and after carrier-recovery DPLL. (b) Constellation of demodulated 50 Mbaud 8PSK SCM at 11 OSNR, subcarrier frequency 5 GHz.

For all three channels, a BER value below 10^{-3} is achieved after 40 km of fiber transmission. An OSNR penalty of approximately 2.5 dB for fibre transmission is observed compared to B2B, attributed mainly to chromatic dispersion as no signal impairment compensating algorithm was applied. Finally, Figure 6(b) shows the BER curve as a function of the OSNR for a single carrier at 5 GHz of a 312.5 Mbaud 16QAM. A BER value below 10^{-4} is achieved.

V. Conclusion

Successful signal demodulation of 8PSK SCM and a single carrier 16QAM using the proposed reconfigurable and low complexity RF carrier recovery scheme based on the *k*-means algorithm is experimentally demonstrated. Successful demodulation is achieved after 40 km of SMF transmission for a phase modulated radio-over-fiber link. The proposed digital carrier recovery approach shows prospect for unified networking platforms due its flexibility and low complexity implementation.

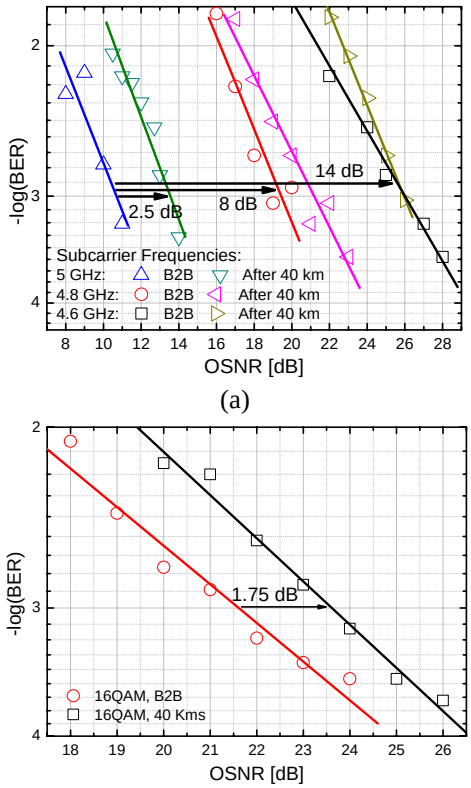

Fig. 6. (a) BER curves as a function of OSNR for the three 8PSK, SCM channels at 50 Mbaud optical phase-modulated RoF link for back-to-back and after 40 km of fiber transmission. (b) BER curve as a function of OSNR for a single carrier at 5GHz of a 312.5 Mbaud 16QAM signal for back-to-back and after 40 km of fiber transmission.

References

[1] K. Tsukamoto, T. Yamagami, T. Higashino and S. Komaki, "Radio on Fiber Technologies and Their Application toward Universal Platform for Heterogeneous Wireless Services," PIERS proceedings, 2009.

[2] D. Zibar, K.J. Larsen and I. Tafur Monroy, "Digital coherent receiver for subcarrier multiplexed phase-modulated radio-over-fibre signals," *Electronics Letters*, vol. 45, no. 11, May 2009.

[3] M. Seimetz, "Performance of Coherent Optical Square-16-QAM-Systems based on IQ-Transmitters and Homodyne Receivers with Digital Phase Estimation," Proc. Of OFC 2006, NWA4.

[4] T. Pfau, S. Hoffmann and R. Noé, "Hardware-Efficient Coherent Digital Receiver Concept With Feedforward Carrier Recovery for M-QAM Constellations," *Journal of Lightwave Technology* vol. 27, no. 8, April 15, 2009.

[5] N. Guerrero G., D. Zibar, A. Caballero, I. Tafur Monroy, "Experimental 2.5 Gbit/s QPSK WDM Phase Modulated Radio-over-Fiber Link with Digital Demodulation by a K-means Algorithm," *IEEE Photonics Technology Letters*, vol. 22, no. 5, pp. 335-337, 2010.

Paper 5: Optical phase-modulated radio-over-fiber links with k-means algorithm for digital demodulation of 8PSK subcarrier multiplexed signals

Guerrero Gonzalez Neil, Zibar Darko, Yu Xianbin, Tafur Monroy Idelfonso. "Optical phase-modulated radio-over-fiber links with k-means algorithm for digital demodulation of 8PSK subcarrier multiplexed signals", in *the Optical Fiber Communication Conference and Exposition and the National Fiber Optic Engineers Conference, OFC'2010,* San Diego, CA, USA., March 2010.

Optical Phase-Modulated Radio-over-Fiber Links with K-means Algorithm for Digital Demodulation of 8PSK Subcarrier Multiplexed Signals

Neil Guerrero Gonzalez, Darko Zibar, Xianbin Yu and I. Tafur Monroy
DTU Fotonik, Department of Photonics Engineering, Technical University of Denmark, DK-2800 Kgs. Lygnby, Denmark.

Abstract: A *k*-means algorithm for phase recovery of three, 50 Mbaud, 8PSK subcarrier multiplexed signals at 5 GHz for optical phase-modulated radio-over-fiber is proposed and experimentally demonstrated after 40 km of single mode fiber transmission.

OCIS codes: (060.1660) Coherent communications, (120.5060) Phase modulation

1. Introduction:

Sub-carrier multiplexing (SCM) with multi-level phase shift keying (PSK) modulation in coherently detected optical phase-modulated radio-over-fiber (RoF) systems allows for substantial increase of bit rates without increasing the symbol rate or the required bandwidth [1]. However, to accomplish it, an optical coherent receiver based on digital signal processing is required for linear signal demodulation [2, 3]. Recently, several digital coherent receiver schemes for single and multiple carrier transmission have been reported for intensity/phase modulated RoF links [1, 3, 4]. A major identified challenge for such systems is phase recovery in the presence of phase noise and other signal impairments [5]. Most of the considered approaches for phase recovery such as those based on maximum likelihood, decision-driven and non-data dependency schemes for PSK signals [3,6] face serious complexity challenges when moving to a higher number of phase levels or for other complex modulation formats [5]. In this paper, we propose and experimentally demonstrate a clustering algorithm called *k*-means [7] for radio-frequency (RF) phase recovery of multi-channel 8PSK multiplexed signals in optically phase-modulated RoF links. Since the operation principle of *k*-means is based on two-dimensional Euclidian distances and average operations on the data, it requires extraction of more statistical information, for example compared to the Viterbi & Viterbi algorithm. However; raising the complex data to the *m*-power for an *m*-level modulation format is not required [7]. We successfully demonstrate signal demodulation of 3 channels subcarrier multiplexed optically phase-modulated RoF link, employing 50 Mbaud 8PSK modulation of subcarriers around a 5 GHz frequency after 40 km of standard Single Mode Fibre (SMF) transmission.

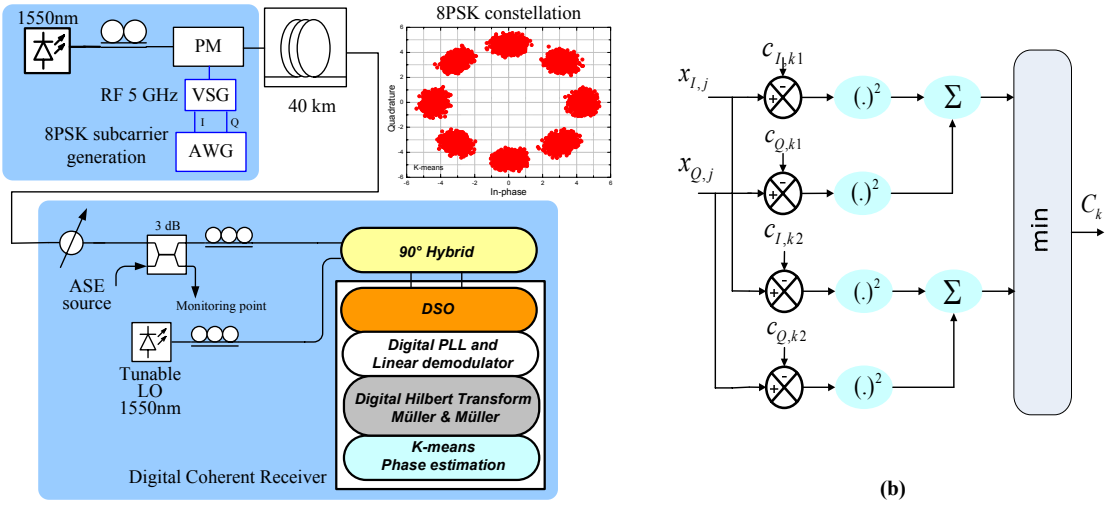

Fig.1 (a) Experimental setup for demonstration of three-channel subcarrier-multiplexed phase-modulated optical signal, employing 50 Mbaud 8PSK modulation (frequency band: 4.6 GHz – 5.4 GHz) and using digital coherent detection. (b) Outline of the proposed RF phase recovery approach based on a k-means algorithm.

2. Experimental setup

The experimental setup for a phase-modulated radio-over-fibre optical link employing multi-channel

978-1-55752-884-1/10/$26.00 ©2010 IEEE

subcarrier modulation is shown in Fig. 1(a). In Fig. 1(a) it is also shown an example of a constellation diagram of a 50 Mbaud 8PSK data signal (5 GHz RF carrier frequency) recovered from the three-channel subcarrier-multiplexed phase-modulated optical signal after phase compensation. The transmitter consists of a tuneable Distributed Feedback Laser (DFB), with a linewidth of ~3 MHz in the range of 1550 nm. The output of the transmitter laser is then connected to an optical phase modulator (PM). We use an Agilent N8241A arbitrary waveform generator (AWG) to generate three 50 Mbaud 8PSK modulated digital data streams. The generated digital data signals are then modulated onto 3 subcarriers with frequencies at 0, 200 and 400 MHz. Square root of raised-cosine filter is applied to the digital data streams in order to limit the signal bandwidth and reduce Interference Inter-symbols (ISI) between subcarriers. The outputs of the AWG are I and Q components of the modulated subcarriers and are then simultaneously fed to the Vector Signal Generator (VSG) where they are up-converted to a 5GHz carrier frequency. The output of the VSG is a 50 Mbaud multichannel SCM in the frequency range from 4.6 GHz to 5.4 GHz. The RF power driving the PM is set to 11 dBm.

The optically phase modulated signal is launched into the optical fiber with an average power level of -1.8 dBm and transmitted over 40 km. The received optical power level was measure to be -9.5 dBm. The fiber is a standard single mode fiber (SMF) type. As a Local Oscillator (LO), a tuneable external cavity laser is used, with ~100 kHz linewidth and 0 dBm input power was delivered to the 90° optical hybrid. The in-phase and quadrature resultant signals after the 90° optical hybrid are detected with two pairs of balance photodiodes, with 7.5 GHz 3-dB bandwidth. The detected photocurrents are digitized using a sampling oscilloscope at 40 Gs/s for offline processing. The employed digital receiver uses carrier-recovery digital phase-locked loop (PLL) [3], linear signal demodulation [3], and a subcarrier demodulation approach including a digital Hilbert transform [1], our proposed k-means algorithm is used for RF phase estimation and signal demodulation.

3. The *k*-means algorithm for RF phase recovery

Once the resultant I and Q signals, after coherent detection, are digitized and processed through the DPLL, the linear signal demodulator, the digital Hilbert transform and the Müller and Müller synchronizer [3], a set of n two-dimensional data points forming the 8PSK constellation is given. By estimating coordinates of clusters centres of the constellation, phase off-set estimation is a straightforward computation spatial coordinates of each cluster can be calculated. Fig. 1(b) shows the schematic diagram of our approach for RF recovery using *k*-means.

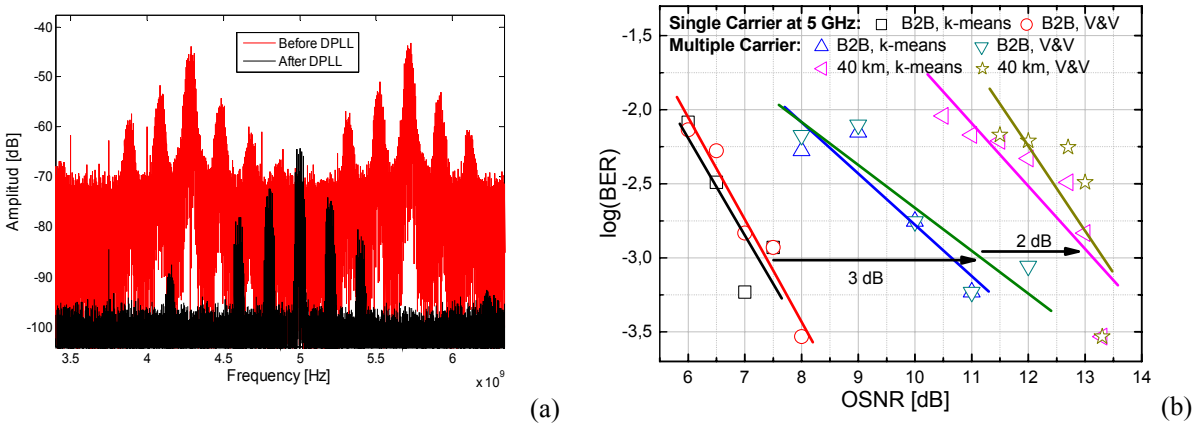

Fig.2 (a) Frequency spectrum of the sampled complex optical signal before and after carrier-recovery DPLL. (b) BER as function of OSNR for Viterbi & Viterbi and k-means phase estimators for subcarrier at 5 GHz for back-to-back and 40 km transmission.

For each complex 8PSK data point, its two-dimensional Euclidian distance to every initial cluster centre $C_{I,k}$, $C_{Q,K}$ (fixed from an initial subset of data points) is computed by squaring the arithmetical difference to the reference centres coordinates and adding up results from both the In-phase and Quadrature components. A complex data point is assigned to a class k centre to which its distance is the shortest. Subsequently, the cluster centres are refined iteratively by calculating the average value of centres in each class per iteration.

4. Experimental Results

Fig. 2(a) shows the frequency spectrum of the three-channel subcarrier-multiplexed phase-modulated optical signal. It is shown that the reconstruction of the whole optical field is achieved after removing the frequency offset between the lasers by the DPLL. Double-sideband subcarriers occupying the frequency range from 4.6 to 5.4 GHz are clearly observed in the shown frequency spectrum. Fig. 2(a)

also shows that the subcarriers located at 4.8 and 4.6 GHz have their respective amplitudes 10 and 20 dB lower than the amplitude of the central subcarrier as a consequence of the frequency response of the used AWG. This amplitude difference is also reflected in Fig. 3(a) and explained in the next paragraph. Figure 2(b) shows the BER curves for the subcarrier located at 5 GHz, after phase compensation, using the proposed k-means and a Viterbi & Viterbi phase estimators. No substantial difference is observed between Viterbi & Viterbi and k-means performance confirming its good operation.

In addition to the multichannel subcarrier (MSC) scenario, we consider for the back-to-back (B2B) case a single carrier (SC) at 5GHz carrier frequency for reference purposes. The BER curves for B2B transmission for MSC/SC are presented in Fig. 3(a). For a fixed RF power driving the PM, there is a penalty of 3 dB between the carrier at 5GHz transmitted in a SC and MSC configuration. At BER value of 10^{-3}, OSNR penalties of 8 dB and 14 dB, compared to that of the subcarrier at 5GHz for the MSC scenario, can be observed for the subcarriers at 4.8 GHz and 4.6 GHz, respectively. This is due the difference in amplitude between subcarriers shown in Fig. 2(a). For the 40 km fibre transmission case, we consider only MSC simultaneous transmission. In Fig. 3(b), the BER curve of each demodulated individual subcarrier channel is computed as a function of OSNR after transmission. For all three channels, a BER value below 10^{-3} is achieved. Compared to the subcarrier at 5GHz, the subcarriers at 4.8 GHz and 4.6 GHz experience OSNR penalties of 8 dB and 13 dB respectively. A OSNR penalty of approximately 2 dB for after fibre transmission is observed compared to back-to-back attributed mainly to chromatic dispersion as no signal impairment compensating algorithm was applied.

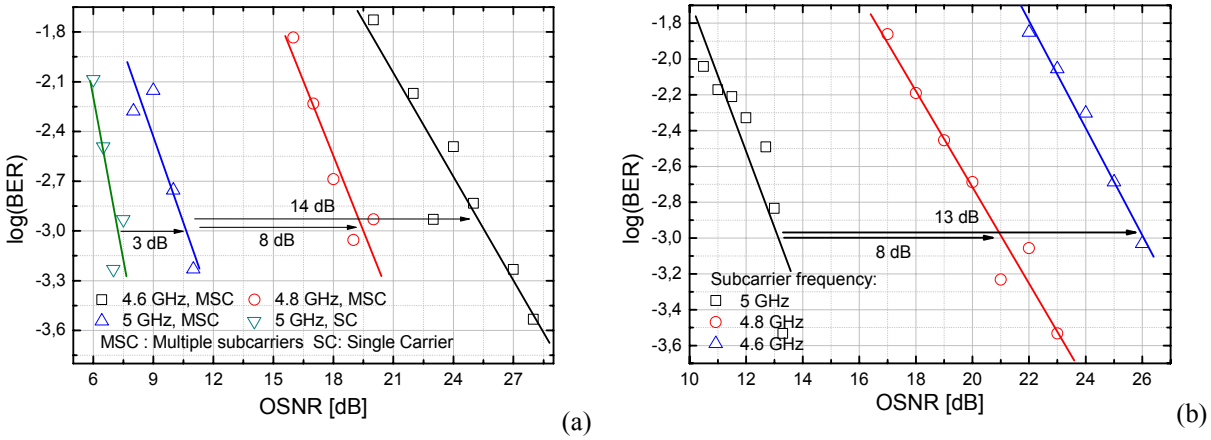

Fig.3 (a) Back-to-back BER curves as a function of OSNR for a single carrier at 5 GHz carrier frequency and for the three 8PSK, SCM channels at 50 Mbaud optical phase-modulated RoF link. (b) BER curves as a function of OSNR for the three channels SCM channels after 40 km of fibre transmission.

5. Conclusions

Successful signal demodulation of three channels subcarrier multiplexed signal, using a proposed *k*-means algorithm for RF phase recovery, for 50 Mbaud, 8PSK modulation (frequency band: 4.6 GHz – 5.4 GHz), has been experimentally shown after 40 km of SMF transmission for a phase modulated radio-over-fiber link. The proposed *k*-means algorithm for RF phase recovery shows prospect for operation with higher order modulation formats due its flexible configurationally and simplicity for digital implementation.

6. References

[1]. D. Zibar, K.J. Larsen and I. Tafur Monroy, "Digital coherent receiver for subcarrier multiplexed phase-modulated radio-over-fibre signals," Electronics Letters, vol. 45, no. 11, 21st May 2009.

[2]. T. R. Clark, and M. L. Dennis, "Coherent Optical Phase-Modulation Link," IEEE Photonics Technology Letters, vol. 19, no. 16, pp. 1206-1208, August 15, 2007.

[3]. D. Zibar, X. Yu, C. Peucheret, P. Jeppesen and I. Tafur Monroy, "Digital Coherent Receiver for Phase-Modulated Radio-Over-Fiber Optical Links", IEEE Photon,. Techol. Lett., vol. 21, no. 3, pp. 155-157, Feb. 2009.

[4]. N. Guerrero G., D. Zibar, A. Caballero, I. Tafur Monroy, "Experimental 2.5 Gbit/s QPSK WDM Coherent Phase Modulated Radio-over-Fibre Link with Digital Demodulation by a K-means Algorithm," Proc. of ECOC 2009, P3.15.

[5]. T. Pfau, S. Hoffmann and R. Noé, "Hardware-Efficient Coherent Digital Receiver Concept With Feedforward Carrier Recovery for M-QAM Constellations," Journal of Lightwave Technology vol. 27, no. 8, April 15, 2009

[6]. S.J. Savory, "Electronic Signal Processing in Optical Communications" Proc. of SPIE, vol. 7136, pp. 71362C-1 - 71362C-9, 2008.

[7]. J. G. Proakis, Digital Communications. McGraw-Hill (1989). Chapter 2, pp. 120-126.

Paper 6: K-means Algorithm for joint Frequency and Phase Offset Compensation in Digital Receivers for Phase-Modulated Radio-over-Fiber Links

Guerrero Gonzalez Neil, Zibar Darko, Yu Xianbin and Tafur Monroy Idelfonso. "K-means Algorithm for joint Frequency and Phase Offset Compensation in Digital Receivers for Phase-Modulated Radio-over-Fiber Links", under review in *Optical Fiber Technology*, 2011.

K-means Algorithm for joint Frequency and Phase Offset Compensation in Digital Receivers for Phase-Modulated Radio-over-Fiber Links

Neil Guerrero Gonzalez[1,*], Darko Zibar[1], Idelfonso Tafur Monroy[1]

[1] *DTU Fotonik, Technical University of Denmark, Oersteds Plads 343, DTU Campus, 2800 Kgs. Lyngby, Denmark*

** Neil Guerrero Gonzalez*

DTU Fotonik, Technical University of Denmark

Oersteds Plads 343, DTU campus, Office 214

2800 Kgs. Lyngby, Denmark

Tel.: +45 2639 5313

Email: nggo@fotonik.dtu.dk

Abstract

A joint RF frequency and phase offset compensation based on the *k*-means algorithm for digital coherent receivers for optical phase-modulated (PM) radio-over-fiber (RoF) signals is proposed and experimentally validated. The algorithm estimates the phase rotation on the constellation diagram between consecutive time-blocks of the received signal followed by subsequent phase de-rotation of each time-block constellation diagram. The proposed algorithm compensates up to 30 kHz of frequency offset using 500 data-symbols per time-block and is experimentally validated on 8-phase-shift-keying (8PSK) modulation format signals after 40 km of optical transmission.

Keywords: carrier recovery; radio-over-fiber; coherent communication; digital receivers component

1. Introduction

Optical phase-modulated (PM) radio over fiber (RoF) systems are a promising candidate for next generation broadband access networks in a range of applications such as last mile solutions for delivering integrated service to end-users as well as extend the existing radio coverage and capacity by simplifying antenna base station (see Fig. 1) [1]. However, optical PM links require an optical coherent receiver combined with digital signal processing (DSP) modules for detection and linear signal demodulation [1, 2]. Furthermore, the integration of DSP modules into coherent receivers has brought additional benefits to PM RoF links. For instance, the increase on spur-free dynamic range (SFDR) compared to intensity-modulation direct-detection (IM-DD) [3] and optical transmission of advanced modulated radio-frequency (RF) signals [4] are straight consequences of having the optical field fully mapped into the electronic domain for further signal processing.

Such electronic processing for PM RoF systems can be classified into two stages: optical and RF frequency/phase offset compensation. This fact is because PM RoF systems have the information encoded into the phase of a RF carrier which then modulates the phase of the optical carrier. The first module (the digital phase-locked-loop, DPLL [2, 5]) removes the frequency/phase offset between the local oscillator (LO) and the optical carrier. Then, a second module is needed to remove the RF phase offset (RF carrier recovery) before signal demodulation. Carrier recovery (CR) is one of the most essential DSP functions in digital coherent receivers. CR consists of tracking and compensating rotations of the received constellation due to the phase mismatch between the transmitted signal and the local carrier used for frequency

down-conversion at the receiver [6]. The Viterbi-and-Viterbi algorithm [7] has been widely used for CR assuming constant carrier phase within the consecutive fourth powered symbols used for estimating the phase-offset. Lately, several CR algorithms have been proposed including feedback phase-locked loop and feedforward phase estimation [8].

However, time-varying rotations of the constellation diagram caused by uncompensated optical frequency offset between the LO and the optical carrier (usually in the order of kHz) reduce the estimation performance of RF carrier recovery schemes. In fact, the DPLL used in the first stage for optical frequency/phase offset compensation is limited to track frequency-offset values in the range of kHz due the very high computational cost required by numerical methods to increase the resolution of the spectral analysis of the signal.

Recently, we have proposed for digital demodulation of PM RoF signals a reconfigurable RF carrier recovery approach based on the *k*-means algorithm for quadrature phase shift keying (QPSK), 8PSK and 16 quadrature amplitude modulated (QAM) RF signals [4]. The *k*-means is a clustering algorithm applied on the constellation diagram where the RF phase-offset (see Fig. 3) is estimated by calculating the angle of centroids belonging to each cluster (complex data-symbols on the constellation diagram) [9].

In this paper we propose a joint RF frequency/phase offset compensation based on the *k*-means algorithm. The proposed approach is able to track up to 30 kHz of frequency offset using 500 data-symbols per time-block for 312.5 Mbaud 8PSK RoF signal after 40 km of optical transmission. Additionally, the parallel structure of the

proposed scheme allows iterative RF carrier recovery simplifying even more the digital receiver.

2. Experimental details

The experimental setup for a phase-modulated radio-over-fibre optical link employing 8PSK RF carrier modulation is shown in Fig. 2. The transmitter consists of a tuneable Distributed Feedback Laser (DFB), with a linewidth of ~3 MHz in the range of 1550 nm. The output of the transmitter laser is then connected to an optical phase modulator (PMod). We use an Agilent N8241A arbitrary waveform generator (AWG) to generate a 312.5 Mbaud 8PSK modulated digital data stream. Square root of raised-cosine filter is applied to the digital data in order to limit the signal bandwidth and reduce Interference Inter-symbols (ISI). The RF power driving the PMod is set to 11 dBm. The In phase (I) and Quadrature (Q) components outputs of the AWG are then simultaneously fed to the Vector Signal Generator (VSG) where they are up-converted to a 5GHz carrier frequency. The optically modulated PM signal is launched into the optical fiber with an average power level of -1.8 dBm and transmitted over 40 km. The received optical power level was measure to be -9.5 dBm. The fiber is a standard single mode fiber (SMF) type. As a Local Oscillator (LO), a tuneable external cavity laser is used, with ~100 kHz linewidth. Input power of 0dBm was delivered to the 90° optical hybrid. The in-phase and quadrature resultant signals after the 90° optical hybrid are detected with two pairs of balance photodiodes, with 7.5 GHz 3-dB bandwidth. The detected photocurrents are digitized using a sampling oscilloscope at 40 Gs/s for offline processing.

3. The Proposed Frequency and Phase Offset Compensation Algorithm

Fig. 3 shows the schematic diagram of the proposed frequency/phase offset compensation for a QPSK signal in presence of remained frequency offset. For a large number of data-samples, time-varying rotations on the constellation diagram due to uncompensated frequency-offset from the DPLL causes spreading effects on data-symbols (clusters). Such spreading effect (see Fig. 3 left side) increases the number of errors because the overlapping of rotated noisy data-symbols (*y*). To reduce the effect of remaining frequency-offset on the RF signal, we proposed to compensate the phase rotation between consecutive time-blocks of the signal by using the *k*-means algorithm [10]. The *k*-means is a scalable and flexible clustering algorithm which estimates centroids of clusters on a two dimensional (2D) space (the constellation diagram). Since the phase-offset is a rotation of the whole 2D constellation diagram of RF signals, *k*-means can be used for phase-offset estimation by calculating the angle of centroids after the clustering process [9].

Fig. 3 (right side) and Eq. 1 illustrates the splitting process of an initial constellation formed by *2N* data samples (Fig. 3, left side) into two consecutive time-blocks containing each of them *N* data symbols (the dark and the clear time-blocks).

$$y(1:2N) = [y_{clear}(1:N), y_{dark}(N+1:2N)] \quad \text{(Eq. 1)}$$

The maximum frequency-offset value to be estimated given a certain number of data-symbols per time-block can be calculated by applying the Eq. 2. The constant k for PSK signals is proportional to the maximum allowed symbol phase-deviation on the constellation diagram without interfering neighbour symbols (for instance, $\pi/8$

for 8PSK signals). The constant k for 8PSK signals is equal to $1/16$. Therefore, frequency-offset compensation using 500 data-symbols per time-block removes frequency-offset values up to 40 kHz for 312.5 Mbaud 8PSK signals under very high optical signal-to-noise ratios.

$$Frequecy\_Offset = \frac{Baud\_rate}{k.(data-symbols/time-block)} \quad \text{(Eq. 2)}$$

To estimate the centroid of each PSK cluster, the proposed RF carrier recovery based on the *k*-means algorithm [9] is applied separately to the two constellations for estimating phase-offset values α and β. The time-varying phase rotation represented by the angular difference $\alpha - \beta$ is removed by de-rotating the constellation of the time-block ahead in time (y_{dark}) by $\alpha - \beta$ degrees. Therefore, the new time-block represented by $\tilde{y}_{dark}$ is obtained by applying the Eq. 3.

$$\tilde{y}_{dark} = y_{dark} e^{-j(\alpha-\beta)} \quad \text{(Eq. 3)}$$

4. Results

Fig. 4 shows an example of the constellation of demodulated back-to-back (B2B) 8PSK RF signal for an optical-signal-to-noise-ratio (OSNR) of 18 dB at 0.1-nm resolution bandwidth before and after frequency/phase offset compensation. In Fig. 4(a) it is seen the spreading effect on clusters produced by the uncompensated frequency offset. By splitting the RF signal into blocks of 1000 complex 8PSK data-

symbols and processing each of them following the approach illustrated in Fig. 3, clusters become more separated as it is shown in Fig. 4(b).

The bit error rate (BER) curves as a function of the OSNR for the 312.5 Mbaud 8PSK RoF signal with and without frequency offset compensation after 40 km of fiber transmission are presented in Fig. 5(a). The 8PSK constellation composed of 4.075 8PSK data-symbols (32.600 bits) is partitioned into time-blocks of 500 data symbols each, for frequency offset compensation. An improvement of 2.7 dB in the system performance is observed after frequency offset compensation.

To analyze the impact of the length of time-blocks in the performance of the proposed approach, we calculate the BER curve as a function of the number of data-symbols per time-block for two different values of OSNR at 0.1-nm resolution bandwidth (Fig. 5(b)). By generating a controlled frequency offset of 10 kHz at the digital receiver, we observe for both cases (20 dB and 22 dB of OSNR) a decrease of one order in the BER value (from 10-4 to 10-3) when the length of time-blocks is twice longer. The optimum length of the time-blocks must be estimated before signal demodulation (calibration stage) with a minimum value of 200 data-symbols to guarantee *k*-means convergence.

Fig. 6 shows the measured BER curve as a function of different controlled frequency-offset added at the digital receiver for three different values of OSNR. BER values below 10^{-3} are achieved up to 30 KHz of frequency offset for all three cases of OSNR (18 dB, 20 dB and 22dB). The length of time-blocks was fixed at 500 data-symbols.

5. Conclusions

We have proposed and experimentally demonstrated a joint frequency and phase offset compensation algorithm for digital coherent receivers for optical phase-modulated radio-over-fiber systems. Our approach is based on iterative phase de-rotation of the constellation diagram of consecutive time-blocks of the RF signal. The partitioning process of signals allows a parallel implementation of the proposed compensation algorithm relaxing computational costs in future real time applications. Successful demodulation for frequency offset values up to 30 kHz on a 312.5 Mbaud 8PSK phase-modulated radio-over-fiber signal is demonstrated after 40 km of transmission.

References

[1] N. J. Gomes, M. Morant, A. Alphones, B Cabon, J. E. Mitchell, C Lethien, M. Csörnyei, A. Stöhr and S. Iezekiel, Radio-over-fiber transport for the support of wireless broadband services, J. Opt. Networking, vol. 8, pp.156-178, Feb. 2009.

[2] D. Zibar, X. Yu, C. Peucheret, P. Jeppesen and I. Tafur Monroy, Digital Coherent Receiver for Phase-Modulated Radio-Over-Fiber Optical Links, IEEE Photon. Technol. Lett., vol. 21, no. 3, pp. 155-157, Feb. 2009

[3] T. R. Clark and M. L. Dennis, Coherent optical phase-modulation link, IEEE Photon. Technol. Lett., vol. 19, no. 16, pp. 1206–1208, Aug. 2007.

[4] N. Guerrero Gonzalez, D. Ziba and I. Tafur Monroy, Cognitive Digital Receiver for Burst Mode Phase Modulated Radio over Fiber Links, in Proc. European Conference on Optical Communications, (ECOC 2010), Torino, Italy, 2010, Paper P6.11.

[5] H. Meyr, M. Moeneclaey and S. A. Fechtel, Digital Communication Receivers: Synchronization, Channel Estimation and Signal Processing. Wiley, 1998. Chapter 5.

[6] Z. Tao, L. Li, L. Liu, W. Yan, H. Nakashima, T. Tanimura, S. Oda, T. Hoshida and J. C. Rasmussen, Improvements to Digital Carrier Phase Recovery Algorithm for High-Performance Optical Coherent Receivers, IEEE J. of Sel. Topics in Quantum Electronics, vol. 16, no. 5, pp. 1201-1209, Sept. 2010.

[7] A. J. Viterbi and A. M. Viterbi, Nonlinear estimation of PSK-modulated carrier phase with application to burst digital transmission, IEEE Trans. Inf. Theory, vol. IT-29, no. 4, pp. 543–551, Jul. 1983.

[8] M. G. Taylor, Phase estimation methods for optical coherent detection using digital signal processing, J. Lightw. Technol., vol. 27, no. 7, pp. 901–914, Apr. 2009.

[9] N. Guerrero G., D. Zibar, A. Caballero, I. Tafur Monroy, Experimental 2.5 Gbit/s QPSK WDM Phase Modulated Radio-over-Fiber Link with Digital Demodulation by a K-means Algorithm, IEEE Photon. Technol. Lett., vol. 22, no. 5, pp. 335-337, 2010.

[10] C. M. Bishop, Pattern Recognition and Machine Learning, Springer 2006, pp. 430-455.

Biography

 **Neil Guerrero** received the B.Sc. degree in electronics engineering from the Universidad Nacional de Colombia, Manizales, in 2005; a Graduate Diploma in M.Eng.Sc. degree from the Universidad Nacional de Colombia, Manizales, in 2007. He is currently pursuing a Ph.D. in Photonics at the Technical University of Denmark, with the metro-access and short range systems research group of the department of Photonics Engineering.

 **Darko Zibar** was born on December 9th, 1978, in Belgrade former Yugoslavia. He received the M.Sc. degree in Telecommunication in 2004 from the Technical University of Denmark and the Ph.D. degree in 2007 from the Department of Communications, Optics and Materials, COM$\bullet$DTU within the field of optical communications. He was a Visiting Researcher with Optoelectronic Research Group led by Prof. John E. Bowers, at the University of California, Santa Barbara (UCSB) from January 2006 to August 2006, and January 2008 working on coherent receivers for phase-modulated analog optical links. From Febryaru 2009 until Luly 2009, he was Visiting Researcher with Nokia-Siemens Networks working on digital clock recovery for 112 Gb/s polarization multiplexed systems. Currently, he is employed at DTU Fotonik, Technical University of Denmark as the Assistant Professor. His research interests are in the area of coherent optical communication, with the emphasis on digital demodulation and compensation techniques.

Darko Zibar is a recipient of the Best Student Paper Award at the IEEE Microwave Photonics Conference (MWP) 2006, for his work on novel optical phase demodulator based on a sampling phase-locked loop as well as Villum Kann Rasmussen postdoctoral research grant in 2007.

Idelfonso Tafur Monroy received the M.Sc. degree in multichannel telecommunications from the Bonch-Bruevich Institute of Communications, St. Petersburg, Russia, in 1992, the Technology Licenciate degree in telecommunications theory from the Royal Institute of Technology, Stockholm, Sweden, and the Ph.D. degree from the Electrical Engineering Department, Eindhoven University of Technology, The Netherlands, in 1999.

He is currently Head of the metro-access and short range communications group of the Department of Photonics Engineering, Technical University of Denmark. He was an Assistant Professor until 2006 at the Eindhoven University of Technology. Currently, he is a Professor at the Technical University of Denmark. He has participated in several European research projects, including the ACTS, FP6, and FP7 frameworks (APEX, STOLAS, LSAGNE, MUFINS). At the moment, he is in involved the ICT European projects Gi-GaWaM, ALPHA, BONE, and EURO-FOS. His research interests are in hybrid optical-wireless communication systems, coherent detection technologies and digital signal processing receivers for baseband and radio-over-fiber links, optical switching, nanophotonic technologies, and systems for integrated metro and access networks, short range optical links, and communication theory.

Figure captions

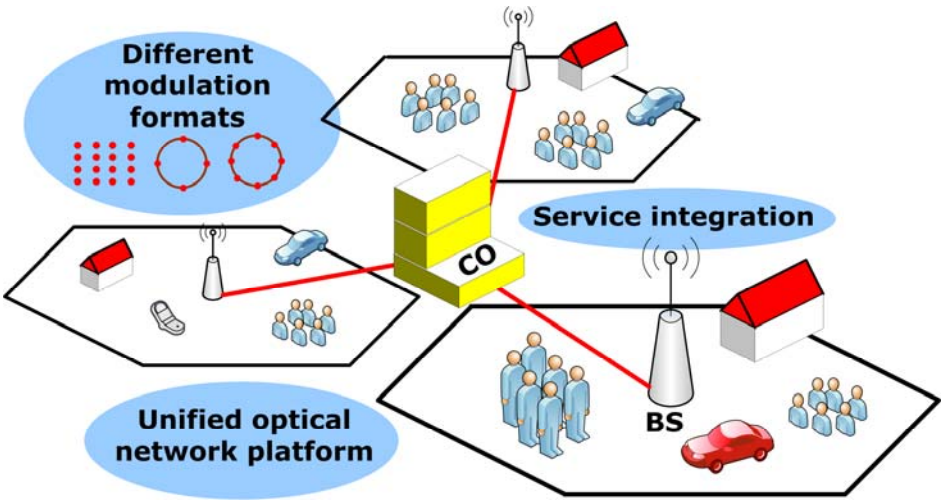

Fig 1. Next generation broadband access networks supporting mixed services, mix bit rate and diverse modulation formats.

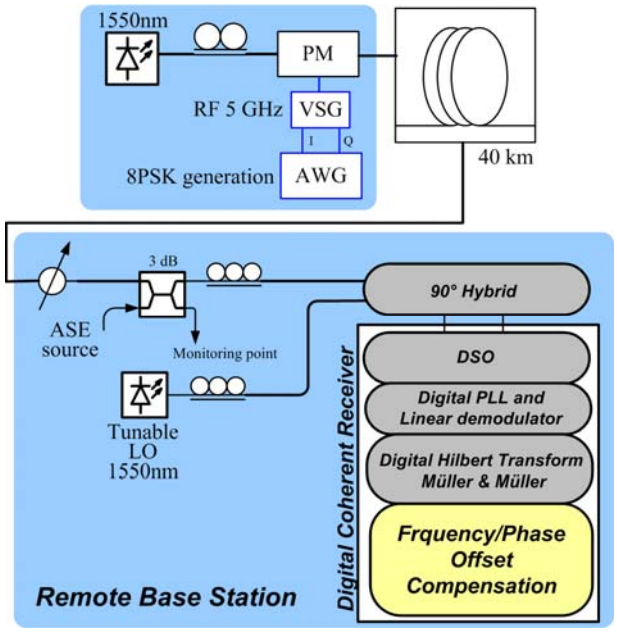

Fig.2. Experimental set-up for the demonstration of coherent phase-modulated RoF optical link. PBS: polarization Beam Splitter, VSG: Vector Signal Generator.

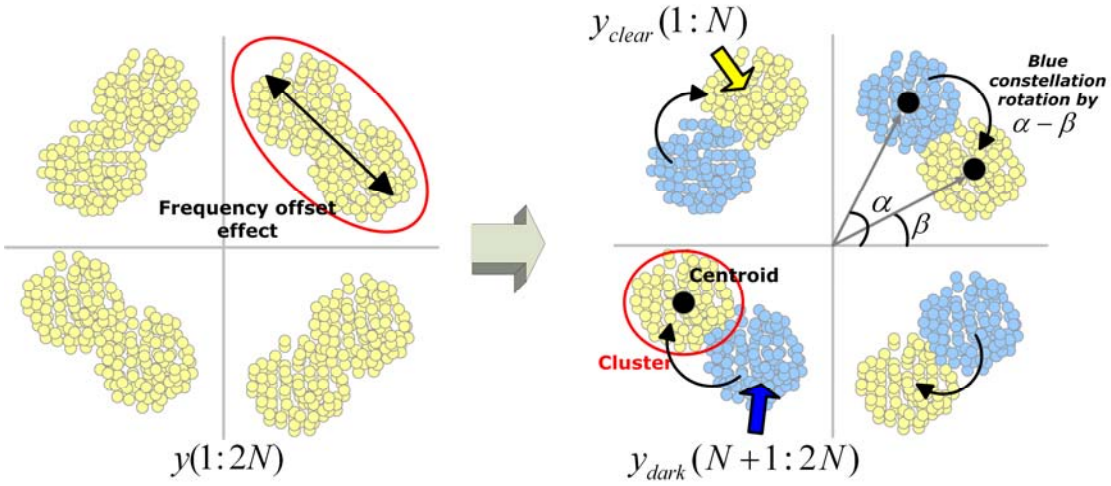

Fig.3. Schematic diagram of the proposed frequency and phase offset compensation approach

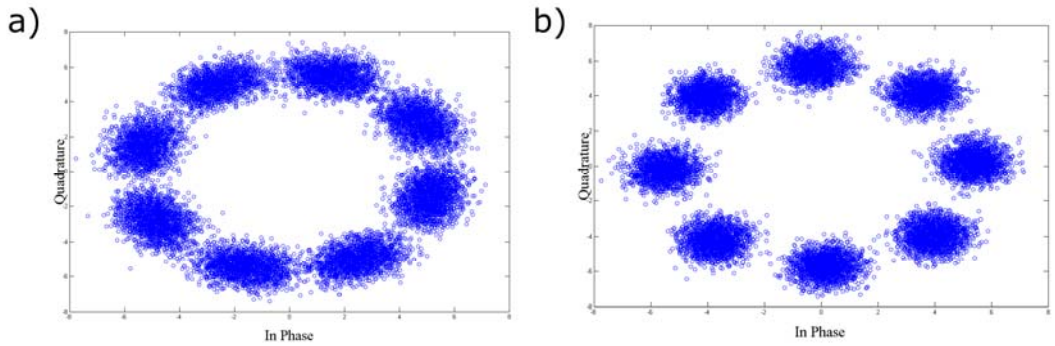

Fig.4. (a) 8PSK constellation diagram without frequency offset compensation. (b) 8PSK constellation diagram after frequency offset compensation.

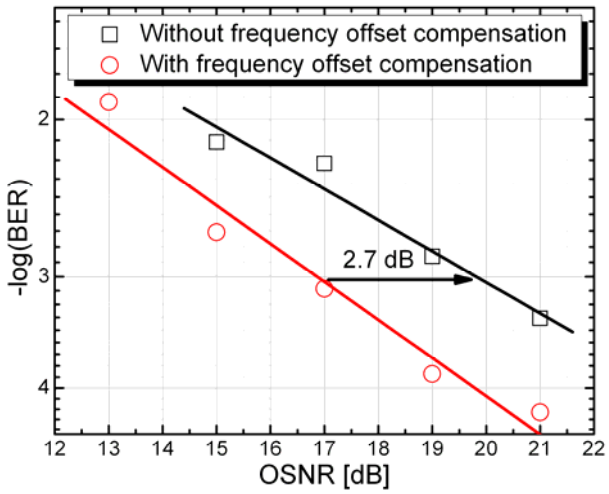

Fig.5. (a) BER curves as a function of OSNR at 0.1-nm resolution bandwidth with and without frequency offset compensation after 40 km of optical fiber transmission.

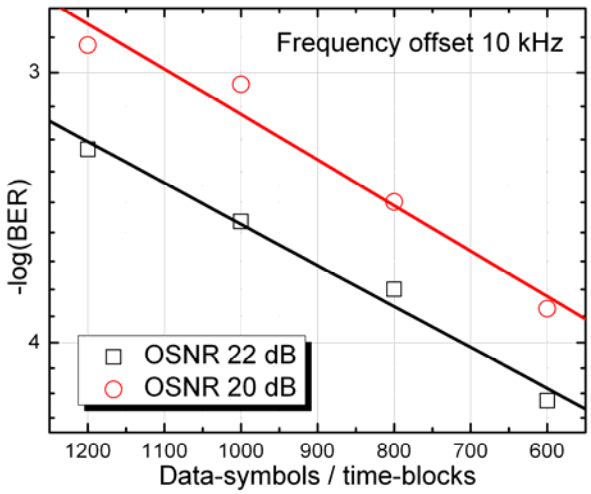

Fig.5 (b) BER curves as a function of the number of data-symbols per time-block for two different values of OSNR at 0.1-nm resolution bandwidth (20 dB and 22 dB) after 40 km of fiber transmission.

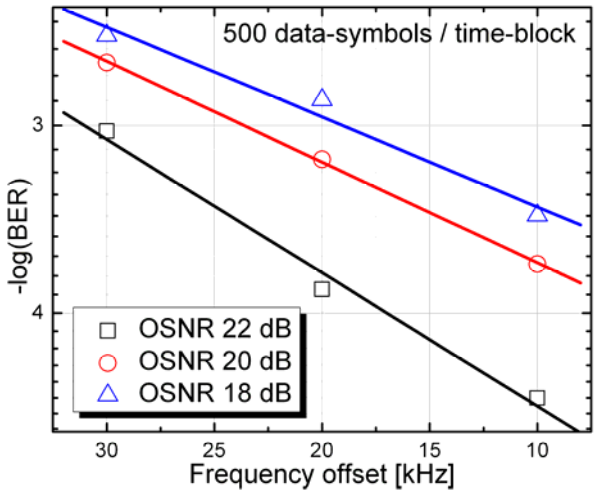

Fig.6. BER curves as a function of frequency offset values for three different conditions of OSNR at 0.1-nm resolution bandwidth (18 dB, 20 dB and 22 dB).

Paper 7: Cognitive digital receiver for burst mode phase modulated radio over fiber links

Guerrero Gonzalez Neil, Zibar Darko, Tafur Monroy Idelfonso. "Cognitive digital receiver for burst mode phase modulated radio over fiber links", in *the 36th European Conference on Optical Communication, ECOC'2010,* Torino, Italy, Paper P6.11, September 2010.

Cognitive Digital Receiver for Burst Mode Phase Modulated Radio over Fiber Links

Neil Guerrero Gonzalez[(1)], Darko Zibar[(1)] and Idelfonso Tafur Monroy[(1)]

[(1)] DTU Fotonik, Technical University of Denmark, Kgs. Lyngby, Denmark, nggo@fotonik.dtu.dk

Abstract *A novel cognitive receiver for modulation format recognition with reconfigurable carrier recovery scheme is proposed and experimentally demonstrated for phase modulated radio-over-fibre links. Demodulation of burst-mode mixed modulation formats (PSK and QAM) is demonstrated after 40km of transmission.*

Introduction

The next generation of broadband access networks is striving for a convergence of wired and wireless service delivery to the end users over a unified networking platform[1] (see Fig. 1). In addition to the increasing demand for greater bandwidth, in combination with diverse modulation formats and mixed bit rates of emerging services, access networks will need to be flexible while keeping the overall cost and complexity low[2]. The challenge of designing digital receivers compatible with different standards has started to be addressed by the Wireless Personal Area Networks (WPAN)[2] research community. However, in current WPANs, bit rates are low. For the next generation hybrid wireless-optical links which rely on radio-over-fiber (RoF) systems, a new set of challenges is added such as high-bit-rates and signal distortions from both the optical channel and the wireless environment. To our knowledge, no solutions for cognitive receivers for radio-over-fibre links employing optical phase modulation have been reported so far.

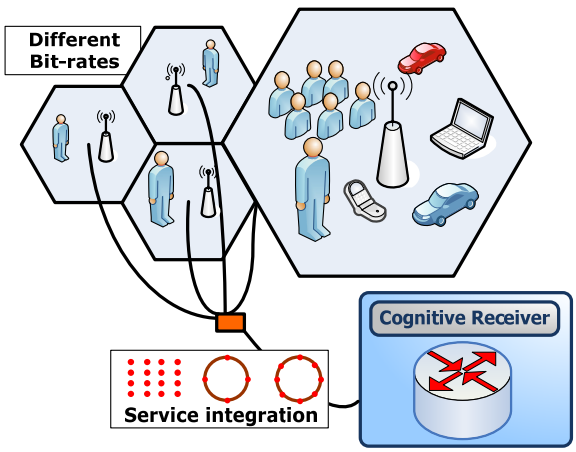

Fig. 1: Next generation broadband access networks supporting mixed services, mix bit rate and diverse modulation formats.

In this paper, we propose a cognitive digital receiver capable of signal modulation format recognition with corresponding reconfigurable carrier recovery scheme for phase shift keying (PSK) and quadrature amplitude modulated (QAM) signals. We experimentally demonstrate its successful operation for an optically phase-modulated RoF link transporting bursts of mixed modulation formats at 312.5 Mbaud QPSK, 8PSK and 16QAM data payloads. Error free operation achieved including 40 km of fiber transmission.

Setup Description

The experimental setup for a phase-modulated RoF optical link transporting burst mode mixed modulation formats (QPSK, 8PSK and 16QAM) is shown in Fig. 2. The transmitter consists of a tuneable Distributed Feedback Laser (DFB), with a linewidth of ~3 MHz in the range of 1550 nm. The output of the transmitter laser is then connected to an optical phase modulator (PM). We use an Agilent N8241A arbitrary waveform generator (AWG) to generate bursts of 312.5 Mbaud QPSK, 8PSK and 16QAM modulated digital data streams (see Fig. 2).

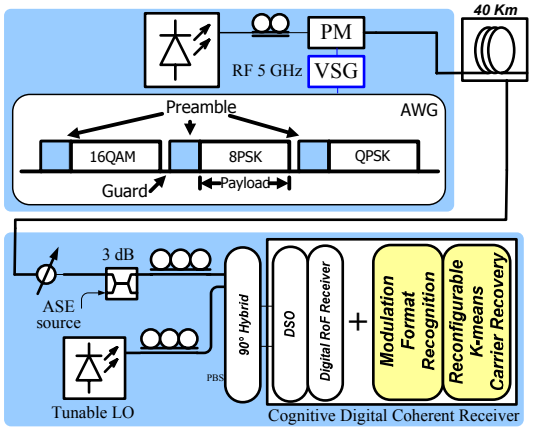

Fig. 2: General outline for the experimental setup for demonstration of burst mode mixed modulation formats phase-modulated RoF signals using the cognitive digital receiver.

Each burst is comprised of a 200-bit preamble of alternating ones and zeros and

978-1-4244-8535-2/10/$26.00 ©2010 IEEE

4000 symbols data payload. The 200-bit burst tail may also be used to facilitate the reception of a burst payload of an unknown length. The outputs of the AWG are the In-phase and Quadrature (I&Q) components of the modulated burst signal and are then simultaneously fed to the Vector Signal Generator (VSG) where they are up-converted to a 5GHz carrier frequency.

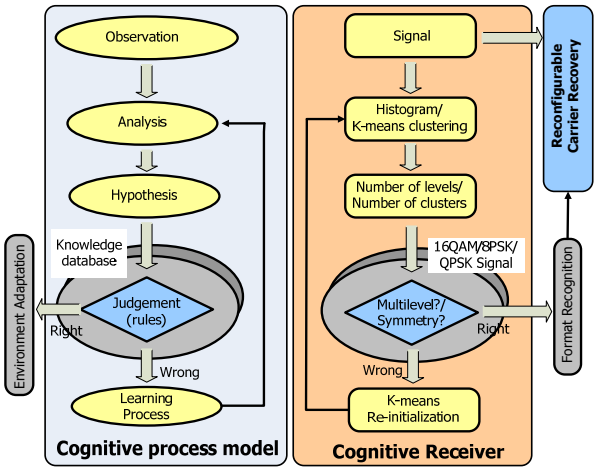

Fig. 3: Schematic diagrams of a cognitive process model and a Cognitive receiver.

The radio frequency (RF) power driving the PM is set to 10 dBm. The optically phase modulated signal is launched into the optical fiber with an average power level of -11 dBm and transmitted over 40 km of standard single mode fiber (SMF). The received optical power level was measured to be -19 dBm. As Local Oscillator (LO), a tuneable external cavity laser is used, with ~100 kHz linewidth and 0 dBm input power was delivered to the 90° optical hybrid. The in-phase and quadrature resultant signals after the 90° optical hybrid are detected with two pairs of balance photodiodes, with 7.5 GHz 3-dB bandwidth. The detected photocurrents are digitized using a sampling oscilloscope at 40 GSa/s for offline processing. The employed cognitive digital receiver uses optical carrier-recovery digital phase-locked loop[3] (PLL), linear signal demodulation[3], a subcarrier demodulation approach including a digital Hilbert transform[3] and our proposed signal modulation format recognition algorithm followed by a reconfigurable radio frequency (RF) carrier recovery scheme based on the *k*-means algorithm; as explained in the next section.

The Cognitive Digital Receiver

Fig 3 shows the schematic diagram of a generic cognitive process model and the corresponding functions in our proposed cognitive digital receiver. Digitized I&Q samples enter the cognitive receiver. The signal modulation format recognition (SMFR) is based on the statistical analysis of the signal and will provide the updating information to the carrier recovery module for subsequent demodulation. A first step is the estimation of the number of clusters on the two-dimensional (2D) I&Q constellation diagram and the number of levels on the histogram (hypothesis stage). The operation of finding the number of clusters is achieved by the *k*-means clustering algorithm on the constellation diagram. According to the generic cognitive process depicted in Fig. 2 (left) a testing stage based on rules follows.

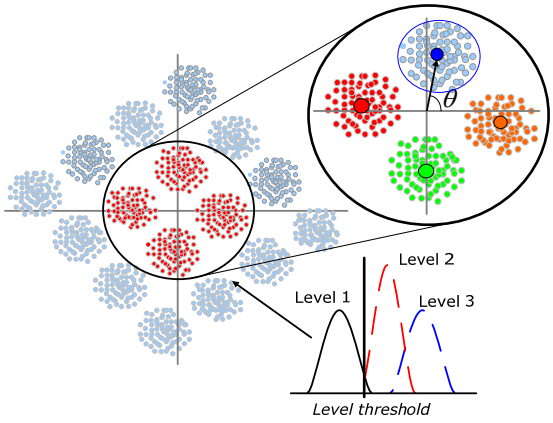

Fig. 4: Carrier recovery scheme for 16QAM signals.

Rules for format recognition judgement are derived according to modulation type characteristics and stored on a knowledge database. For example, for PSK and QAM signals, the number of levels on the magnitude histogram and the number of clusters on the constellation diagram are the two criteria to be judge for recognition of modulation format. Format identification among QAM and PSK signals is based on the number of levels (first rule) on the magnitude histogram. In the case of format identification between *m*-PSK modulation formats, a rule of symmetry must be satisfied for clusters recognized by the *k*-means algorithm. If the rule is not satisfied, the initial state of the *k*-means algorithm (the number of clusters expected to be found) is varied. This *k*-means re-initialization plays the role of the learning process in our cognitive receiver and it will go through all possible formats in the knowledge database until successful identification is achieved. Successful signal modulation format identification is achieved when the symmetry condition is satisfied for the number of clusters

found on the constellation.

Reconfigurable Carrier Recovery

The ability to demodulate signals with different modulation formats requires reconfigurable carrier recovery schemes. We adjust the input signal to the *k*-means algorithm for carrier recovery of square QAM signals by extracting symbols from the constellation with the lowest amplitude level on the magnitude histogram. Extracted symbols are treated as a sub-QPSK constellation and *k*-means carrier recovery is applied[4]. Fig 4 illustrates the principle of operation of *k*-means for a rotated 16QAM signal.

Results

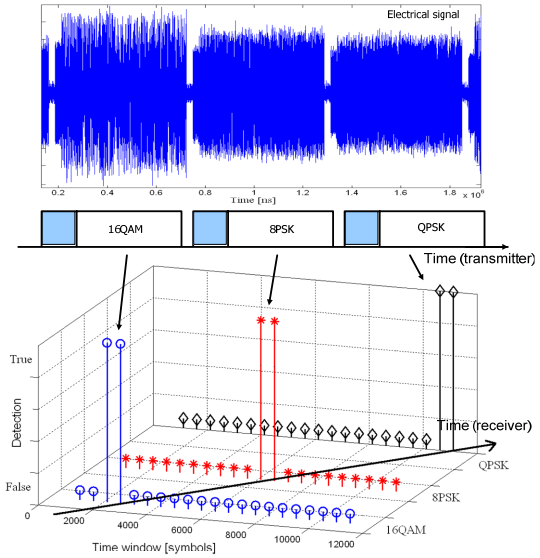

Fig. 5: Signal modulation format recognition for three data payloads with alternated QPSK, 8PSK and QAM modulation formats.

Fig 5 shows the results for signal modulation format detection for the case of three bursts of 4000-symbols data payloads each with alternating 16QAM, 8PSK and QPSK modulation formats. For this work 3500 symbols are used for recognition of modulation format. The SMFR is implemented as a sliding time-window. Modulation format recognition performance is shown over time (for the receiver) and it is consistent to the burst-mode signal transmitted. To demonstrate the performance of the cognitive feature of our digital receiver, we show in Fig 6 the bit error rate (BER) curves for back-to-back (B2B) and after 40 km of fiber transmission as a function of the optical signal to noise ratio (OSNR). For all three data payloads with alternated modulation formats a BER value below 10^{-3} is achieved for both scenarios. The difference on OSNR penalty for the QPSK data payload after transmission on Fig 6(b) is caused by burst power variations.

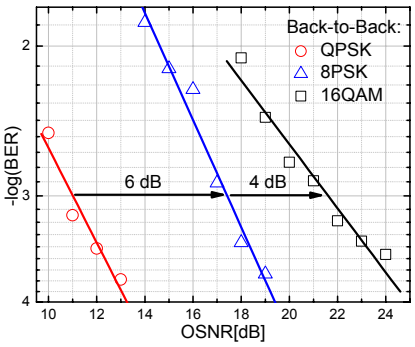

(a)

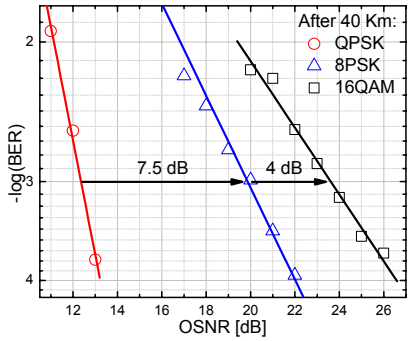

(b)

Fig. 6: (a) Back-to-back BER curves as a function of OSNR for all three payloads with alternated modulation formats at 312.5 Mbaud optical phase-modulated RoF link. (b) BER curves as a function of OSNR after 40 km of fibre transmission.

Conclusions

We experimentally demonstrated a cognitive digital receiver with integrated functions for signal modulation format recognition and reconfigurable carrier recovery based on the *k*-means algorithm. Successful demodulation of burst-mode mixed QPSK, 8PSK and 16QAM modulation formats in a phase-modulated RoF link is demonstrated after 40 km of transmission. The proposed cognitive digital receiver shows prospect for next generation access networks due its adaptability and flexibility.

References

1 Z. Jia et al., J. Lightwave Technol. **25**, 3452 (2007).
2 H. Schwetlick et al., Proc. ISCE'09, 761-764 (2009).
3 D. Zibar et al., PTL **21,** 155-157 (2009).
4 N. Guerrero et al., PTL **22,** 335-337 (2010).

Paper 8: Reconfigurable Digital Coherent Receiver for Metro-Access Networks Supporting Mixed Modulation Formats and Bit-rates

Guerrero Gonzalez Neil, Caballero Jambrina Antonio,
Borkowski Robert, Arlunno Valeria, Thang Pham Tien, Rodes Roberto, Zhang Xu, Binti Othman Maisara, Prince Kamau, Yu Xianbin, Bevensee Jensen Jesper, Zibar Darko and Tafur Monroy Idelfonso. "Reconfigurable Digital Coherent Receiver for Metro-Access Networks Supporting Mixed Modulation Formats and Bit-rates", accepted for oral presentation at *the Optical Fiber Communication Conference and Exposition and the National Fiber Optic Engineers Conference OFC'2011,* Los Angeles, USA., March 2011.

Reconfigurable Digital Coherent Receiver for Metro-Access Networks Supporting Mixed Modulation Formats and Bit-rates

Neil Guerrero Gonzalez, Antonio Caballero Jambrina, Robert Borkowski, Valeria Arlunno, Tien Thang Pham, Roberto Rodes, Xu Zhang, Maisara Binti Othman, Kamau Prince, Xianbin Yu, Jesper Bevensee Jensen, Darko Zibar, and Idelfonso Tafur Monroy

DTU Fotonik, Department of Photonics Engineering, Technical University of Denmark, DK-2800 Kgs. Lyngby, Denmark.
nggo@fotonik.dtu.dk.

Abstract: Single reconfigurable DSP coherent receiver is experimentally demonstrated for mixed-format and bit-rates including QPSK, OFDM, IR-UWB for wireline and wireless signal types. Successful transmission over a deployed fiber link is achieved.
OCIS codes: (060.1660) Coherent communications, (120.5060) Phase modulation

1. Introduction:

Next generation metro-access networks will need to support diverse broadband services including converged wireless and wireline optical access over a unified fiber platform, satisfying bandwidth requirements [1] as well as fulfilling stringent power budget and chromatic dispersion constrains [2]. Another important attribute of future metro-access networks is agile re-configurability to seamlessly accommodate for emerging new services and increased bandwidth requirements [1]. Furthermore, the introduction of mixed modulation formats, bit-mixed rates, support for burst mode transmission into the metro-access networking scenario is creating a highly heterogeneous environment that represents a new challenge to tackle in the near future. Approaches looking for solutions to one or more of the above issues are radio-over-fiber systems for integrating baseband and wireless service delivery over optical fiber access networks [3]. Another approach is developing multi-rate receivers for optical network units (ONUs) from 2.5 Gbit/s-40 Gbit/s to accommodate for mixed bit-rate or service bit-rate on demand [4]. Another promising approach proposed recently is coherent detection based passive optical networks to support closely spaced channels with increased receiver sensitivity to cope with the required large number of users and to extend the reach of metro-access networks [5]. Although experimental demonstrations of converged service delivery have been reported in the literature [2, 3] they use a dedicated receiver for each modulation or bit-rate. In this paper we present and experimentally demonstrate a single, reconfigurable, digital receiver supporting mixed modulation formats, baseband and wireless-over-fiber, with reconfiguration in the digital signal processing domain. We successfully demonstrate its operation for 20 Gbps non-return-to-zero quadrature phase-shift keying (NRZ-QPSK), optically phase-modulated 5 GHz OFDM radio-over-fiber and 2 Gbps impulse radio ultrawideband (IR-UWB), and 5 Gbps directly modulated vertical cavity surface emitting laser (VCSEL) after 78 km of deployed fiber link.

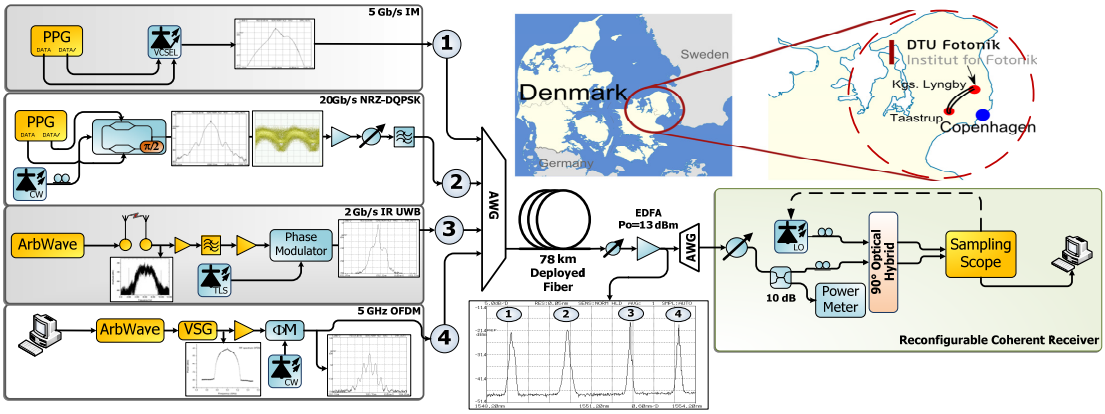

Fig.1 Experiment layout, showing optical and electrical RF spectra at key points; route of installed optical fiber are also shown. Reconfigurable receiver construction allows local oscillator (LO) tuning for channel selection. PPG: pulse pattern generator; ArbWave: arbitrary waveform; VSG: vector signal generator.

2. System description

Fig. 1 shows a block diagram of the heterogeneous optical network and setup used in the experiment. The field-deployed fiber connects the Kgs. Lyngby campus of the Technical University of Denmark (DTU) and the Taastrup suburb of Copenhagen. The fiber is a G.652 standard single-mode fiber (SMF) type (16.5 ps/nm km chromatic dispersion, 0.20 dB/km attenuation). The total link loss was 27 dB. ITU standard operating wavelengths were used for all channels at 200 GHz separation due to equipment availability. Total launch power into the deployed fiber was kept to +4 dBm. At the receiver side, emulating the central office, an erbium doped fiber amplifier (EDFA) was used as preamplifier followed by an optical bandpass filter to reduced ASE noise. The optical power level to the receiver was set to -11 dBm. A tunable external cavity laser was used as local oscillator (LO) for all the received signal types; with a linewidth of 100 kHz. The in-phase and quadrature signals after the 90° optical hybrid were detected with two pairs of balanced photodiodes, having full width at half maximum bandwidth of 7.5 GHz. The detected photocurrents were digitized using a sampling oscilloscope at 40 GSa/s for offline processing. The employed single digital receiver used a digital dispersion compensation module followed by an optical carrier-recovery digital phase-locked loop (PLL) and linear signal demodulation [6] for phase-modulated OFDM and IR-UWB RoF subsystems. Instead of a DPLL, a frequency offset compensation module was used for the NRZ-QPSK optical signal. Reconfiguration for each modulation format was performed by digitally switching between the signal demodulation DSP blocks. Below we present the set-up for each of the signal formats considered.

Gbps Intensity-modulated VCSEL: a pulse pattern generator (PPG) at 5 Gbps directly modulated a 1550 nm VCSEL. Single drive configuration was used for the VCSEL with a driving peak-peak voltage of 1 V. A pseudo random binary sequence (PRBS) with a length of 2^{15}-1 was used for this experiment. The bias current of the VCSEL was used to tune the wavelength to the assigned AWG channel. Bias current was set to 14 mA. The output power of the VCSEL launched into the fiber was measured to be 0.5 dBm.

20 Gbps QPSK baseband: the transmitter of the baseband QPSK subsystem included a PPG to providing a PRBS (215-1) and a MZ modulator to generate a QPSK signal at the wavelength of 1550.5 nm. The value of the signal laser linewidth was 2 MHz.

2 Gbps phase-modulated IR-UWB: an Arbitrary Waveform Generator (AWG) with 24 GSa/s sampling rate was utilized to program a 5th order derivative Gaussian pulse for good compliance with FCC mask [7]. A PRBS with a word length of 2^{11}-1 with bipolar modulation at a bit rate of 2 Gbps was used. The UWB signal was transmitted using a Skycross omni-directional antenna (SMT-3TO10M-A, 0dBi gain) and received after 1 m wireless transmission by a Geozondas directive antenna (AU-3.1G10.6G-1, from +4.65 dBi to +12.4 dBi gain within the UWB frequency range). The received signal was amplified by a low noise amplifier, filtered by a high-pass filter and then amplified again to drive the optical phase modulator. The wavelength of this channel was set at 1552.54 nm. The DSP algorithm in the receiver side included matched filtering and a decision block.

5 GHz OFDM RoF: the OFDM baseband signal was generated in software using a 2^{15}-1 PRBS as input data stream. 256 4-QAM subcarriers were used with 26 samples (10%) cyclic prefix per OFDM symbol. The OFDM frame is composed of two Schmidl training symbols [8] followed by eight data symbols. The signal was fed to an AWG with a 1.25 GSa/s rate which results in a bit rate of 500 Mbps. The signal is then upconverted to a frequency of 5 GHz using a free-running Vector Signal Generator (VSG) whose output is amplified to drive an optical phase modulator supplied with a continuous wave (CW) light at 1553.78 nm. At the receiver, the DSP algorithm implemented a digital PLL, timing offset estimation using a smoothed Schmidl timing metric followed by a carrier frequency offset estimation [8]. The training sequence enabled equalization of each OFDM sub-channel.

3. Results

To demonstrate the performance of our reconfigurable digital coherent receiver, we show in Fig. 2 the measured bit error rate (BER) curves for back-to-back (B2B) and after 78 km of deployed fiber transmission (considering both single and all simultaneous channel performance) as a function of the received optical power. For all four subsystems, a BER value below 10^{-3} (FEC threshold) is achieved for all considered scenarios. **5 Gbps coherently detected, intensity-modulated VCSEL:** as we can see in Fig. 2(a), the VCSEL coherently detected subsystem achieves a sensitivity of -24 dBm for both B2B and 78 km deployed fiber. Chromatic dispersion was completely compensated by DSP, and no penalty was appreciated compared with the B2B case. **20 Gbps QPSK baseband:** Fig. 2(b) shows that fiber transmission incurred 1 dB power penalty (at 10^{-3} BER) difference. Moreover in the simultaneous presence of the other three channels, there was an observable 0.5 dB penalty both for back to back and after transmission; however the reconfigurable receiver showed successful operation.

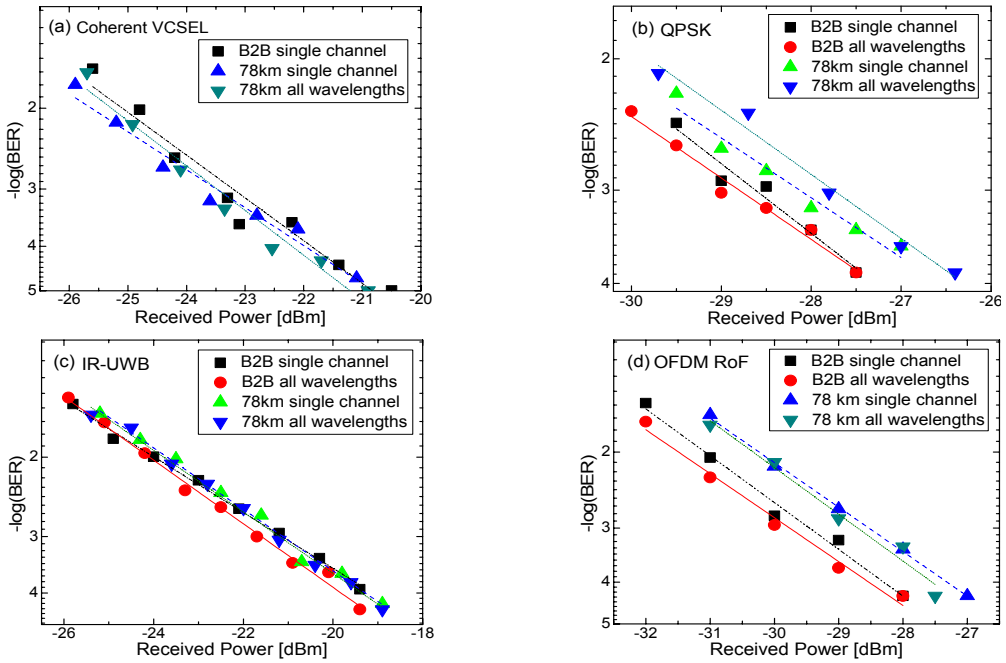

Fig.2 Measured BER performances for (a) 5 Gbps intensity-modulated VCSEL, (b) 20 Gbps QPSK baseband, (c) 2 Gbps phase-modulated IR-UWB, and (d) 5 GHz OFDM RoF.

2 Gbps phase-modulated IR-UWB: as shown in Fig. 2(c) the measured BER performances of the UWB subsystem were consistent for all cases. Errors occurred when the received optical power was less than -21.5 dBm. The BER performance is below the FEC limit when the received power was higher than -23 dBm. **5 GHz OFDM RoF:** Fig. 2(d) shows that for the case of four simultaneously integrated channels, OFDM suffered nearly 0.5 dB of power penalty, for both B2B and 78 km fiber transmission compared to single OFDM channel transmission yielding a receiver sensitivity at a BER of 10^{-4} of 28 dBm for the B2B system, and -27.5 dBm for the 78 km optical transmission link, respectively. The reconfigurable receiver showed stable operation for the 4-QAM OFDM RoF subsystem.

4. Conclusions

A single reconfigurable DSP enabled coherent receiver is experimentally demonstrated for mixed modulation formats and bit rates. In our reported experiment, four different types of wireline and wireless services including 20 Gbps QPSK baseband, 5Gbps OOK, 5 GHz OFDM RoF and 2 Gbps IR-UWB are successfully demodulated after transmission over 78 km deployed fiber link. The receiver used the same optical front-end, is able to switch among baseband and wireless types of signals by DSP reconfiguring to baseband only. This demonstrated digital reconfigurable coherent receiver has potential to enable unified support for signal detection on highly heterogeneous next generation metro- access networks.

5. References

[1]. K, Sato and H. Hasegawa, "Optical Networking Technologies That Will Create Future Bandwidth Abundant Networks", JOCN **1**, 81-83 (2009).

[2]. K. Prince, J. B. Jensen, A. Caballero, X. Yu, T. B. Gibbon, D. Zibar, N. Guerrero, A. V. Osadchiy, and I. Tafur Monroy, "Converged Wireline and Wireless Access Over a 78-km Deployed Fiber Long-Reach WDM PON", PTL **21**, 1274-1276, (2009).

[3]. M. Popov, "The Convergence of Wired and Wireless Services Delivery in Access and Home Networks", in Proc. OFC (San Diego, CA 2010), paper OWQ6.

[4]. H. Kimura, Y. Sakai, N. IIyama and K. Kumozaki, "Service Rate Matching Optical Receiver Module with Bit Rates Over 40Gb/s for PS-based WDM PON Systems", in Proc. LEOS (Newport Beach, CA 2008), pp. 669-70.

[5]. H. Rohde, S. Smolorz, E. Gottwald and K. Kloppe, "Next Generation Optical Access: 1 Gbit/s for Everyone", in Proc. ECOC (Vienna, Austria 2009), paper 10.5.5

[6]. D. Zibar, X. Yu, C. Peucheret, P. Jeppesen and I. Tafur Monroy, "Digital Coherent Receiver for Phase-Modulated Radio-Over-Fiber Optical Links", PTL **21**, 155-157 (2009).

[7]. X. Yu, T. B. Gibbon, M. Pawlik, S. Blaaberg, and I. Tafur Monroy, "A Photonic Ultra-Wideband Pulse Generator Based on Relaxation Oscillations of a Semiconductor Laser", Optics Express **17**, 9680-9687 (2009).

[8]. T. Schmidt and D. Cox, "Robust Frequency and Timing Synchronization for OFDM", IEEE Trans Commun **45**, 1613-1621. (1997).

Paper 9: Adaptive order n-QAM Optical OFDM Link with Optical Phase Modulation and Digital Coherent Detection

Arlunno Valeria, Borkowski Robert, Guerrero Gonzalez Neil, Caballero Antonio, Prince Kamau, Jensen Jesper Bevensee, Zibar Darko, Larsen Knud J. and Tafur Monroy Idelfonso. "Adaptive order n-QAM Optical OFDM Link with Optical Phase Modulation and Digital Coherent Detection", under review in *Microwave and Optical Technology Letters* 2011.

Adaptive order n-QAM Optical OFDM Link with Optical Phase Modulation and Digital Coherent Detection

Valeria Arlunno, Robert Borkowski, Neil Guerrero Gonzalez, Antonio Caballero, Kamau Prince, Jesper Bevensee Jensen, Darko Zibar, Knud J. Larsen and Idelfonso Tafur Monroy
DTU Fotonik, Department of Photonics Engineering, Technical University of Denmark, DK-2800 Kgs. Lygnby, Denmark.
vaar@fotonik.dtu.dk

Abstract: Successful digital coherent demodulation of asynchronous optical phase-modulated adaptive order QAM (4, 16 and 64) OFDM signals is achieved by a single reconfigurable digital receiver after 78 km of optical deployed fiber transmission.
OCIS codes: (060.2330) Fiber optics communications; (060.2360) Fiber optics links and subsystems; (060.5060) Phase modulation.

1. Introduction

Orthogonal frequency division multiplexing (OFDM) is a promising modulation format for optical communications, as it provides large immunity to chromatic dispersion (CD) and polarization mode dispersion (PMD) effects and also provides high spectral efficiency [1-3]. This is due to the fact that OFDM implements a large number of orthogonal radio frequency (RF) subcarriers, each having a lower symbol rate than the bit rate of the message source [1,2]. Recently, coherent detection optical OFDM (CO-OFDM) using digital signal processing (DSP) has been proposed as a promising alternative to maximize the spectral/power efficiency by exploiting the advantages of digital signal processing (DSP) such as linear and nonlinear fiber impairments compensation in the digital domain and software reconfigurability [2,3].

So far optical intensity modulation for CO-OFDM has been dominantly employed due to its simplicity; however, it suffers from higher sensitivity to fiber nonlinearities due to the relative large peak-to-average power ratio [1]. Optical phase modulation (PM) has the potential to improve robustness to fiber nonlinearities by encoding the information in the optical phase and thus maintaining a constant optical power. Furthermore, optically phase-modulated links can also potentially enable large dynamic range, high-capacity and higher spectral efficiency for transmission of microwave radio frequency (RF) signals over optical fiber links [3-6].

In this paper, we report on the use of optical phase modulation for CO-OFDM transmission links supported by a reconfigurable DSP receiver that allows for adaptation of the modulation order of the transmitted signal. We demonstrate performance using QAM constellations having 4, 16 and 64 points. We report on experiments employing 78 km of SMF deployed fiber and 40 km of SMF. For all reported experiments, a bit error rate (BER) value better than 10^{-3} was achieved for all employed OFDM subcarriers; complying with the forward error correction (FEC) limit. Our results demonstrate the transmission robustness of phase modulated OFDM links and their potential for use in scenarios with need for flexible modulation format assignment to subcarriers.

2. System Setup

The general outline of the experimental setup for the adaptive order 4-QAM, 16-QAM and 64-QAM phase-modulated (PM) coherent optical (CO) OFDM link is shown in Fig. 1. The PM CO-4QAM-OFDM signal was transmitted over 78 km of field-deployed fiber while a standard single mode fiber (SMF) was employed for optical transmission of the PM CO-16QAM-OFDM signal.

The baseband adaptive order n-QAM OFDM signal was obtained from a pseudorandom binary sequence (PRBS) of length $2^{15}-1$ bits. In all cases, 256 subcarriers without oversampling were used with 26 samples (10%) cyclic prefix per OFDM symbol. OFDM frame is composed of two Schmidl training symbols [7], followed by eight data symbols. The use of these two training symbols makes receiver independent of transmitter synchronization and allows us to avoid a clock reference for synchronizing the arbitrary waveform generator (AWG) and digital storage oscilloscope (DSO) in our experimental setup.

The software-generated OFDM baseband signal was upsampled by a factor of 5 and fed to a 1.25 GSa/s AWG. Resultant electrical OFDM signal with a bit rate of 0.5 Gb/s for 4-QAM and 1 Gb/s for 16-QAM were upconverted to a carrier frequency of 5 GHz and a 6 GHz respectively by using a free-running Vector Signal Generator (VSG). The output power of the VSG was fixed at −25 dBm. Output of the VSG was then amplified to 2 dBm and used to drive an optical phase modulator (PM) supplied with a continuous laser (CW) laser at 1553.78 nm. At the receiver,

a 90° optical hybrid was used to mix the received optical data signal with the tunable external cavity local oscillator laser. Samples taken from the sampling scope with a sample rate of 40 GSa/s were processed offline. First, carrier-recovery digital PLL and linear demodulation was performed without any dispersion compensation algorithm. The signal was downconverted to baseband and timing offset estimated using a smoothed Schmidl timing metric followed by a carrier frequency offset estimation algorithm [7]. In contrast to [3], the system presented here is fully asynchronous PM CO-OFDM transmission link, whose receiver and transmitter are not triggered by a common clock signal. The phase offset and amplitude for every channel is corrected by using the training sequence as an equalization reference. A structure typical for an OFDM receiver is then used.

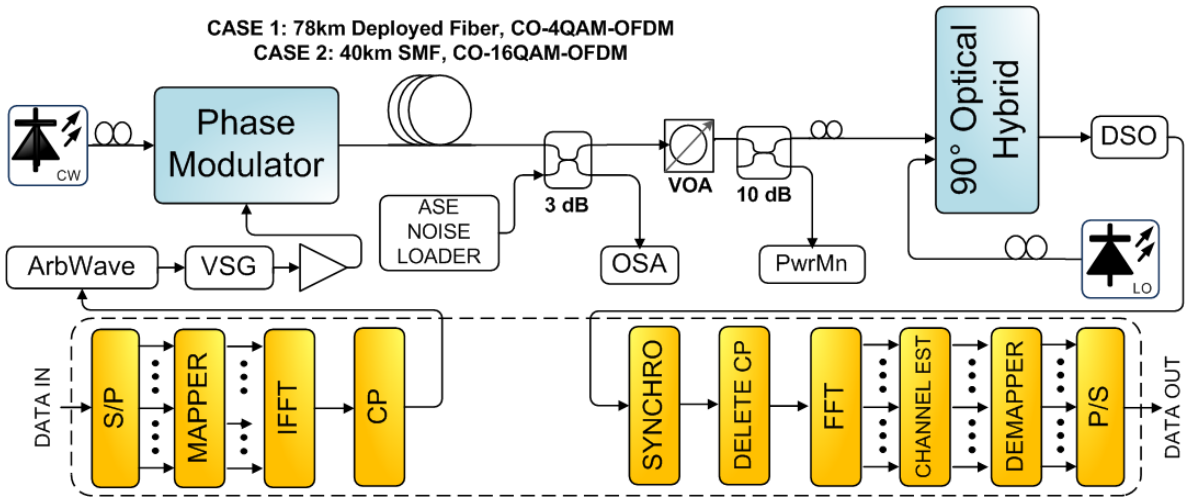

Fig.1. Experiment layout; ArbWave: arbitrary waveform; VSG: vector signal generator; OSA: optical Spectrum Analyzer; PwrMn: power measurement point; DSO: digital sampling oscilloscope.

In the case of CO adaptive n-QAM OFDM the generating software has been modified as to support 4 different modulation formats. Namely, 4-QAM modulation is used on the first subcarrier of every OFDM symbol, 16-QAM on the second, QPSK on the third and 8-QAM on the fourth; this arrangement is then repeated as to fill all 256 subcarriers in use.

3. Experimental Results

The measured BER performances of the 4-QAM and 16-QAM OFDM signal for the back-to-back (B2B) system and optical link transmission are shown in Fig. 2(a); in the first case the signal has been transmitted over 78 km of deployed SMF, while in the second over 40 km of SMF. As insets, the received constellation diagram of the 250 Mbaud 4-QAM and 16-QAM PM CO-OFDM signal at 10^{-4} BER in B2B configuration are shown; the constellation points look clear and well separated.

Fig. 2(b) is a contour plot showing the relation between the radio frequency (RF) output power measured at the output of the VSG and the optical received power at the input of the coherent receiver to obtain specific BER values for B2B CO-16QAM-OFDM. For instance, a BER value at 10^{-4} is measured by setting VSG output power anywhere in the range between 1 dBm and 2 dBm and the optical received power (via a variable optical attenuator) between −16 dBm and −14 dBm. For 16QAM-OFDM (Fig. 2(a)) the RF power was fixed at 2 dBm, corresponding to a modulation index value of 0.36 rad.

Fig. 3(a) shows the constellation diagram for the initial CO-64QAM-OFDM trial with a BER value of 10^{-3}, while Fig. 3(b) shows constellation diagrams used for the initial m-QAM CO-OFDM trial with a BER value of 10^{-3}. In the second case, the reported results are obtained for an RF power equal to 2 dBm.

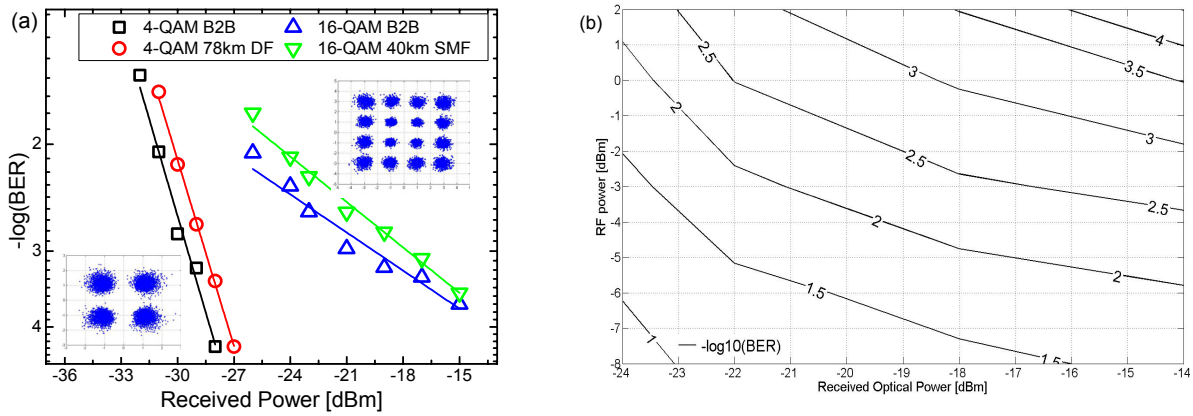

Fig. 2a) OFDM BER as a function of the Received Optical Power [dBm] for Back to Back and optical transmission; DF: deployed fiber; b) Contour plot RF optical power versus Received Optical Power for 16-QAM OFDM.

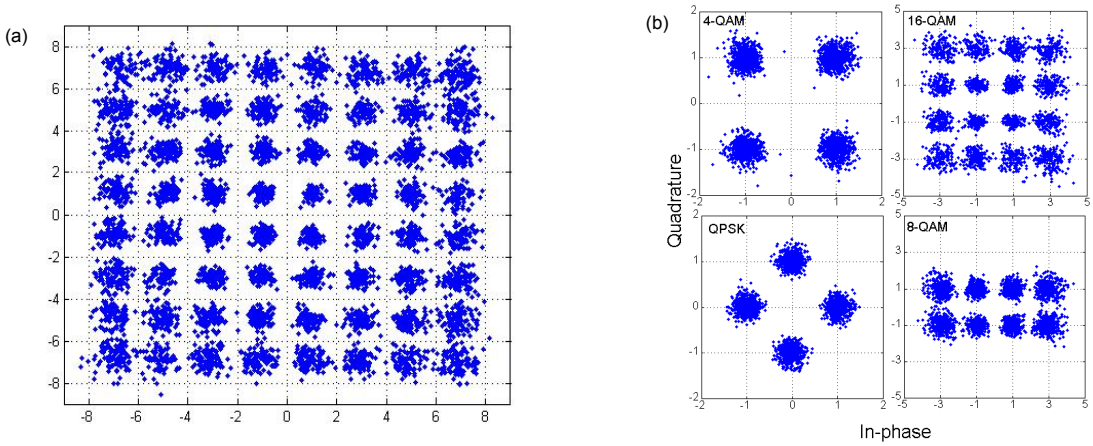

Fig.3. Received OFDM constellation diagrams: a) all 64-QAM subcarriers superimposed; b) first-fourth subcarriers of the adaptive n-QAM

4. Conclusions

Successful signal demodulation of phase-modulated (PM) coherent optical (CO) 4-QAM and 16-QAM OFDM signals after fiber transmission (78 km of field deployed fiber for 4-QAM and 40 km of SMF for 16-QAM) have been experimentally demonstrated by using a single reconfigurable digital receiver. We also have demonstrated the easy reconfigurability of the implemented digital receiver capable of achieving bit error rate values at 10^{-3} for back-to-back PM CO-64QAM-OFDM and CO adaptive n-QAM OFDM without hardware changes in the experimental setup. Phase-modulated coherent optical OFDM systems are a promising solution for applications in converged wireless/wireline service delivery in optical networking scenarios with reconfigurable digital coherent receivers.

5. References

[1] B. Djordjevic and B. Vasic, "Orthogonal frequency division multiplexing for high-speed optical transmission", Optics Express 14, 9, (2006).

[2] W. Shieh and C. Athaudage, "Coherent optical orthogonal frequency division multiplexing", Electronics Letters **42**, 10, (2006).

[3] Z. Wu, H. Wen, X. Zheng, H. Zhang and Y. Guo,, "Phase Modulated Coherent Optical OFDM by Phase Restioration of Optical Field", in Proc. of Microwave Photonics (Montreal, Canada, 2010), paper TH4-15.

[4] T. R. Clark and M. L. Dennis, "Coherent optical phase-modulation link", PTL **19**, 16, 1206-1208, (2007).

[5] D. Zibar, I. T. Monroy, C. Peucheret, L. A. Johansson, J. E. Bowers and P. Jeppesen, "DSP based coherent receiver for phase-modulated radio-over-fibre optical links", in Proc. Optical Fibre Communication Conf., (Anaheim, CA, 2008), paper OThH3.

[6] D. Zibar, X. Yu, C. Peucheret, P. Jeppesen and I. T. Monroy, "Digital Coherent Receiver for Phase-Modulated Radio-over-Fiber Optical Links", ", PTL, **21**,. 3, 2009.

[7] T. M. Schmidl and D. C. Cox, "Robust frequency and timing synchronization for OFDM", IEEE Trans. Commun., **45**, pp. 1613-1621, (1997).

Paper 10: Robust BPSK Impulse Radio UWB-over-Fiber Systems Using Optical Phase Modulation

Pham Tien-Thang, Guerrero Gonzalez Neil, Yu Xianbin, Zibar Darko, Dittmann Lars and Tafur Monroy Idelfonso. "Robust BPSK Impulse Radio UWB-over-Fiber Systems Using Optical Phase Modulation," accepted for oral presentation at *the Optical Fiber Communication Conference and Exposition and the National Fiber Optic Engineers Conference OFC'2011,* Los Angeles, USA., March 2011.

Robust BPSK Impulse Radio UWB-over-Fiber Systems Using Optical Phase Modulation

Tien-Thang Pham, Neil Guerrero Gonzalez, Xianbin Yu, Darko Zibar, Lars Dittmann, and Idelfonso Tafur Monroy

DTU Fotonik, Department of Photonics Engineering, Technical University of Denmark, DK-2800 Kgs. Lyngby, Denmark.
Tel: + +45 45 25 37 77, Fax: +45 45 93 65 81, E-mail: ptit@fotonik.dtu.dk

Abstract: The impact of fiber dispersion on the performance of optical phase modulated impulse-radio-ultrawideband (IR-UWB) signals is experimentally investigated. 2Gbps BPSK IR-UWB over 78km fiber transmission is successfully achieved by using digital coherent detection.

OCIS codes: (060.1660) Coherent communications, (060.5625) Radio frequency photonics.

1. Introduction

With the recent development of integrated electronic circuits and digital signal processing (DSP), optical coherent receivers using DSP are becoming a practical and feasible solution for high speed systems. Digital coherent detection is a dominating approach for long-haul high capacity transmission systems [1]. Recently, it has also been proposed for optical access networks due to its very good channel selectivity, including optical phase modulated radio-over-fiber (RoF) systems which have several advantages compared to intensity-modulated RoF systems, such as no need of bias voltage, no fundamental limit on modulation depth, high linearity [2, 3], and 6 dB receiver performance advantage over intensity modulation counterpart [4].

On the other hand, ultrawideband (UWB) has been considered as a promising technology for short-range, high-speed wireless communication systems [5]. Regulated by the U.S. Federal Communications Commission (FCC), power spectral density of UWB signals is limited below -41.3dBm/MHz. Therefore, wireless transmission distance is very limited. In this context, UWB-over-fiber, similar to radio-over-fiber technology, is a potential technology to extend the reach with assistance of flexible UWB generation and distribution. Several approaches have been proposed to optically generate impulse radio (IR) UWB signals at the central office (CO) and distribute to end-users [6, 7, 8]. Recently, we also demonstrated that UWB-over-fiber could be integrated seamlessly into a WDM-PON that supports both wireline and wireless services [9]. In fact, in such long reach UWB-over fiber transmission systems, fiber chromatic dispersion will critically affect the signal performance, since UWB signals occupy a large bandwidth up to 6.5 GHz. Therefore it is important to conceive a robust IR-UWB optical fiber signal distribution approach with seamless integration with the major trend of employing advanced digital coherent receivers for universal support of several services and modulation formats.

In this paper we consider optical phase-modulated transmission and coherent detection of IR-UWB-over-fiber in a coherent-detection PON scenario. We demonstrate an uplink transmission of 2-Gbps binary phase shift keying (BPSK) IR-UWB signals. The influences of the chromatic dispersion of various single mode fiber links (from 20 km in conventional access networks to up to 78 km in long-reach access networks) are experimentally investigated. The result proves the robustness of our system and its integration capability into a digital coherent receiver structure.

2. Coherent optical access networks

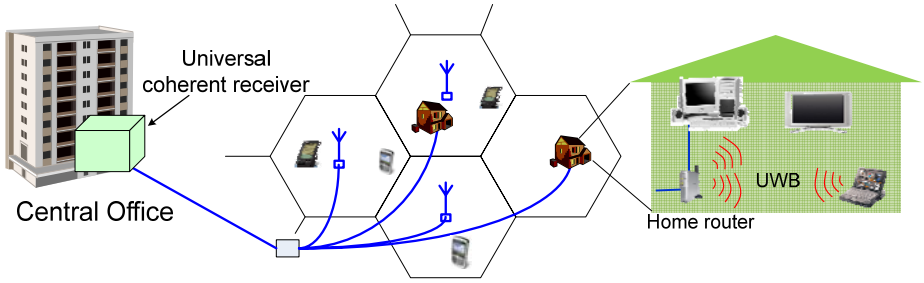

Fig. 1. Hybrid optical-wireless signal transport over optical access network supported by a universal coherent receiver.

Fig. 1 shows a schematic diagram for a prospective converged wireless-optical network. Both wireline and wireless services are transported in the same fiber infrastructure. With the advantages of DSP, a universal and reconfigurable coherent-detection based DSP receiver can be employed in the CO to detect all types of signals. Moreover, the utilization of the universal receiver allows the CO to adaptively tackle the requirements for large number of users,

diversity of services and reach extension, as it has potential to support large number of channels with very close channel spacing and increased receiver sensitivity.

3. Experimental setup

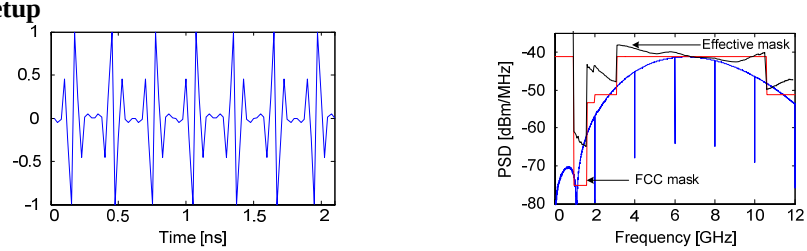

a) b)

Fig.2. a) BPSK-modulated UWB sequence (1 0 1 1 0 0 1). b) Spectrua of the 2Gbps BPSK-UWB signals.

To emulate a UWB wireless signal generation terminal, an arbitrary waveform generator (AWG) with a 24-GSa/s sampling rate was used. The generated UWB pulse is a 5th derivative Gaussian shape for its good compliance with the FCC mask [6]. In the experiment, a pseudo-random bit sequence (PRBS) at a bit rate of 2 Gbps with a word length of 2^{11}-1 was used. Bipolar modulation is employed for the UWB signal in order to avoid spectral lines at multiplication of pulse repetition frequency for on-off-keying modulation [10], and thus to be able to radiate further wirelessly. Fig. 2 shows an example of UWB sequence and the UWB spectra generated by the AWG. We can see PI phase shift is perfectly introduced between bit '1' and '0', and no spectral spike lines are observed. The effective mask is the allowed mask when the frequency response of the transmitting antenna is taken into account.

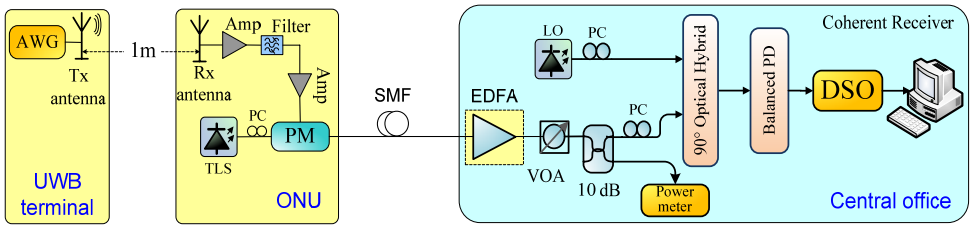

Fig. 3. Experimental setup. AWG: arbitrary waveform generator, TLS: tunable laser source, PM: phase modulator, EDFA: Erbium doped fiber amplifier, SMF: single mode fiber, VOA: variable optical attenuator, LO: local oscillator, DSO: digital storage oscilloscope.

Fig. 3 shows the experimental setup. The UWB signal from the AWG was transmitted wirelessly through an Omni-antenna (SMT-3TO10M-A) and received by a directive antenna (AU-3.1G10.6G-1). The wireless transmission distance was set at 1 m. The received UWB signals from the receiver antenna were amplified and filtered out by a high-pass filter, to remove frequency components below 3.1 GHz before driving an optical phase modulator (PM). The lightwave launched into the PM with 4 dBm power was emitted from a tunable laser source (TLS). The modulated optical signals were then transmitted over a spool of single mode fibers (SMF) with different length (23, 40, 58 and 78 km fiber). The 78-km long link is a deployed fiber; in this case an erbium doped fiber amplifier (EDFA) was used as pre-amplifier to compensate 25 dB losses of the optical link.

In the coherent receiver, a tunable external cavity laser with a linewidth of 100 kHz was used as local oscillator (LO). The in-phase and quadrature signals after a 90° optical hybrid were detected by two pairs of balanced photodiodes with 7.5 GHz full-width-half-maximum (FWHM) bandwidth. The detected photocurrents were digitized by a sampling scope at 40 GSa/s for offline digital signal processing (DSP). The employed single digital receiver included a digital dispersion compensation module, which is followed by an optical carrier-recovery digital phase-locked loop (PLL) [9] and a linear signal demodulator. In the digital linear demodulation module, the DSP algorithm performs functions of high-pass filtering, matched filtering with the original UWB pulse, synchronization and threshold decision [10]. The dispersion parameter for dispersion compensation (DC) module was 17ps/nm/km.

4. Experimental results

In the experiment, 70,000 UWB bits were used to assess the performance of the UWB signals in each case. Fig. 4a shows the BER curves in cases of back-to-back (B2B), after 23, 40 and 58 km fiber transmission, with and without dispersion compensation as well. As illustrated in the figure, 23, 40 and 58 km fiber without DC caused approximately 1.4, 3.1 and 4.3 dB power penalties at a BER of 10^{-4}, respectively. When digital DC was applied in the digital domain, power penalties were then less than 0.5 dB for all the transmission cases. Fig.4b shows the comparison of the measured BER performance between B2B and 78 km fiber transmission cases. The use of the EDFA introduced about 1 dB power penalty while 78-km fiber caused about 7 dB. However, similar to the shorter

transmission distances, this power penalty can also be compensated completely by using digital dispersion compensation. Fig. 4c simply summaries the measured power penalties caused by the chromatic dispersion.

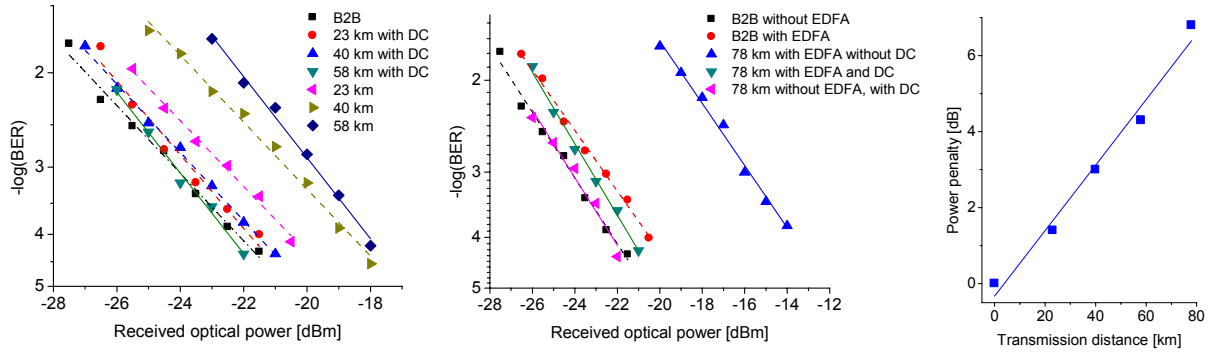

a) b) c)

Fig. 4. BER performance of the UWB signals with and without dispersion compensation after (a) 23km, 40km and 58km and (b) 78km fiber transmission, c) Summarized power penalties caused by chromatic fiber dispersion.

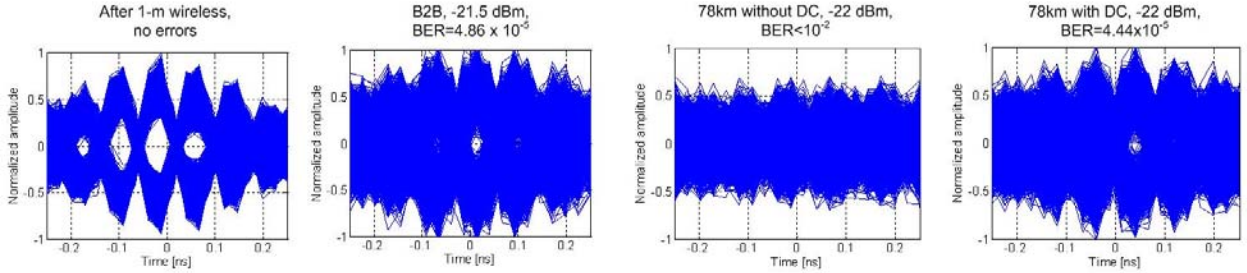

Fig. 5. Eye-diagrams of the received BPSK UWB signals

Fig. 5 illustrates the eye-diagrams of 10,000 UWB bits at different positions in the 78-km transmission system. The eye diagram after wireless transmission but before fiber transmission was clear and open. After 78-km fiber transmission, the eyes at -22-dBm optical power were completely close due to the chromatic dispersion. However, after using digital dispersion compensation, the eye-diagrams and the transmission performance were similar to B2B.

5. Conclusions

We experimentally demonstrated an optical phase modulated UWB-over-fiber system using digital coherent detection for the transport of 2-Gbps BPSK IR-UWB signals in a coherent detection PON. Our experimental results indicate that a DSP receiver has the capability of overcome fiber transmission impairments, and the power penalty caused by the chromatic fiber dispersion is completely compensated in the digital coherent receiver. Therefore, it can be foreseen that a universal, reconfigurable DSP receiver will make it possible to seamlessly integrate also IR-UWB into the diverse services supported in next generation high capacity optical access networks.

6. References

[1] J. Renaudier, G. Charlet, O. Bertran-Pardo, et al, "Transmission of 100Gb/s Coherent PDM-QPSK over 16x100km of standard fiber with allerbium amplifiers," *Opt. Express* **17**, 5112-5119 (2009).

[2] D. Zibar, et al, "Digital coherent receiver for phase-modulated radio-over-fiber optical links," *IEEE Photon. Techn. Lett.* **21**, 155-157, (2009).

[3] T. R. Clark, M. L. Dennis,"Coherent optical phase-modulation link," *IEEE Photon. Techn. Lett.* **19**, 1206–1208, (2007).

[4] F. Gardner, "Phase-lock techniques," 3rd edition, (John Wiley and Sons, 2004).

[5] D. Porcino, W. Hirt, "Ultra-wideband radio technology: Potential and challenges ahead," *IEEE Comm. Mag.*, **41**, 66–74, (2003).

[6] X. Yu, T. B. Gibbon, M. Pawlik, S. Blaaberg and I. T. Monroy, "A photonic ultra-wideband pulse generator based on relaxation oscillations of a semiconductor laser," *Optics Express* **17**, 9680–9687, (2009).

[7] S. Pan, J. P. Yao, "Switchable UWB pulses generation using a phase modulator and a reconfigurable asymmetric Mach-Zehnder interferometer," *Opt. Lett.* **34**,160-162, (2009).

[8] A. K.-Anandarajah, P. Perry, et al, "An IR-UWB photonic distribution system," *IEEE Photon. Techn. Lett.* **20**, 1884 – 1886, (2008).

[9] K. Prince, J. B. Jensen, A. Caballero, et al, "Converged wireline and wireless access over a78-km deployed fiber long-reach WDM PON," *IEEE Photon. Technol. Lett.* **21**, 1274–1276, (2009).

[10] T. B. Gibbon, X. Yu, I. T. Monroy, "Photonic ultra-wideband 781.25 Mbit/s signal generation and transmission incorporating digital signal processing detection," *IEEE Photon. Techn. Lett.* **21**, 1060-1062, (2009).

Paper 11: Range extension and channel capacity increase in impulse-radio ultra-wideband communications

Rodes Lopez Roberto, Yu Xianbin, Caballero Jambrina Antonio, Jensen Jesper Bevensee, Gibbon Timothy Braidwood, Guerrero Gonzalez Neil, Tafur Monroy Idelfonso. "Range extension and channel capacity increase in impulse-radio ultra-wideband communications", *Tsinghua Science and Technology*, vol. 15, no. 2, pp. 169-173, April 2010.

TSINGHUA SCIENCE AND TECHNOLOGY
ISSN 1007-0214 05/16 pp169-173
Volume 15, Number 2, April 2010

Range Extension and Channel Capacity Increase in Impulse-Radio Ultra-Wideband Communications*

Roberto Rodes, Xianbin Yu**, Antonio Caballero, Jesper Bevensee Jensen,
Timothy Braidwood Gibbon, Neil Guerrero Gonzalez, Idelfonso Tafur Monroy

DTU Fotonik, Department of Photonics Engineering, Technical University of Denmark, DK-2800, Kgs. Lyngby, Denmark

Abstract: We theoretically analyze the channel capacity of a 5th-order Gaussian pulse-based ultra-wideband (UWB) system and experimentally demonstrate 2 Gbit/s UWB-over-fiber transmission systems incorporating wireless transmission. Both electrical and photonic UWB pulse generation methods are employed and its performance is compared. By utilizing optimum UWB pulse design and employing a digital signal processing (DSP) receiver, a bit-error-rate above the forward error correction (FEC) limit for 8 meters of wireless emission is obtained in our photonic generation UWB system. A noticeable increase in the channel capacity is achieved compared to previously reported results.

Key words: impulse radio ultra-wideband; UWB-over-fiber; channel capacity; personal area networks

Introduction

Ultra-wideband (UWB) wireless communication is an emerging technology for short range, high speed systems in future wireless local area networks (WLANs). The main characteristic of this technology is the extremely low radiated power over a wide frequency bandwidth. In accordance with the Federal Communications Commission (FCC) regulation which was first released in 2002[1], a maximum emission power spectral density (PSD) of –41.3 dBm/MHz from 3.1 to 10.6 GHz is allowed. Meanwhile, the employment of the ultra-wide frequency band (7.5 GHz) potentially allows UWB information transmission at a high bit-rate.

Recently, UWB-over-fiber has been shown to be extremely valuable in extending UWB reach and several experiments featuring UWB-over-fiber transmission systems have been demonstrated[2-4]. However, the trade-off between UWB Shannon channel capacity, propagation distance, and radiation of low power close to the noise level imposes serious hurdles to extending wireless distance reach for high-speed signals[4]. Considerable effort has therefore recently been devoted to simultaneously increasing wireless distance and bit rate. Thus far, 500 Mbit/s×65 cm[5], 1.025 Gbit/s×20 cm[6], and 1 Gbit/s×90 cm[7] have been demonstrated.

In this paper, we present our efforts towards extending the wireless reach range of an impulse radio (IR)-UWB fiber system. UWB pulse design, UWB signal generation, digital signal processing (DSP) receiver implementation, channel capacity analysis, and experiment results will be presented.

1 Theory of UWB Channel Capacity

A study of the Shannon channel capacity with respect to the UWB wireless transmission length is of great importance to evaluate the transmission link performance. The Shannon limit states the upper bound of information data rate can be transmitted through a

Received: 2009-12-14
* Partly supported by a Marie Curie International Incoming Fellowship and ICT-ALPHA Project within the 7th European Community Framework Programme
** To whom correspondence should be addressed.
E-mail: xiyu@fotonik.dtu.dk; Tel: 45-45253796

channel for a given signal power S, and additive white Gaussian noise power N, within a bandwidth B.

$$C = B \cdot \log_2(1+\mathrm{SNR}) \tag{1}$$

where C is the maximum channel capacity. SNR is the signal-to-noise ratio.

In 2004 Levitt[8] computed a theoretical channel capacity of UWB communications assuming a lossless system and an ideal FCC limit emission from 3.1 - 10.6 GHz. In fact, the received SNR of a UWB radio system can be written as[9]

$$\mathrm{SNR} = 10 \cdot \lg \frac{P_{Tx}}{BkT} + L_{\mathrm{air}} + L_{Rx} \tag{2}$$

where P_{Tx} is the pulse shape dependent and effective radiated power, B is the bandwidth of the system, k is Boltzmann's constant, T is the nominal noise temperature, L_{Rx} is the receiver loss, and L_{air} is the free-space path loss between antennas defined link, and

$$L_{\mathrm{air}} = 20\lg\left(\frac{c}{4\pi df}\right) \tag{3}$$

where d is the air link length. Therefore, Shannon's channel capacity limit C can be represented with respect to the wireless distance of the system by computing Eqs. (1) - (3), while the parameters P_{Tx}, B, kT, L_{Rx}, and f are constants for a specific system.

2 Effective IR-UWB Pulses

The more efficient use of the UWB frequency band below the FCC mask, the higher the radiation power, and hence the longer the wireless transmission distance. Previous study proved that UWB pulses with shapes following high order Gaussian derivatives have good compliance with the FCC mask[10]. The 5th-order derivative Gaussian pulse is the lowest order fitting the FCC mask, which makes it the simplest shape in terms of minimal zero-level crossing. In addition, the central frequency of the pulse increases with the higher derivative orders. Therefore, the 5th order has the relatively lowest central frequency, and the lowest air attenuation. The 5th-order Gaussian derivative pulse is given by the equation,

$$y(t) = A\left(-\frac{t^5}{\sqrt{2\pi}\sigma^{11}} + \frac{10t^3}{\sqrt{2\pi}\sigma^{9}} - \frac{15t}{\sqrt{2\pi}\sigma^{7}}\right)\exp\left(-\frac{t^2}{2\sigma^2}\right) \tag{4}$$

where the optimum deviation σ is 60 ps and A is used to normalize the pulse amplitude.

Figure 1 shows the pulse in time domain and Fig. 2 shows the corresponding power spectral density. It is noticeable that the spectrum of a 5th-order derivative Gaussian pulse is effectively compliant with the FCC mask. By integrating the PSD of 5th-order pulse under the FCC power limit, a maximum transmitted power of 0.2769 mW is obtained.

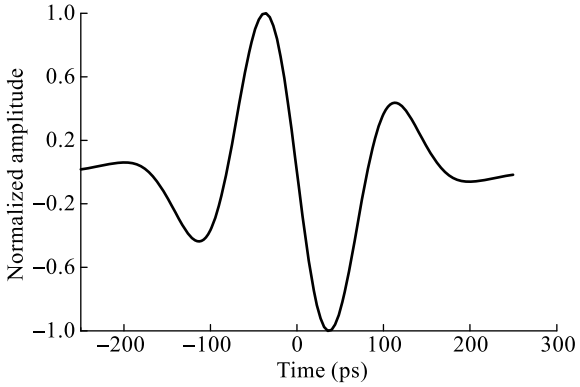

Fig. 1 Normalized 5th-order derivative Gaussian pulse

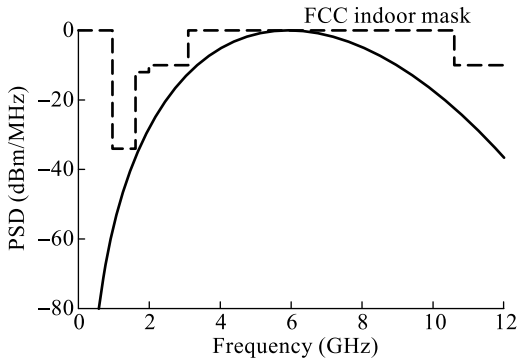

Fig. 2 Normalized PSD of the 5th-order Gaussian pulse and FCC mask

3 Experiment Setup

The experimental setup used to demonstrate UWB pulse generation and transmission is shown in Fig. 3. In the experiment, the UWB pulse is generated using two different approaches: electrical and optical generations.

3.1 Generation of UWB pulses

The electrical generation is performed by controlling an arbitrary waveform generator with 9 GHz bandwidth and a sample rate of 24 GSa/s, as shown in Fig. 3a. At the output of the AWG, an on-off keying pulse sequence with a pseudo-random bit sequence (PRBS) of word length 2^{11}–1 is generated.

The photonic generation setup is shown in Fig. 3b. The principle was described in Refs. [11,12]. A conventional pulse pattern generator set to 10 Gbit/s bit

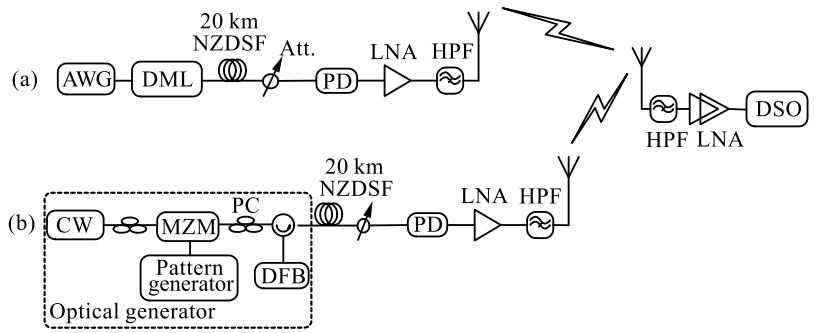

AWG, arbitrary waveform generator; DML, directly modulated laser; CW, continuous-wave laser; PC, polarization controller; NZDSF, non-zero dispersion shift fiber; DFB, distributed feedback laser; LNA, low noise amplifier; PD, photodiode; MZM, Mach-Zehnder modulator; DSO, digital sampling scope; HPF, high-pass filter

Fig. 3 Experimental setup

rate is used to drive an optical intensity Mach-Zehnder modulator. Five-bit patterns '10000' and '00000' are used to represent a binary one and zero, respectively. This results in a 2 Gbit/s effective IR-UWB bit rate. An optical circulator (OC) is used to separate the light-wave launched into the DFB from its output lightwave. Cross-gain modulation inside the DFB in combination with relaxation oscillations results in an optical pulse whose shape is close to a 5th-order derivative Gaussian pulse. Both pulses generated by electrical and photonic methods are shown in time domain in Fig. 4. We can notice that compared to the pulse in Fig. 1, the pulse photonically generated is a reversed 5th-order pulse.

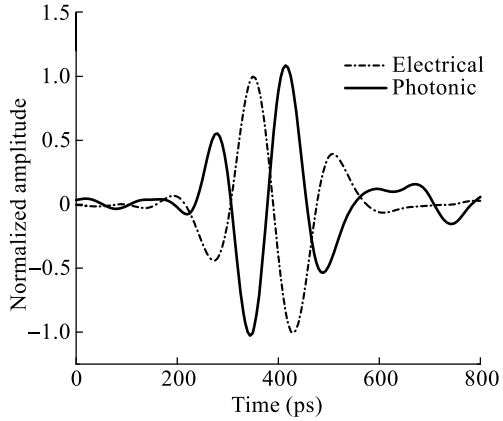

Fig. 4 Measured pulses generated by electrical and photonic means

The systems in Fig. 3 share the same transmission link and the same receiver. The optical transmission link consists of a 20 km NZDSF. Before wireless emission, a broadband electrical LNA with an 8 dB gain is used. Subsequently, an HPF with cut-off frequency of 3.1 GHz is used to feed the transmitter antenna, assuring the signal fits inside the spectrum available for UWB technology. Figure 5 shows the measured PSD after the transmitter antenna (omni-directional antenna Skycross SMT-3TO10M-A[13]). It is evident that both spectra meet the FCC requirements and fit the FCC mask. However, due to the AWG bandwidth, the spectra generated by electrical means exhibit greater attenuation in the high frequency band.

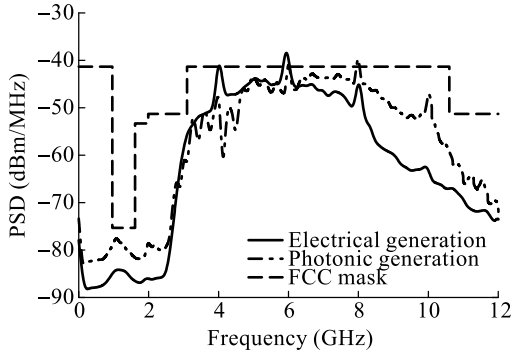

Fig. 5 Measured PSDs of electrically and photonically generated pulses in the experiment

3.2 DSP receiver

In order to extend the wireless distance and recover the corresponding UWB signal with its extremely low power after air transmission, a high performance receiver with high gain, low noise, and broadband amplification is highly desirable. In the experiment a receiver with high gain of around 59 dB is implemented. The receiver consists of a directive antenna (Geozondas AU-3.1G10.6G-1), with around 10 dB gain at a frequency of 6.5 GHz[14], and a 2-stage broadband amplifier with a total gain of 49 dB. An LNA is set as the first stage, which provides a total noise figure of 3 dB. Finally, a DSO, with a 40 GSa/s sampling rate over a 13 GHz bandwidth, digitizes and stores the received

signal. A DSP algorithm based on correlation is programmed to demodulate the signal offline.

The block diagram of the DSP algorithm is shown in Fig. 6. The received signal from the DSO is firstly filtered by a bandpass filter, and correlated with a 5th-order derivative Gaussian pulse. The synchronization after envelope detection is then performed by calculating the maximum variance of the signal envelope and shifting the signal to the middle of the pulse period for optimum sampling. Finally, adaptive thresholding and a bit-for-bit comparison are used to calculate bit-error-rate (BER).

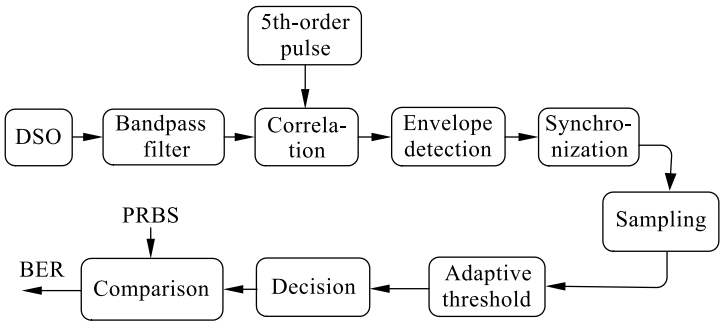

PRBS: pseudo random bit sequence

Fig. 6 Block diagram of the DSP algorithm

4 Experimental Results and Channel Capacity Analysis

We measure the bit-error-rate results based on the system discussed in Section 3. By changing the wireless distance, the BER at 4, 6, and 8 m for both systems are measured and presented in Fig. 7. We can observe that only BER after 8 m emission in the electrical generation system exceeds the forward error correction (FEC) limit of 2×10^{-3}. We can also notice that the photonic generation system has better performance. This is mainly due to the 9 GHz bandwidth limitation of the AWG. In addition, non-linear modulation of the DFB introduces signal degradation in the electrical generation link[15].

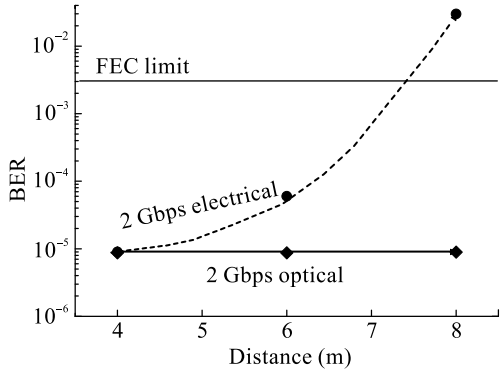

Fig. 7 Experimental BER results for electrical and photonic generation systems

Figure 8 shows the theoretical and experimental channel capacity, as well as Levitt theoretical channel capacity and the previously reported experimental results. Table 1 displays the constants used in calculating our theoretical channel capacity. In the calculation, we took into account the system loss, and the fact that the 5th-order pulse does not completely fill the FCC mask. Compared to the Levitt result, our predicted curve thus provided a more accurate approximation of the fundamental limit for our UWB system. Most importantly, we have also contributed to achieving a noticeable increase in the experimental distance and bit-rates compared to previously published wireless UWB transmission experiments. Our results are, to our knowledge, the closest to the channel capacity limit achieved thus far, even though the ranges are still below half of the fundamental maximum distance.

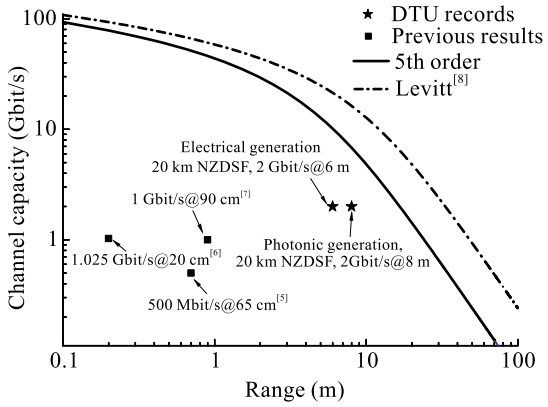

Fig. 8 Analysis of theoretical and experimental channel capacity

Table 1 Parameters used in the calculation

Parameters	Value
P_{Tx}	0.2769 mW
B	7.5 GHz
kT	$1.38\times10^{-23}\times290$ eV
L_{Rx}	−3 dB
f	6.85 GHz

5 Conclusions

We have theoretically analyzed the channel capacity for a 5th-order Gaussian pulse-based UWB system. Taking into account the system loss and the emission power of the 5th-order pulse our calculation provides a better approximation of the fundamental limit for our UWB system than the Levitt formulation. Furthermore, we have experimentally demonstrated two 2 Gbit/s IR-UWB systems based on electrical and photonic pulse generation methods. The experimental results shown have contributed to achieve a noticeable increase in the wireless distance and bit rate (2 Gbit/s× 8 m). These results present UWB over fiber as a potentially attractive solution for fiber-to-the-home (FTTH) networks, providing high-speed wireless services to the end-users.

References

[1] Federal Communications Commission. Revision of part 15 of the commission's rules regarding ultra-wideband transmission systems. February 14, 2002.

[2] Llorente R, Alves T, Morant M, et al. Ultra-wideband radio signals distribution in FTTH networks. *IEEE Photon. Technol. Lett.*, 2008, **20**(11): 945-947.

[3] Gibbon T B, Yu X, Monroy I T. Photonic ultra-wideband 781.25 Mbit/s signal generation and transmission incorporating digital signal processing detection. *IEEE Photon. Technol. Lett.*, 2009, **21**(15): 1060-1062.

[4] Yu X, Gibbon T B, Monroy I T. Experimental demonstration of all-optical 781.25 Mbit/s binary phase coded UWB signals generation and transmission. *IEEE Photon. Technol. Lett.*, 2009, **21**(17): 1235-1237.

[5] Abtahi M, Mirshafiei M, LaRochelle S, et al. All-optical 500-Mb/s UWB transceiver: An experimental demonstration. *Journal of Lightwave Technology*, 2008, **26**(15): 2795-2802.

[6] Hanawa M, Mori K, Nakamura K, et al. Dispersion tolerant UWB-IR-over-fiber transmission under FCC indoor spectrum mask. In: Conference on Optical Fiber Communication (OFC 2009). San Diego, USA, 2009: 1-3.

[7] Tan C M, Ong L C, Yee M L, et al. Transmission of ultra wide band radio using multimode radio-over-fiber system. In: Asia-Pacific Microwave Conference Proceedings (APMC 2005). Suzhou, China, 2005, **2**: 3-5.

[8] Levitt L. Fundamental communication range limitation of ultra wideband communications for military application. In: 24th Army Science Conference. Orlando, USA, 2004: Paper BS-41.

[9] Siwiak K, Petroff A. A path link model for ultra wide band pulse transmissions. In: Proc. of the IEEE 53rd Vehicular Technology Conference (VTC Spring 2001). Barcelona, Spain, 2001, **2**: 1173-1175.

[10] Sheng H. On the spectral and power requirements for ultra-wideband transmission. In: IEEE International Conference on Communications, 2003: 738-742.

[11] Yu X, Gibbon T B, Pawlik M, et al. A photonic ultra-wideband pulse generator based on relaxation oscillations of a semiconductor laser. *Opt. Express*, 2009, **17**(12): 9680-9687.

[12] Gibbon T B, Yu X, Gamatham R, et al. 3.125 Gb/s impulse radio UWB over fiber transmission. In: ECOC2009. Vienna, Austria, 2009: P6.01.

[13] http://www.skycross.com/Products/PDFs/SMT-3TO10M-A.pdf, 2009.

[14] http://www.geozondas.com/Old_Site/Antenna_AU-3-1G10-6G-1/Antenna_AU-3-1G10-6G-1.htm, 2009.

[15] Rodes R, Caballero A, Yu X, et al. A comparison of electrical and photonic pulse generation for IR-UWB on fiber links. *Photonics Technology Letters*, 2010, **22**(5): 264-266.

Paper 12: 3.125 Gb/s impulse radio ultra-wideband photonic generation and distribution Over a 50 km Fiber With Wireless Transmission

Gibbon Timothy Braidwood, Yu Xianbin, Gamatham Romeo, Guerrero Gonzalez Neil, Rodes Lopez Roberto, Jensen Jesper Bevensee, Caballero Jambrina, Antonio, Tafur Monroy Idelfonso. "3.125 Gb/s impulse radio ultra-wideband photonic generation and distribution Over a 50 km Fiber With Wireless Transmission", *IEEE Microwave and Wireless Components Letters*, vol. 20, no. 2, pp. 127-129, February 2010.

3.125 Gb/s Impulse Radio Ultra-Wideband Photonic Generation and Distribution Over a 50 km Fiber With Wireless Transmission

Timothy Braidwood Gibbon, Xianbin Yu, Romeo Gamatham, Neil Guerrero Gonzalez, Roberto Rodes, Jesper Bevensee Jensen, Antonio Caballero, and Idelfonso Tafur Monroy

***Abstract*—A 3.125 Gb/s photonic impulse radio ultra-wideband signal is created using the incoherent optical field summation resulting from the cross gain modulation of an uncooled distributed feedback laser injected with an external cavity laser. After 50 km of fiber and wireless transmission over 2.9–3.3-m, successful detection using a digital signal processing receiver is achieved.**

***Index Terms*—Digital signal processing, photonic signal generation, ultra-wideband (UWB), wireless transmission.**

I. Introduction

ULTRA-WIDEBAND (UWB) radio is a rapidly emerging technology capable of supporting bandwidth intensive applications by radiating extremely low power levels into the environment within an unlicensed region of the spectrum, below the noise floor of other wireless technologies such as Global Positioning System (GPS), WiMax and Universal Mobile Telecommunications System (UTMS) [1]. As governed by the Federal Communications Commission (FCC), UWB operates from 3.1–10.6 GHz at radiation levels below $-41.3\,\mathrm{dBm/MHz}$. Wireless UWB can however only propagate several meters due to the low power levels. Photonic UWB signals transmitted through fiber are thus extremely useful for distributing UWB in converged optical/ short range wireless access networks. For broadcast applications such as high definition TV this approach has the added benefit that the UWB transmission equipment can be localized in a central office, thereby sharing capex and opex costs amongst many users.

Two major challenges confronting the practical implementation of UWB optical-wireless access networks are the generation of high speed photonic impulse radio UWB (IR-UWB) signals, and the challenge of extending wireless reach. Previous demonstrations include photonic IR-UWB generation at 500 Mb/s with pulse shaping and 65 cm wireless transmission [2], 625 Mb/s photonic generation with frequency up-conversion [3], 781.25 Mb/s [4], [5] and 3.125 Gb/s [6] photonic generation using an uncooled DFB laser, 1.025 Gb/s photonic generation with 20 cm wireless [7], 1.625 Gb/s photonic generation with wireless transmission over an unspecified distance [8], and 90 cm wireless at 1 Gb/s [9].

In this letter we report to date the furthest and highest bit rate wireless transmission of an IR-UWB signal generated in the photonic domain. A 3.125 Gb/s photonic IR-UWB signal is generated based on the incoherent optical field summation resulting from cross gain modulation (XGM) of an uncooled distributed feedback (DFB) laser injected with a 12.5 Gb/s modulated external cavity laser (ECL). The photonic IR-UWB signal is transmitted over 50 km of fiber followed by a 2.9 m wireless link. The signal is subsequently recovered without errors using an offline digital signal processing (DSP) receiver.

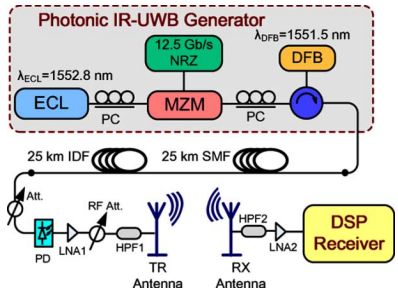

Fig. 1. Experimental setup used for the generation of 3.125 Gb/s photonic IR-UWB signals along with the subsequent fiber and wireless transmission.

II. Experiment Setup and Operation Principle

Fig. 1 shows the experimental setup. A 1552.8 nm ECL intensity modulated at 12.5 Gb/s is injected into the first-order sidemode of an uncooled DFB laser with a central wavelength of 1551.5 nm. A polarization controller (PC) placed before the circulator is used to adjust the state of polarization of the modulated ECL to ensure that the resultant XGM introduced within the DFB laser is maximized.

The signal exits the IR-UWB generator with an optical power of 3.3 dBm and is launched into 25 km of single mode fiber (SMF) followed by 25 km of matching inverse dispersion fiber (IDF). The combined fiber loss is 12.8 dB. The IR-UWB pulse is subsequently detected by a photodiode (PD) with a 12 GHz 3 dB bandwidth, before wireless retransmission with an omni-directional UWB antenna. A high pass filter (HPF1) is used to remove frequency components below 3.1 GHz. A low noise amplifier (LNA1) and RF attenuator are used to ensure

Manuscript received July 14, 2009; revised October 27, 2009. First published January 22, 2010; current version published February 10, 2010.

T. B. Gibbon, X. Yu, N. G. Gonzalez, R. Rodes, J. B. Jensen, A. Caballero, and I. Tafur Monroy are with the DTU Fotonik-Department of Photonics Engineering, Technical University of Denmark, Lygnby DK-2800, Denmark (e-mail: tbgi@fotonik.dtu.dk).

R. Gamatham is with the DTU Fotonik-Department of Photonics Engineering, Technical University of Denmark, DK-2800 Kgs. Lygnby, Denmark. He is also with the Department of Physics, Nelson Mandela Metropolitan University, Port Elizabeth, South Africa.

Color versions of one or more of the figures in this letter are available online at http://ieeexplore.ieee.org.

Digital Object Identifier 10.1109/LMWC.2009.2039049

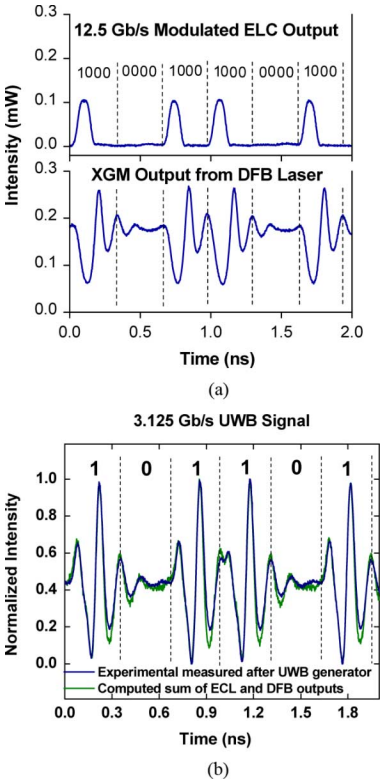

Fig. 2. (a) The ECL and DFB laser signals measured individually using a 0.4 nm FWHM filter at the output of the IR-UWB generator. (b) The IR-UWB signal resulting from the incoherent summation of the ECL and DFB signals.

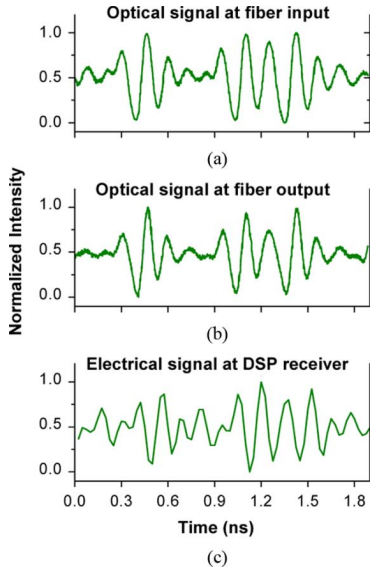

Fig. 3. Optical signals at (a) the fiber input and (b) fiber output for the IR-UWB bit sequence 010110. (c) Electrical signal at the DSP receiver after fiber transmission over 50 km and wireless transmission over 2.9 m.

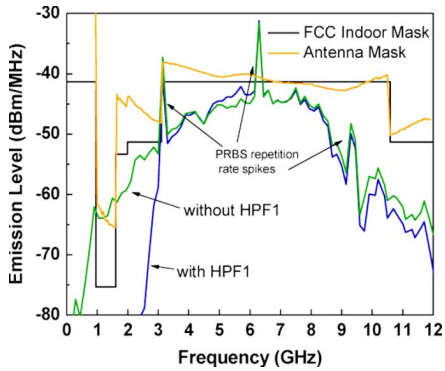

Fig. 4. Electrical spectrum at the input to the transmitter antenna, both with and without the high pass filter (HPF1).

that the radiated power levels comply with the FCC indoor requirements. The wireless signal is received by a directional antenna directed towards the transmitter. HPF2 is used to filter 0.9, 1.8, and 2.1 GHz GSM interference, and no absorbers were used. The received signal is processed by a DSP receiver comprising of an Agilent 40 GSa/s Digital Storage Oscilloscope and a custom offline DSP algorithm.

III. Generation of 3.125 Gb/s Optical IR-UWB

Injection of the intensity modulated signal from the ECL introduces XGM in the DFB laser. This causes the carrier and photon density inside the DFB laser active region to change with time, accompanied by relaxation oscillations which results in a complex pulse shape at the DFB laser output [10]. Both phase modulated [11] and [12] and intensity modulated [6] IR-UWB pulses can be produced from the incoherent sum of the ECL and DFB outputs. Fig. 2 illustrates the generation principle for a 101101 intensity modulated IR-UWB bit sequence. The ECL modulated at 12.5 Gb/s with the sequence 1000 0000 1000 1000 0000 1000 produces XGM of the DFB laser with associated overshoot and relaxation oscillations as shown in Fig. 2(a). IR-UWB bits are created from the incoherent sum of the ECL and DFB outputs as shown in Fig. 2(b). The 12.5 Gb/s modulation sequences 1000 and 0000 of the ECL correspond to 1 and 0 IR-UWB bits respectively, at an effective IR-UWB bit rate of 3.125 Gb/s.

The IR-UWB pulse resembles that of an inverted fifth-order Gaussian derivative, which is known to demonstrate good agreement to the FCC requirements [13]. The generation method shown here shares similarities to that used in [4] and [5], where an optically injected DFB laser was used to create a 781.25 Mb/s photonic IR-UWB signal. Unlike [4] and [5] however, there is no optical filter after the circulator in Fig. 1 to remove the ECL wavelength, and hence good compliance to the FCC requirements at higher bit rates can be achieved through the incoherent summation of the DFB and ECL optical fields. Were the ECL wavelength to be filtered as in [4], [5], the UWB pulse would have the shape of the DFB output shown in Fig. 2(b) instead of the ideal inverted fifth order Gaussian derivative.

IV. IR-UWB Transmission Results

Fig. 3(a) shows the optical signal directly after the IR-UWB generator for the bit sequence 010110. In comparison with Fig. 3(b) it is evident that the signal shape is well preserved after the 50 km fiber link. The IDF that is used to compensate the SMF dispersion has the added advantage compared to dispersion compensating fiber of being used as a transmission fiber, thus extending network reach.

From Fig. 4 it is evident that the IR-UWB pulse at the input to the transmitter antenna shows good compliance with the FCC

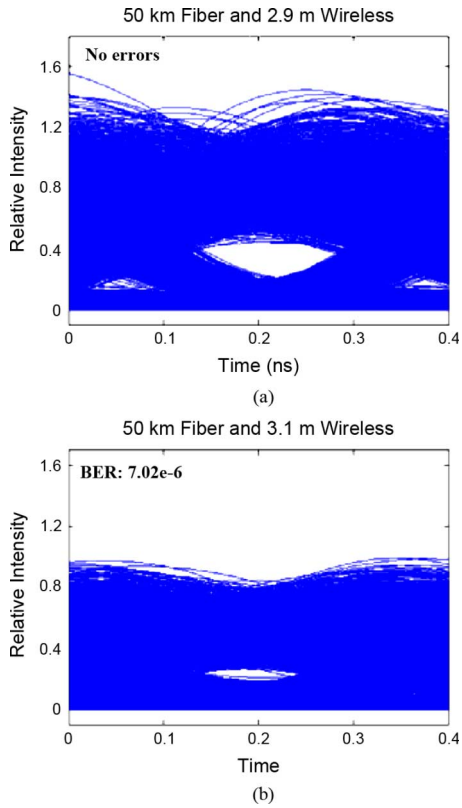

Fig. 5. Eye diagrams with 20000 bits for IR-UWB transmission over 50 km fiber link followed by (a) 2.9 m wireless, (b) 3.1 m wireless.

mask when using HPF1 to remove low frequency components below 3.1 GHz. The frequency response and gain of the transmitter antenna plays a role in shaping the transmitted wireless pulse. The effective antenna mask, which was calculated as described in [2], takes this into account and provides the overall conditions for FCC compliance. The spikes in the spectrum with 3.125 Gb/s spacing are a measurement artifact originating from the PRBS repetition rate, and in accordance with the FCC regulation such spikes may protrude around 20 dB above the FCC mask [14].

In order to assess transmission performance, 1 million IR-UWB bits following a $2^7 - 1$ PRBS pattern were transmitted over the fiber and wireless link and recorded using a 40 GSa/s Digital Storage Oscilloscope. The bit error rate was subsequently computed using a DSP algorithm in a bit-for-bit comparison between the transmitted and received bits. The DSP algorithm features noise filtering, bit correlation, and distinguishing between "1" and "0" IR-UWB bits by comparing the average power within the central window of each bit slot to an optimally determined decision threshold [4] and [5]. For 50 km IR-UWB over fiber followed by 2.9 m wireless, 1 million bits were transmitted error-free. An example of the signal at the DSP receiver is shown in Fig. 3(c). Wireless distances of 3.1 m and 3.3 m yielded bit error rates of 7.02e-6 and 5.89e-3, respectively. The corresponding eye diagrams after DSP processing for 2.9 m and 3.1 m wireless transmission are shown in Fig. 5. The results were very similar for back-to-back wireless transmission without the fiber, yielding no errors in 1 million bits at 3.1 m, and a bit error rate of 4.27e-3 for 1 million bits at 3.3 m.

V. Conclusion

In this letter, we reported to date the furthest and highest bit rate wireless transmission of an IR-UWB signal generated in the photonic domain. A 3.125 Gb/s photonic IR-UWB signal was created using the incoherent optical field summation resulting from cross gain modulation of an uncooled distributed feedback laser injected with an external cavity laser. The photonic components used are all conventional to optical fiber access systems. The IR-UWB signal was sent over 50 km of fiber followed by 2.9 m wireless, and subsequently recovered without error in 1 million bits using a digital signal processing receiver. The results highlight the potential of IR-UWB as a candidate for supporting extremely bandwidth intensive applications in converged optical/ short range wireless access networks.

References

[1] D. Porcine, P. Research, and W. Hirt, "Ultra-wideband radio technology: Potential and challenges ahead," *IEEE Commun. Mag.*, vol. 41, no. 7, pp. 66–74, Jul. 2003.

[2] M. Abtahi, M. Mirshafiei, S. LaRochelle, and L. A. Rusch, "All-Optical 500 Mb/s UWB transceiver: An experimental demonstration," *IEEE J. Lightwave Technol.*, vol. 26, no. 15, pp. 2795–2802, 2008.

[3] Q. Chang, Y. Tian, T. Ye, J. Gao, and Y. Su, "A 24-GHz ultra-wideband over fiber system using photonic generation and frequency up-conversion," *IEEE Photon. Technol. Lett*, vol. 20, no. 19, pp. 1651–1653, Oct. 2008.

[4] T. B. Gibbon, X. Yu, D. Zibar, and I. T. Monroy, "Novel ultra-wideband photonic signal generation and transmission featuring digital signal processing bit error rate measurements," in *Proc. OFC/NFOEC'09*, Mar. 2009, p. OTuB8.

[5] T. B. Gibbon, X. Yu, and I. T. Monroy, "Photonic ultra-wideband 781.25 Mbit/s signal generation and transmission incorporating digital signal processing detection," *IEEE Photon. Technol. Lett*, vol. 21, no. 15, pp. 1060–1062, Aug. 2009.

[6] T. B. Gibbon, X. Yu, and I. T. Monroy, "3.125 Gb/s impulse radio UWB over fiber transmission," in *Proc. ECOC'09*, Vienna, Austria, Sep. 2009, p. P6.01.

[7] M. Hanawa, K. Mori, K. Nakamura, A. Matsui, Y. Kanda, and K. Nonaka, "Dispersion tolerant UWB-IR-over-fiber transmission under FCC indoor spectrum mask," in *Proc. OFC/NFOEC'09*, Mar. 2009, p. OTuJ3.

[8] H. Shams, A. Kaszubowska-Anandarajah, P. Perry, and L. P. Barry, "Optical generation, fiber distribution and air transmission of ultra wide band over fiber system," in *Proc. OFC/NFOEC'09*, Mar. 2009, p. OWR2.

[9] C. M. Tran, L. C. Ong, M. L. Yee, B. Luo, and P. K. Tang, "Transmission of ultra wide band radio using multimode radio-over-fiber system," in *Proc. APMC'05*, Suzhou, China, Dec. 2005, vol. 2, p. P2.89.

[10] X. Yu, T. B. Gibbon, M. Pawlik, S. Blaaberg, and I. T. Monroy, "A photonic ultra-wideband pulse generator based on relaxation oscillations of a semiconductor laser," *Opt. Express*, vol. 17, no. 12, pp. 9680–9687, 2009.

[11] X. Yu, T. B. Gibbon, D. Zibar, and I. T. Monroy, "A novel incoherent scheme for photonic generation of biphase modulated UWB signals," in *Proc. OFC/NFOEC'09*, Mar. 2009, p. JWA60.

[12] X. Yu, T. B. Gibbon, and I. T. Monroy, "Experimental demonstration of all-optical 781.25 Mbit/s binary phase coded signals generation and transmission," *IEEE Photon. Technol. Lett*, vol. 21, no. 17, pp. 1235–1237, Sep. 2009.

[13] H. Sheng, P. Orlik, A. M. Haimovich, L. J. Cimini, and J. Zhang, "On the spectral and power requirements for ultra-wideband transmission," in *ICC2003*, May 2003, vol. 1, pp. 738–742.

[14] *Revision of Part 15 of the Commission's Rules Regarding Ultra-Wideband Transmission Systems*. Washington, DC: Federal Communications Commission, 2002.

Paper 13: Converged wireline and wireless access over a 78-km deployed fiber long-reach WDM PON

Prince Kamau, Jensen Jesper Bevensee, Caballero Jambrina Antonio, Yu Xianbin, Gibbon Timothy Braidwood, Zibar Darko, Guerrero Gonzalez Neil, Osadchiy Alexey Vladimirovich, Tafur Monroy Idelfonso. "Converged wireline and wireless access over a 78-km deployed fiber long-reach WDM PON", *IEEE Photonics Technology Letters*, vol. 21, no. 17, pp. 1274-1276, September 2009.

Converged Wireline and Wireless Access Over a 78-km Deployed Fiber Long-Reach WDM PON

Kamau Prince, *Student Member, IEEE*, Jesper Bevensee Jensen, Antonio Caballero, Xianbin Yu, Timothy Braidwood Gibbon, Darko Zibar, Neil Guerrero, Alexey Vladimirovich Osadchiy, and Idelfonso Tafur Monroy

***Abstract*—In this letter, we demonstrate a 78.8-km wavelength-division-multiplexing passive optical network supporting converged transport of 21.4-Gb/s nonreturn-to-zero differential quadrature phase-shift keying, optical phase-modulated 5-GHz radio-over-fiber, fiber and air transmission of 3.125-Gb/s pulse ultrawideband, and 256-quadratic-amplitude modulation wireless interoperability for microwave access.**

***Index Terms*—Coherent optical systems, converged access networks, ultrawideband (UWB) signaling, wireless interoperability for microwave access (WiMAX).**

I. Introduction

HYBRID optical/wireless access network architectures are considered a promising solution for large-scale deployment of broadband access as they combine the advantages of high capacity offered by optical access with the flexibility provided by wireless networks [1], [2]. Simultaneous transport of wireline and wireless types of signals, fulfilling power budget, dispersion, and other quality requirements for both signal types, over a common fiber infrastructure is an important aspect for hybrid optical wireless access networks.

We report on a converged wireless and wireline, wavelength-division multiplexing (WDM) passive optical network (PON) access link over a 78.8-km-long commercially deployed optical fiber in Copenhagen. We successfully implemented an eight-channel, single-fiber, WDM transmission system simultaneously supporting 85.6-Gb/s baseband via four 21.4-Gb/s nonreturn-to-zero (NRZ) differential quadrature phase-shift keying (DQPSK) channels, 500 Mb/s via two coherently detected phase-modulated radio-over-fiber (RoF) channels, 3.125 Gb/s via impulse radio ultrawideband (UWB), and intensity-modulated, direct-detected RoF link with quadratic-amplitude modulation (QAM) at 12 megabaud (MBd). Air transmission was demonstrated after fiber transmission for the UWB and WiMAX signals.

Manuscript received April 21, 2009; revised June 08, 2009. First published July 10, 2009; current version published August 19, 2009. This work was supported in part by the European Union FP7 Information Communication Technology (ICT)-ALPHA and in part by the ICT GigaWaM projects.

The authors are with the Department of Photonics Engineering, Technical University of Denmark, DK-2800 Kgs. Lyngby, Denmark (e-mail: kpri@fotonik.dtu.dk; jebe@fotonik.dtu.dk; acaj@fotonik.dtu.dk; xiyu@fotonik.dtu.dk; tbgi@fotonik.dtu.dk; dazi@fotonik.dtu.dk; nggo@fotonik.dtu.dk; avos@fotonik.dtu.dk; idtm@fotonik.dtu.dk).

Color versions of one or more of the figures in this letter are available online at http://ieeexplore.ieee.org.

Digital Object Identifier 10.1109/LPT.2009.2025699

II. System Layout

Fig. 1 shows a block diagram of the field trial and setup used in the experiment. The field-deployed fiber connects the Kongens Lyngby campus of the Technical University of Denmark (DTU) and facilities located in the suburb of Taastrup. The fiber is a G.652 standard single-mode fiber (SMF) type (16.5 ps/nm·km chromatic dispersion, 0.20 dB/km attenuation, polarization dispersion coefficient < 0.20 ps/$\sqrt{\text{km}}$). The total link loss was measured at 25 dB. The eight WDM channels employed were separated by 200 GHz, at standard International Telecommunication Union (ITU) wavelengths, denoted by $\lambda_1 = 1549.3$ nm through $\lambda_8 = 1560.0$ nm. Four wavelengths (λ_{5-8}) were used for NRZ-DQPSK: two $(\lambda_{2,4})$ for coherent RoF, λ_3 for UWB, and λ_1 for WiMAX. Launch power into the deployed fiber was set to 0 dBm for each of the eight channels. A dispersion-compensating fiber (DCF) was used at the transmitter; this also ensured decorrelated signals at the input to the transmission fiber. A preamplifier erbium-doped fiber amplifier (EDFA) overcame transmission losses before wavelength demultiplexing by arrayed waveguide grating (AWG). AWG spacing of 200 GHz was used due to equipment availability; we anticipate good system performance with closer spacing [3].

A. NRZ-DQPSK Baseband

The transmitter setup comprises four DFB lasers at wavelengths $\lambda_5 - \lambda_8$ multiplexed in an AWG and NRZ-DQPSK modulated using an inphase/quadrature (I/Q) modulator driven by two electrical pseudorandom bit sequences (PRBSs) of length $2^7 - 1$ bits and bit rate 10.7 Gb/s, resulting in a per-channel bit rate of 21.4 Gb/s at a symbol rate of 10.7 GBd. The $2^7 - 1$ bit pattern length was selected due to limitations of the bit error rate tester (BERT) functionality. Since we used phase modulation, no pattern dependency was expected from nonlinear effects in the transmission fiber. After transmission and wavelength demultiplexing, the NRZ-DQPSK signals were demodulated using a one-symbol delay Mach–Zehnder interferometer (MZI) and detected by a pair of balanced photodetectors (BPDs). The BER of each DQPSK tributary was measured independently, and we report the average obtained.

B. Coherent RoF

A 5-GHz RF carrier at $+8$ dBm was BPSK modulated at 250 Mb/s, and used to optically phase modulate signals at wavelengths of λ_2 and λ_4. At the receiver, the desired channel was optically mixed with a continuous-wave local oscillator (LO) signal, derived from a tunable laser source at 0 dBm output power, and coherently detected using a 90° optical hybrid with integrated photodetectors. The in-phase (I) and quadrature (Q)

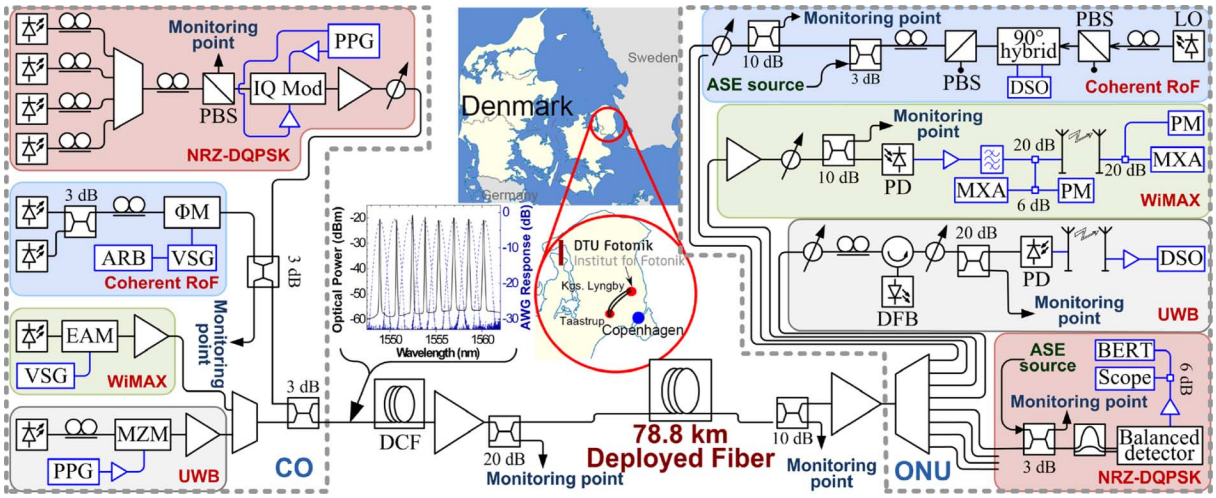

Fig. 1. Detail of the experimental setup. PPG: pulse pattern generator; PBS: polarization beam splitter; PM: optical phase modulator; ARB: arbitrary waveform generator; VOA: variable optical attenuator. ASE added to evaluate system OSNR sensitivity for phase-modulated signals: precompensating DCF-implemented decorrelation of RoF and NRZ-DQPSK signals. (Inset) Spectra of launched WDM optical signal (solid line) and AWG response (dashed line).

electrical signals were sampled at 40 GSa/s by a sampling oscilloscope (SO) with a 13 GHz bandwidth. The stored signals were processed offline using DSP algorithms described in [3] to perform signal demodulation and BER evaluation.

C. Impulse Radio UWB

A lightwave at λ_3 (1552.80 nm wavelength) was modulated by a 12.5-Gb/s pattern "1000" using a Mach–Zehnder modulator (MZM). An uncooled DFB laser was optically injected with the incoming signal from the fiber link. Under optical injection, cross-gain modulation and relaxation oscillations governing the dynamic response of the DFB shape its output signal [4]. The incoherent combination of the injected and DFB wavelengths after photodetection generated a pulse with a postdetection RF spectrum that is compliant with the impulse radio UWB mask. Air transmission of 40 cm was implemented. These UWB signals were sampled by a 40 GSa/s sampling scope with 13 GHz bandwidth, and processed offline using a DSP algorithm.

D. WiMAX

An electroabsorption modulator (EAM) fed by an optical carrier at λ_2 was modulated with a 256-QAM RF signal, centered at 5.8 GHz, obtained from an Agilent E4438C vector signal generator (VSG); a boost EDFA and a variable optical attenuator (VOA) controlled the launch power. A preamplified receiver was implemented with a 30-dB gain EDFA, an optical bandpass filter (BPF), and a 10-GHz PIN photodiode. The electrical signal obtained was amplified by 35 dB, filtered by 25 MHz RF duplexers for 5 GHz unlicensed ISM band operation, and radiated by a 12 dBi omnidirectional 5 GHz antenna. The wireless signal was detected with an identical antenna at 40 cm separation, and amplified and assessed with an Agilent 9020 MXA vector signal analyzer (VSA) with the 89 600 VSA signal analyzer software. We report error vector magnitude (EVM) sensitivity to RF source power at both ends of the wireless link for the single active wavelength and for all WDM transmitters active. We additionally assessed the performance with extra 40 km of uncompensated SMF, after DF and preamp and the postdetection eye diagram.

III. Results

A. NRZ-DQPSK Baseband

The BER of the four NRZ-DQPSK-modulated baseband channels back-to-back (B2B) and after fiber transmission is plotted in Fig. 2(a) with filled symbols/solid lines for the back-to-back case and hollow symbols/dashed lines for the transmitted. OSNR requirement for a BER of 10^{-9} was observed between 22 dB (λ_5) and 23.3 dB for λ_8. At λ_7, a penalty of 0.3 dB was observed after transmission; for all other channels, no penalty was measured. The eye diagrams before and after transmission shown in Fig. 2(b) show no transmission distortion, thus confirming good transmission properties.

B. Coherent RoF

A 250-MBd BPSK data signal modulating a 5-GHz RF carrier for each WDM channel was successfully recovered after transmission through the dark fiber with input power to the coherent receiver set to -15.77 and -16.77 dBm, respectively. In Fig. 2(b), the BER curves for back-to-back and after fiber transmission are computed as a function of OSNR values from 7 to 12 dB. We observed a receiver sensitivity penalty of 0.5 dB at λ_2 for BER at 10^{-3}, whereas a 2 dB penalty was observed in channel 4, which we believe was caused by partial misalignment of the source with the AWG passband.

C. Impulse Radio UWB

We generated 3.125-Gb/s ON–OFF key (OOK) modulation with $2^7 - 1$ PRBS; an example of "1110111" pattern and the resulting RF spectrum are shown in Fig. 3(a). The frequency spectra observed are compatible with the FCC (indoor) UWB mask. We used a sample size of 684 kilosamples, and a DSP algorithm was employed to calculate the BER offline. From the BER measurement curves, we observed less than 0.5 dB penalty between B2B and fiber transmission (for both single-channel and WDM transmissions).

D. WiMAX

We successfully transported 256-QAM signals at 12 MBd over the deployed fiber and an additional 40 km SMF with no

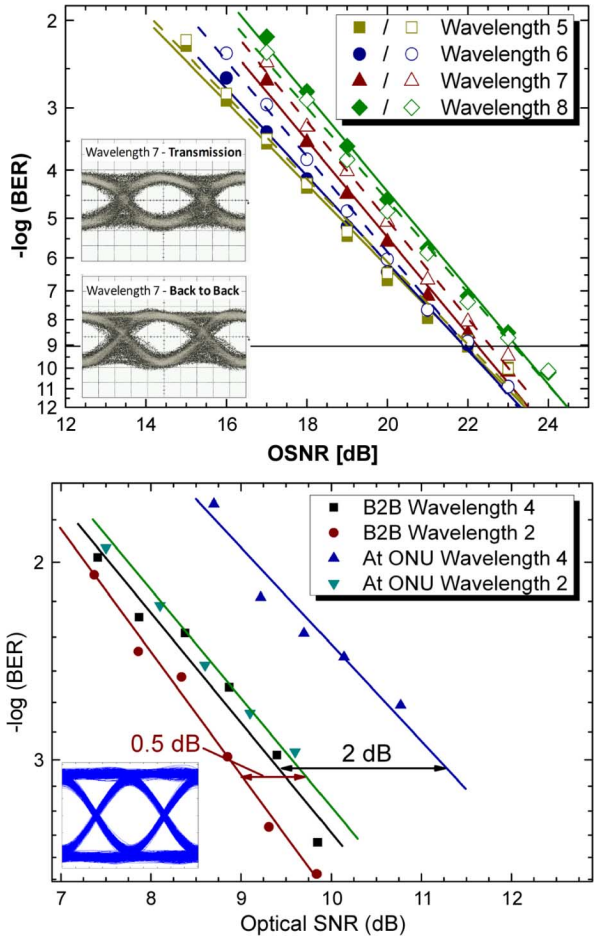

Fig. 2. BER results. (Top) 21.4-Gb/s NRZ-DQPSK. (Bottom) Coherent RoF. Sample eye diagrams are also shown.

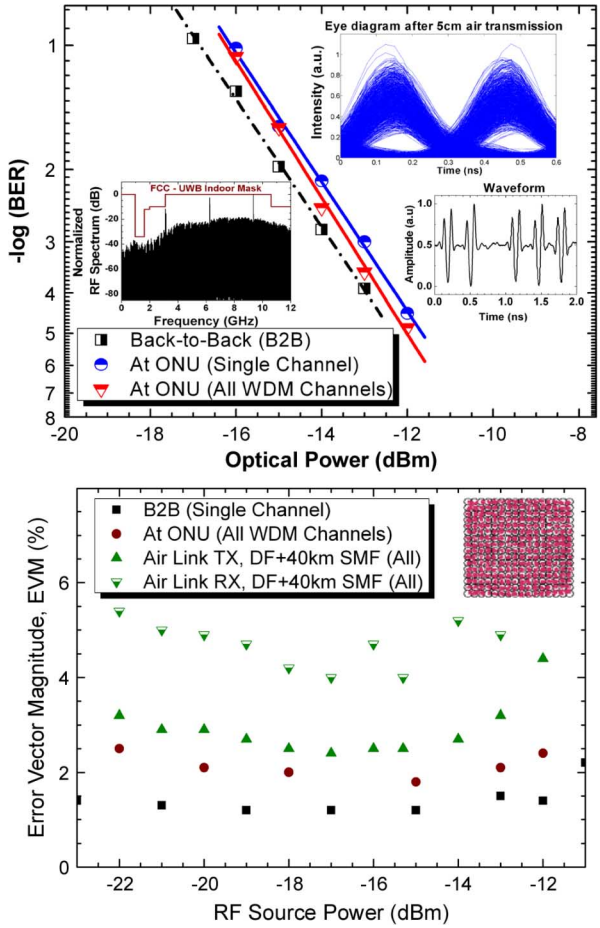

Fig. 3. (Top) BER results, RF spectrum, and eye diagrams obtained for 3.125-Gb/s UWB. (Bottom) WiMAX EVM sensitivity and constellation.

further optical amplification, with below 3% EVM at the remote transmit antenna, as shown in Fig. 3(b). System spur-free dynamic range was 74 dB/Hz$^{2/3}$.

IV. Conclusion

We successfully demonstrated combined transport over a single 78.8-km field-installed fiber of NRZ-DQPSK-modulated baseband access at 21.4 Gb/s per channel, coherent RoF at 250 Mb/s per channel, impulse-radio UWB at a record speed of 3.2 Gb/s, and a 256-QAM WiMAX signal at 12 MBd. For the UWB and WiMAX signals, air transmission was included after the fiber link. This is the first known demonstration of its kind, and it proves that the existing standard SMF based fiber infrastructure can support the seamless coexistence of various wireless and wireline signals for future converged broadband access networks. Prior results [5] also suggest the feasibility of WDM transmission with 100-GHz channel separation.

Acknowledgment

The authors would like to thank M. M. Nedergaard and D. Fryd of the Agilent Technologies Denmark for access to RF signal quality evaluation platforms, and N. Raun of GlobalConnect Denmark for access to the deployed fiber.

References

[1] S. Sarkar, S. Dixit, and B. Mukherjee, "Hybrid wireless-optical broadband-access network (WOBAN): A review of relevant challenges," *J. Lightw. Technol.*, vol. 25, no. 11, pp. 3329–3340, Nov. 2007.

[2] W.-T. Shaw, S.-W. Wong, N. Cheng, K. Balasubramanian, X. Zhu, M. Maier, and L. G. Kazovsky, "Hybrid architecture and integrated routing in a scalable optical-wireless access network," *J. Lightw. Technol.*, vol. 25, no. 11, pp. 3443–3451, 2007.

[3] D. Zibar, X. Yu, C. Peucheret, P. Jeppesen, and I. Tafur Monroy, "Digital coherent receiver for phase-modulated radio-over-fiber optical links," *IEEE Photon. Technol. Lett.*, vol. 21, no. 3, pp. 155–157, Feb. 1, 2009.

[4] X. Yu, T. B. Gibbon, D. Zibar, and I. Tafur Monroy, "A novel incoherent scheme for photonic generation of biphase modulated UWB signals," presented at the Opt. Fiber Commun. Conf. (OFC), San Diego, CA, Mar. 2009, Paper JWA60.

[5] J. Jensen, T. Torkle, C. Peucheret, and P. Jeppesen, "Transmission of WDM multilevel 8 × 30 Gbit/s single polarization RZ-D8PSK with a total capacity of 240 Gbit/s," presented at the 33rd Annu. Eur. Conf. Exhib. Opt. Commun. (ECOC), Berlin, Germany, Sep. 2007, Paper P097.

Bibliography

[1] T. Kuri, H. Toda, J. J. Vegas-Olmos,and K. Kitayama. "Reconfigurable Dense Wavelength-Division-Multiplexing Millimeter-Waveband Radio-Over-Fiber Access System Technologies." *Journal of Lightwave Technology,* vol. 28, issue. 16, pp. 2247–2257, 2010.

[2] K. Sato and H. Hasegawa. "Optical Networking Technologies That Will Create Future Bandwidth Abundant Networks." *Journal on Optical Communications Networks,* vol. 1, issue. 2, pp. 81–83, 2009.

[3] F.J. Effenberger, J.i Kani, and Y. Maeda, "Standardization Trends and Prospective Views on the Next Generation of Broadband Optical Access Systems." *IEEE Journal on Selected Areas in Communications,* vol. 28, issue. 6, pp. 773–780, 2010.

[4] Cvijetic, M. "Advanced Technologies for Nex-Generation Fiber Network," in textitProceeding of Optical Fiber Communication Conference 2010, OFC '10. San Diego, CA, USA. Paper OWY1. 2010.

[5] X. Zhou, J. Yu, M.-F. Huang, Y. Shao, T. Wang, P. Magill, M. Cvijetic, L. Nelson, M. Birk, G. Zhang, S. Ten, H. Matthew, and S. Mishra. "32Tb/s ($320 \times 114Gb/s$) PDM-RZ-8QAM transmission over 580km of SMF-28 ultra-low-loss fiber," in textitProceeding of Optical Fiber Communication Conference 2009, OFC '09. San Diego, CA, USA. Paper PDPB4. 2009.

[6] G. K. Chang, A. Chowdhury, Z. Jia, H. C. Chien, M. F. Huang, J. Yu and G. Ellinas. "Key Technologies of WDM-PON for Future Converged Optical Broadband Access Networks." *Journal on Optical Communication Networks,* vol. 1, issue. 4, pp. C35–C50, 2009.

[7] R. Freund, M. Seimetz, L. Molle, T. Baghdasaryan, M. Forzati and J. Mårtensson. "Next Generation Optical Networks Based on Higher-

Order Modulation Formats, Coherent Receivers and Electronic Distortion Equalization." in *ICTON-MW'09*. Paper Th3.1. 2009.

[8] J. B. Jensen, A. V. Osadchiy, D. Zibar, R. Rodes Lopez, V. Arlunno, N. Guerrero Gonzalez, A. Caballero Jambrina, X. Yu, I. Tafur Monroy. "Coherent technologies for next generation flexible converged wireless-wireline access networks," in *Proceeding of Access Networks and In-house Communications (ANIC)*. Karlsruhe, Germany (Invited conference contribution). 2010.

[9] M. Popov. "The Convergence of Wired and Wireless Service Delivery in Access and Home Network," in *Proceeding of Optical Fiber Communication Conference 2010, OFC '10*. San Diego, CA, USA. 2009.

[10] M. Riaz, R.H. Nielsen, J.M. Pedersen, N Prasad, and O.B. Madsen. "On Radio over Fiber for Heterogeneous Wireless Network," in *Proceeding of International Conference on Wireless and Optical Communications Networks*. Cairo. pp. 1–4. 2009.

[11] N. J. Gomes, M. Morant, A. Alphones, B. Cabon, J. E. Mitchell, C. Lethien, M. Csörnyei, A. Stöhr and S. Iezekiel. "Radio-over-fiber transport for the support of wireless broadband services. " *Journal of Optical Networking,* vol. 8, issue. 2, pp. 156-178, 2009.

[12] Y. Pi, Z. Dong, L. Chen, J. Yu. "A Radio-over-Fiber System for Simultaneous Generation of Wired and Wireless Services," in *Proceeding of SPIE, SPIE'08*. Vol. 7136. pp 71361K-1–71361K-9. 2008.

[13] J. J. Vegas Olmos, T. Kuri and K. I. Kitayama. "Dynamic Reconfigurable WDM 60-GHz Millimeter-Waveband Radio-Over-Fiber Access Network: Architectural Considerations and Experiment." *Journal of Lightwave Technology,* vol. 25, issue 11, pp 3374–3380. 2007.

[14] J. J. Vegas Olmos, T. Kuri, T. Sono, K. Tamura, H. Toda, and K. I. Kitayama. "Reconfigurable 2.5-Gb/s Baseband and 60-GHz (155-Mb/s) Millimeter-Waveband Radio-Over-Fiber (Interleaving) Access Network." *Journal of Lightwave Technology,* vol. 26, issue 15, pp 2506–2512. 2008.

[15] Y. Y. Won, H. S. Kim, Y. H. Son and S. K. Han. "Full Colorless WDM-Radio Over Fiber Access Network Supporting Simultaneous Transmission of Millimeter-Wave Band and Baseband Gigabit Signals by Side-

band Routing." *Journal of Lightwave Technology,* vol. 28, issue 16, pp 2213–2218. 2010.

[16] C. Lim, A. Nirmalathas, M. Bakaul, P. Gamage, K. Lee, Y. Yang, D. Novak, and R. Waterhouse. "Fiber-Wireless Networks and Subsystem Technologies." *Journal of Lightwave Technology,* vol. 28, issue. 4, pp. 390–405, 2010.

[17] H. Paul, K-D. Kammeyer. "Equivalent baseband channels of systems using envelope detection." *International Journal of Electronics and Communications,* vol. 63, pp. 533–540. 2009.

[18] K. Prince, I. Tafur Monroy, J. Seoane and P. Jeppesen. "All-optical envelope detection for Radio-over-Fiber links using external optical injection of a DFB laser." *Optics Express,* vol. 16, issue 3, pp. 2005–2014. 2008.

[19] I. Tafur Monroy, K. Prince, J. Seoane, and X. Yu. "Optically Envelope Detected QAM and QPSK RF Modulated Signals in Hybrid Wireless-Fiber Systems." *Microwave and Optical Technology Letters,* vol. 51, issue 3, pp. 864–865. 2009.

[20] D. Porcine, P. Research, and W. Hirt. "Ultra-wideband radio technology: Potential and challenges ahead." *IEEE Commununications Magazine,* vol. 41, issue. 7, pp. 66–74, 2003.

[21] R. Naik, J. Singh, H. P. Le and J. Devlin. "Real Time Reconfigurability for UWB Receiver." in *Proceeding of the 2008 IEEE International Conference on Ultra-wideband ICUWB'2008,* vol. 1, 2008.

[22] C. Carbonelli and U. Mengali. "Synchronization Algorithms for UWB Signals." *IEEE Transactions on Communications,* vol. 54, issue. 2, pp. 329–338, 2006.

[23] D. Wake, A. Nkansah, and N.J. Gomes. "Radio over Fiber Link Design for Next Generation Wireless System. " *Journal of Lightwave Technology,* vol. 28, issue. 16, pp. 2456-2464, 2010.

[24] T. Berceli, and P.R. Rerczfeld. "Microwave Photonics - A Historical Perspective." *IEEE Transactions on Microwave Theory and Thecniques,* vol. 58, issue. 11, pp. 2292—3000, 2010.

[25] Y. Li and P. Herczfeld. "Coherent PM optical link employing ACP-PPLL." *Journal of Lightwave Technology,* vol. 27, issue. 9, pp. 1086—1094, 2009.

[26] T.R. Clark, and M.L. Dennis. "Coherent Optical Phase-Modulation Link." *IEEE Photonics Technology Letters,* vol. 19, issue. 16, pp. 1206—1208, 2007.

[27] T. R. Clark, S. R. O'Connor and M. L. Dennis. "A Phase-Modulation I/Q-Demodulation Microwave-to-Digital Photonic Link." *IEEE Transactions on Microwave Theory and Techiques,* vol. 58, issue. 11, pp. 3039—3058, 2010.

[28] D. Zibar, X. Yu, C. Peucheret, P. Jeppesen and I. Tafur Monroy. "Digital Coherent Receiver for Phase-Modulated Radio-Over-Fiber Optical Links." *IEEE Photonic Techology Letters,* vol. 21, issue. 3, pp. 155–157, 2009.

[29] T. Okoshi, and K. Kikuchi. "Coherent optical fiber communications." *KTK Academic Publishers,* Tokio. 2008.

[30] S. Tsukamoto. "Coherent demodulation of 40-Gbit/s polarization-multiplexed QPSK signals with 16-GHz spacing after 200-km transmission," in *Proceeding of Optical Fiber Communication Conference 2005, OFC '05.* San Diego, CA, USA. Paper PDP29. 2005.

[31] S.Savory., "Electronic Signal Procesing in Optical Communications," in *Proceeding of SPIE, SPIE'08.* Vol. 7136. Invited paper. 2008.

[32] S. Savory. "Digital Coherent Optical Receivers: Algorithms and Subsystems." *IEEE Jourrnal of Selected Topics in Quantum Electronics,* vol. 16, issue. 5, pp. 1164–1179, 2010.

[33] L. G. Kazovsky, G. Kalogerakis and W.-T. Shaw. "Homodyne Phase-Shift-Keying Systems: Past Challenges and Future Opportunities." *Journal of Lightwave Technology,* vol. 24, issue. 12, pp. 4876–4884, 2006.

[34] C.R.S. Fludger, J.C. Geyer, T. Duthel, S. Wiese, and C. Schulien. "Real-time Prototypes for Digital Coherent Receivers," in *Proceeding of Optical Fiber Communication Conference 2010, OFC '10.* San Diego, CA, USA. Paper OMS1. 2010.

[35] A. Leven, N. Kaneda, and S. Corteselli. "Real-Time Implementation of Digital Signal Procesing for Coherent Optical Digital Communication Systems." *IEEE Journal of Selected Topics in Quantum Electronics,* vol. 18, issue. 5, pp. 1227–1234, 2010.

[36] E. M. Ip and J. M. Kahn, "Fiber Impairment Compensation Using Coherent Detection and Digital Signal Processing." *Journal of Lightwave Technology,* invited paper, pp. 502–519, 2010.

[37] R. Noe. "Phase noise-tolerant synchronous QPSK/BPSK baseband-type intradyne receiver concept with feedforward carrier recovery." *Journal of Lightwave Technology,* vol. 23, issue. 2, pp. 802–808, 2005.

[38] E. Ip and J. Kahn. "Feedforward carrier recovery for coherent optical communications." *Journal of Lightwave Technology,* vol. 25, issue. 9, pp. 2675–2692, 2007.

[39] A. J. Viterbi, and A. M. Viterbi. "Nonlinear estimation of PSK-modulated carrier phase with application to burst digital transmission." *IEEE Transaction in Information Theory,* vol. 29, issue. 4, pp. 543–551, 1983.

[40] M. G. Taylor. "Phase estimation methods for optical coherent detection using digital signal processing." *Journal of Lightwave Technology,* vol. 29, issue. 7, pp. 901–914, 2009.

[41] L. Pessoa, H. Salgado, and I. Darwazeh. "Performance evaluation of phase estimation algorithms in equalized coherent optical systems." *IEEE Photonic Technology Letters,* vol. 21, issue. 17, pp. 1181–1183, 2009.

[42] S. Hoffmann, R. Peveling, T. Pfau,O.Adamczyk, R. Eickhoff, and R.Noe. "Multiplier-free real-time phase tracking for coherent QPSK receivers." *IEEE Photonic Technology Letters,* vol. 21, issue. 3, pp. 137–139, 2009.

[43] H. Meyr, M. Moeneclaey and S. A. Fechtel. "Digital Communication Receivers: Synchronization, Channel Estimation and Signal Processing." *Wiley,* chapter 5, 1998.

[44] M. G. Taylor. "Coherent detection method using DSP for demodulation of signal and subsequent equalization of propagation impairments." *IEEE Photonic Technology Letter,* vol. 16, issue. 2, pp. 674–676, 2004.

[45] D. Crivelli, H.Carter, and M. Hueda. "Adaptative digital equalization in the presence of chromatic dispersion PMD and phase noise in coherent fiber optic systems.," in *Proceeding of IEEE Global Telecommun. Conf. GLOBECOM'04,* pp. 2545–2551. 2004.

[46] R. Raheli, and G.Picchi. "Synchronous and fractionally-spaced blind equalization in dually-polarized digital radio links.," in *Proceeding IEEE Int. Conference Communication,* vol. 1, pp. 156–161. 1991.

[47] F. Hauske, M. Kuschnerov, B. Spinnler, B. Lank. "Optical Performance Monitoring in Digital Coherent Receivers." *Journal of Lightwave Technology,* vol. 27, issue. 16, pp. 3623–3631, 2009.

[48] M. Kuschnerov, F. Hauske, K. Piyawanno, B. Spinnler, M. Alfiad, A. Napoli, and B. Lankl. "DSP for coherent single carrier receivers." *Journal of Lightwave Technology,* vol. 27, issue. 16, pp. 3614–3622, 2009.

[49] A. Caballero, D. Zibar, and I. Tafur Monroy. "Digital Coherent detection of multi-gigabit 40 GHz carrier frequency radio-over-fiber signals using photonic downconversion." *Electronics Letters,* vol. 46, issue. 1, pp. 57–58, 2010.

[50] T. Hoshida, H. Nakashima, T. Tanimura, S. Oda, Z. Tao, L. Liu, W. Yan, L. Li and J. C. Rasmussen. "Network Innovations Brought by Digital Coherent Receivers," in *Proceeding of the Optical Fiber Communication Conference, OFC'10.* San Diego, CA, USA. Paper NMB4. 2010.

[51] C. M. Bishop. "Pattern Recognition and Machine Learning." *Springer,* pp. 430–455, 2006.

[52] A. Leven, N. Kaneda, U.-V. Koc, and Y.-K. Chen. "Frequency estimation in intradyne reception." *IEEE Photonic Technology Letters,* vol. 19, issue. 6, pp. 366—368, 2007.

[53] L. C. Hong. "Maximum Likehood BPSK and QPSK Classifier in Fading Enviroment using the EM algorithm," in *Proceeding of the 38th Southeastern Symposium on System Theory,* Paper MC3.4, 2006.

[54] W. Sabrina Lin, and K.J. Ray Liu. "Modulation Forensics for Wireless Digital Communications," in *Proceeding of IEEE International Conference on Acoustics, Speech and Signal Processing ICASSP'08,* Las Vegas, USA. pp. 1789–1792. 2008.

[55] W. Su, J.L. Xu, and M. Zhou. "Real-time Modulation Classification Based On Maximum Likelihood." *IEEE Communications Letters,* vol. 12, issue. 11, pp. 801–803, 2008.

[56] F. Hameed, O.A. Dobre, and D.C. Popescu. "On the Likelihood-Based Approach to Modulation Classification." *IEEE Transactions on Wireless Communications,* vol. 8, issue. 12, pp. 5884–5892, 2009.

[57] S. Norimatsu and K. Iwashita. "Linewidth requirements for optical synchronous detection systems with nonnegligible loop delay time." *Journal of Lightwave Technology,* vol. 10, issue. 3, pp. 341–349, 1992.

[58] L. Li, Z. Tao, T. Hoshida, and J. C. Rasmussen. "Carrier synchronization in 43 Gbit/s coherent QPSK receiver.," in *Proceeding of OECC'07,* Yokohama, Japan. Paper 12B1. 2007.

[59] Z. Tao, L. Li, L. Liu, W. Yan, H. Nakashima, T. Tanimura, S. Oda, T. Hoshida, and J.C. Rasmussen. "Improvements to Digital Carrier Phase Recovery Algorithm for High-Performance Optical Coherent Receivers." *IEEE Journal of Select Topic in Quantum Electronics,* vol. 16, issue. 5, pp. 1201–1209, 2010.

[60] M. Seimetz. "Laser linewidth limitations for optical systems with high-order modulation employing feed-forward digital carrier phase estimation," in *Proceeding of OFC/NFOEC 2008,* Paper OTuM2. 2008

[61] S. Zhang, P. Y. Kam, C. Yu, and J. Chen. "Laser linewidth tolerance of decision-aided maximum likelihood phase estimation in coherent optical M-ary PSK and QAM systems." *IEEE Photonic Technology Letters,* vol. 21, issue. 15, pp. 1075–1077, 2009.

[62] F. Rice, M. Rice, and B. Cowley. "A newalgorithm for 16QAMcarrier phase estimation using QPSK partitioning." *Digital Signal Processing,* vol. 12, issue. 1, pp. 77–86, 2002.

[63] H. Louchet, K. Kuzmin, and A. Richter. "Improved DSP algorithms for coherent 16- QAM transmission," in *Proceeding of ECOC 2008,* Paper Tu.1.E.6. 2008.

[64] M. G. Taylor. "Accurate digital phase estimation for coherent detection using a parallel digital processor," in *Proceeding of ECOC 2005,* vol. 2, pp. 263—264, paper Tu 4.2.6. 2005.

[65] L. M. Pessoa, H. M. Salgado, and I. Darwazeh. "Joint mitigation of optical impairments and phase estimation in coherent optical systems," in *Proceeding of IEEE LEOS Summer Topical Meetings,* pp. 169–170. 2008.

[66] S. Zhang, P. Y. Kam, C. Yu and J. Chen. "Decision-Aided Carrier Phase Estimation for Coherent Optical Communications." *Journal of Lightwave Technology,* vol. 28, issue. 11, pp. 1597–1607, 2010.

[67] J. R. Montalvão Filho, B. Dorizzi and J. C. M. Mota. "Channel Estimation by Symmetrical Clustering." *IEEE Transactions on Signal Processing,* vol. 50, issue. 6, pp. 1459–1469, 2002.

[68] C. Chan. "Optical Performance Monitoring: Advance Techniques for Next-Generation Photonic Networks." *Elsevier,* San Diego, USA, CA. Chapter 10, 2010.

[69] M. Kuschnerov, M. Chouayakh, K. Piyawanno, B.Spinnler, E. de Man, P. Kainzmaier, Mohammad S. Alfiad, A. Napoli, and B. Lankl. "Data-Aided Versus Blind Single-Carrier Coherent Receivers." *IEEE Photonics Journal,* vol. 2, issue. 3, pp. 386–403, 2010.

[70] F. Hauske, M. Kuschnerov, K. Piyawanno, B. Spinnler, E.-D. Schmidt and B. Lankl. "DGD Estimation from FIR Filter Taps in Presence of Higher Order PMD." in *Proceeding of the European Conference on Optical Communications ECOC'2008,* Brussels, Belgium. Paper Tu.1.D.4, 2008.

[71] M. Chouayakh. "Wireless Indoor MIMO Systems: Theoretical Concept and Practcal Implementation with Focus on Low Effort Data Detection." *PhD Thesis report,* chapter 2. Universität der Bundeswehr München, Fakultät für Elektrotechnik und Informationtechnik. August 2009.

[72] J. E. Mitchell. "Radio over fibre Networks: Advanced and Challenges," in *Proceeding of European Conference on Optical Communication 2009, ECOC '09.* Vienna. Paper P4.5. 2009.

[73] D. Zibar, R. Sambaraju, R. Alemany, A. Caballero, J. Herrera and I.T. Monroy. "Radio-Frecuency Transparent Demodulation for Broadband Hybrid Wireless-Optical Links." *IEEE Photonics Technology Letters,* vol. 22, issue. 11, pp. 784–786, 2010.

[74] C-T. Lin, J. Chen, P-T. Shih, W-J Jiang and S. Chi. "Ultra-High Data-Rate 60 GHz Radio-Over-Fiber System Employing Optical Frequency Multiplication and OFDM Format." *IEEE Journal of Lightwave Technology,* vol. 28, issue. 16, pp. 2296–2306, 2010.

[75] G.H. Smith, D. Novak, and Z. Ahmed. "Overercoming chromatic dispersion effects in fiber-wireless systems incorporating external modulators." *IEEE Transaction Microwave Theory Technology,* vol. 45, issue. 8, pp. 1410–1415, 1997.

[76] J.Marti, J.M. Fuster, and R.I. Lamimg. "Experimental Reduction of chromatic dispersion effects in lightwave microwave/millimetre-wave transmission using tapered linearly chirped fibre gratings." *IEEE Electronic Letters,* vol. 33, issue. 13, pp. 1170–1171, 1997.

[77] H. Murata, K. Kaneda, A. Enokihara, and Y. Okamura. "38 GHz signal optical fiber transmission using guided-wave electro-optic single-side-band modulators with polarization reversals," in *Proceeding European Microwave Association,* pp. 112–115. 2006.

[78] A. Stöhr, A. Akrout, R. BuB, B. Charbonnier, F.V. Dijk, A. Enard, S. Fedderwitz, D. Jager, M. Huchard, F. Lecoche, J. Marti, R. Sambaraju, A.G. Steffan, A. Umbach, and M. Weib. "60 GHz radio-over-fiber technologies for broadband wireless service." *Journal Optical Network,* vol. 8, issue. 5, pp. 471–487, 2009.

[79] M. Weib, A. Stöhr, F. Lecoche, and B. Charbonnier. "27 Gbit/s photonic wireless 60 GHz transmission system using 16-QAM OFDM. M. Weib, A. Stöhr, F. Lecoche, and B. Charbonnier," in *Proceeding of International Meeting on Microwave Photonic,* Valencia, pp. 1–3. 2009.

[80] L.Goldberg, R.D. Esman, andK.J. Williams. "27 Gbit/s photonic wireless 60 GHz transmission system using 16-QAM OFDM," in *Proceeding of Inst. Elect. Eng. J Optoelectronic,* vol. 139, issue. 4, pp. 228–295. 1992.

[81] X.S. Yao and L. Maleki. "Optoelectronic oscillator for photonic system." *IEEE Journal of Quantum Electronic,* vol. 32, issue. 7, pp. 1141–1149, 1996.

[82] X.S. Yao and L. Maleki. "Multiloop optoelectronic oscillator." *IEEE Journal of Quantum Electronic,* vol. 36, issue. 1, pp. 79–84, 2000.

[83] D. Strekalov, D. Aveline, N. Yu, R. Thompson, A.B. Matsko, and L. Maleki. "Stabilizing an optoelectronic microwave oscillator with photonic filters." *Journal of Lightwave Technology,* vol. 21, issue. 12, pp. 3052–3061, 2003.

[84] T. Banky, B. Horvath, and T. Berceli. "Optimum configuration of multiloop optoelectronic oscillators." *Journal of Optics Society of America,* vol. 23, issue. 7, pp. 1371–1380, 2006.

[85] T. Berceli, T. Banky, and B. Horvath. "Optoelectronic Generation of stable and low noise microwave singnals.," in *Proceeding of Inst. Elect. Eng. Optoelectronic,* vol. 153, issue. 3, pp. 119–127. 2006.

[86] A.S. Daryoush, H.W. Li, G. Bouwmans, D. Decoster, J. Chazelas, and F. Deborgies. "Performance evaluation of optoelectronic oscillators employing photonic crystal fiber," in *Proceeding 36th Europena Microwave Conference,* Manchester, pp. 1111–1114. 2006.

[87] G. Kovacs, T. Bereli, and P. Herczfeldc. "Quadrature amplitude modulated microwave signal generation using a single electro-optic Nd:YVO solid-state laser." *IEEE Microwave Wireless Components Letter,* vol. 19, issue. 4, pp. 254–256, 2009.

[88] M. Kourogi, C.H. Shin,and M. Ohtsu. "A 134 MHz bandwidth homodyne optical phase-locked-loop of semiconductor laser diodes." *IEEE Photonic Technology Letter,* vol. 3, issue. 3, pp. 270–272, 1991.

[89] A.C. Bordonalli, B. Cai, A.J. Seeds, and P.J. Williams. "Generation of microwave signals by active mode locking in a gain bandwidth restricted laser structure." *IEEE Photonic Technology Letter,* vol. 8, issue. 1, pp. 151–153, 1996.

[90] H.A. Haus, and A. Mecozzi. "Noise of mode-locked laser." *IEEE Journal of Quantum Electronic,* vol. 39, issue. 3, pp. 983–996, 1993.

[91] D.J. Jones, S.A. Diddams, J.K.Ranka, A. Stentz, R.S. Windeler, J.L. Hall, and S.T. Cundiffi. "Carrier-Envelope phase control of femtosecond model-locked laser and direct optical frequency synthesis." *Science,* vol. 288, issue. 5466, pp. 635–639, 2000.

[92] L.A. Johansson, and A.J. Seed. "Milimeter-wave modulate optical signal generation with high spectral purity and wide locking bandwidth

using a fiber-integrated optical phase-lock-loop." *IEEE Photonic Technology Letter,* vol. 12, issue. 6, pp. 635–640, 2000.